Loughborough University

Thesis Access Form

Copy No.....**Location**.....

Author Monique Iris Jackson

Title The Mechanics of the Table Contact Phase of Gymnastics Vaulting

Status of access OPEN

Moratorium Period:.....years, ending...../.....200.....

Conditions of access approved by (CAPITALS):..... M.R.YEADON .....

Supervisor (Signature)..... .....

Department of School of Sport, Exercise and Health Sciences

Author's Declaration: *I agree the following conditions:*

Open access work shall be made available (in the University and externally) and reproduced as necessary at the discretion of the University Librarian or Head of Department. It may also be digitised by the British Library and made freely available on the Internet to registered users of the EThOS service subject to the EThOS supply agreements.

*The statement itself shall apply to **ALL** copies including electronic copies:*

This copy has been supplied on the understanding that it is copyright material and that no quotation from the thesis may be published without proper acknowledgement.

Restricted/confidential work: All access and any photocopying shall be strictly subject to written permission from the University Head of Department and any external sponsor, if any.

Author's signature.....Date.....11.05.10.....

users declaration: for signature during any Moratorium period (Not Open work): ***I undertake to uphold the above conditions:***			
Date	Name (CAPITALS)	Signature	Address

The Mechanics of the Table Contact Phase of Gymnastics Vaulting

By

Monique Iris Jackson

A Doctoral Thesis

Submitted in partial fulfilment of the requirement for the award of Doctor of Philosophy of Loughborough University

May 2010

Research Student Office, Academic Registry
Loughborough University Leicestershire LE11 3TU UK
Switchboard: +44 (0)1509 263171 Fax: +44 (0)1509 223938

Loughborough University

CERTIFICATE OF ORIGINALITY

This is to certify that I am responsible for the work submitted in this thesis, that the original work is my own except as specified in acknowledgments or in footnotes, and that neither the thesis nor the original work contained therein has been submitted to this or any other institution for a degree.

..... (Signed)

11.05.10 ..... (Date)

Abstract

The Mechanics of the Table Contact Phase of Gymnastics Vaulting

Monique Iris Jackson, Loughborough University, 2010

A computer simulation model of the table contact phase of gymnastics vaulting was developed to gain an understanding of the mechanics of this phase of the vault. The model incorporated a gymnast and a vaulting table, and used a novel two-state contact phase representation to simulate the interaction between these two bodies during the table contact phase. The gymnast was modelled in planar form using seven segments, with torque generators acting at the wrist, shoulder, hip and knee joints. The model also allowed for shoulder retraction and protraction, displacement of the glenohumeral joint centre and flexion/extension of the fingers. The table was modelled as a single rigid body that could rotate. The model was personalised to an elite gymnast so that simulation outputs could be compared with the gymnast's performance. Kinematic data of vaulting performances were obtained using a optoelectronic motion capture system. Maximal voluntary joint torques were also measured using an isovelocity dynamometer, and a torque - angle - angular velocity relationship was used to relate joint torques to joint angles and angular velocities. A set of model system parameters was determined using a gymnast-specific angle-driven model by matching four simulations to their respective performances concurrently. The resulting parameters were evaluated using two independent trials, and found to be applicable to handspring entry vaults. The torque-driven model was successfully evaluated, and shown to produce realistic movements, with mean overall differences between simulations and recorded performances of 2.5% and 8.6% for two different handspring entry vaults. The model was applied to further understanding of the mechanics of the table contact phase of gymnastics vaulting. Optimisation showed that there was limited potential (1.3%) for the gymnast to improve performance through technique changes during the table contact phase. However, with additional changes in configuration at table contact post-flight rotation could be increased by 9.8% and post-flight height could be increased by 0.14 m. Angular momentum was found to always decrease during the table contact phase of the vault, although the reductions were less when maximising post-flight rotation.

Publications

Conference Presentations

JACKSON, M. I., YEADON, M. R., and HILEY, M. J. 2010. Modeling Friction to Incorporate Sliding and Stiction: Application to the Contact Phase of Gymnastics Vaulting, *Accepted for presentation at the 6th World Congress on Biomechanics*, 2010

JACKSON, M., YEADON, M. R., and HILEY, M. J. 2010. Computer Simulation of the Contact Phase of Vaulting, *Proceedings of the Biomechanics Interest Group of the British Association of Sport and Exercise Sciences*, 2010, pp 18.

JACKSON, M., YEADON, M. R., and HILEY, M. J. 2008. Relationship Between Vaulting Table Contact Conditions and Vaulting Performance, *Proceedings of the Biomechanics Interest Group of the British Association of Sport and Exercise Sciences*, 2008, pp 31.

Acknowledgments

I would like to express my sincere gratitude to the following people:

- My supervisors Dr M. R. Yeadon and Dr M. J. Hiley for their continued guidance and support throughout this project,
- Dr M. Begon and Dr S. Forrester who have provided assistance and guidance with aspects of the work,
- The members of the Sports Biomechanics and Motor Control Research Group and associates (Matt, Mark, Lesley, Jon, Bob, Alec, Gheorghe, Sarah, Jo, Martin, Neale, Phil, Dave, Sam, Peter, Felix, Michael, Idafe, David, Ciaran, Helen, Akiko) who have provided assistance and friendship during my time in Loughborough,
- My family and friends outside the department who have supported me throughout my studies,
- The School of Sport, Exercise and Health Sciences and British Gymnastics for financial support.

To all my loved ones

Contents

List of Figures

List of Tables

Chapter 1

Introduction

1.1 The Area of Study

Artistic gymnastics is an Olympic sport that attracts competitors from many countries throughout the world. Gymnasts compete in events that test strength, agility, flexibility, coordination and balance. Both men and women compete in vaulting, one of the more explosive events.

To perform a vault, the gymnast runs along the runway, jumps off the vaulting board, briefly contacts the vaulting table with the hands and becomes airborne before landing on the landing mat. Gymnasts aim to maximise the number of twists and somersaults that are performed during the post-flight, whilst maintaining good form. In the past the vault was performed using a vaulting horse but the apparatus was changed in 2001 when the Fédération Internationale de Gymnastique (FIG) approved a new apparatus: the vaulting table.

The rationale for this research study is to analyse gymnastics vaulting to gain an understanding of the mechanics of the movement, and then to use this understanding to identify ways to improve performance. The research will focus in particular on the table contact phase of the vault, as this phase has been identified as requiring further, more detailed analysis (Prassas et al., 2006; Sands et al., 2003).

While there are numerous coaching publications and experimental research studies on vaulting, there is no general consensus about the importance of the table contact phase. While some sources have advocated that vaulting performance is largely determined prior to the table contact phase (Prassas and Giankellis, 2002; Still, 1990), other sources have suggested that the gymnast has the ability to change the outcome of the vault during the table contact phase (Smith, 1982; Boone, 1976). Table contact is, however, a crucial phase, in that the initial conditions for post-flight, such as the gymnast's centre of mass

velocity and angular momentum, are finalised during this phase (Prassas et al., 2006).

Theoretical research studies, that have used simulation models to investigate the biomechanics of gymnastics vaulting, have provided some insight into the mechanics of this activity (Dainis, 1981; Gervais, 1994; Koh et al., 2003a,b; Sprigings and Yeadon, 1997; King et al., 1999; King and Yeadon, 2005). These models, which represented the gymnast as a number of linked rigid segments, allowed different aspects of vaulting technique to be investigated. A limitation of these theoretical research studies is that the table contact phase was generally over-simplified and therefore the mechanics of this phase of the vault is still not well understood.

Few studies currently exist in the literature regarding the use of the vaulting table. The literature is primarily focused on vaulting using the vaulting horse, and therefore the applicability of the literature to current vaulting using the vaulting table is questionable.

A simulation model of vaulting that accurately represents the table contact phase has the potential to provide better understanding of this particular phase of the vault and to answer questions that previously could not be addressed. Furthermore a simulation study based on the vaulting table will not only be more applicable to current vaulting but will also allow findings from previous studies to be verified or refuted for the new apparatus.

1.2 Statement of Purpose

A simulation model of the table contact phase of vaulting will be developed, evaluated and applied. The simulation model will be used to determine the relationships between table contact phase initial conditions and technique, and vaulting performance, thus providing an understanding of the mechanics of the table contact phase of vaulting.

A subject-specific torque-driven computer simulation model of vaulting will be developed. The representation of the gymnast in the torque-driven simulation model, as a number of rigid segments with torque generators at each inter-segment joint, will be similar to existing models (King and Yeadon, 2005; Koh et al., 2003b). The simulation model will, however, differ from existing models by including a separate vaulting table model, to more accurately account for the dynamics of the table. Furthermore, model complexity of the hand/table interface will also be increased compared to previous simulation models

to more accurately represent the interaction between the gymnast and the vaulting table.

Performance, strength and anthropometric data of an elite level gymnast will be collected so that the simulation model may be gymnast-specific. An angle-driven simulation model will be matched to the kinematic performance data so that model parameters can be determined. These parameters will then be used in the torque-driven model, which will be evaluated by comparing simulated motion with the performance data. This method of evaluation is commonly used in conjunction with simulation models (King and Yeadon, 2005; Koh et al., 2003b).

After evaluation the simulation model will be applied to gain an understanding of the mechanics of the table contact phase of gymnastics vaulting. The simulation model will be used to determine the table contact phase technique that will lead to 'optimal' performance, where optimal performance will be characterised by maximised post-flight rotation and height. The simulation model will also be used to determine the relative importance of table contact phase technique and the initial table contact conditions on vaulting performance.

1.3 Research Questions

1. What is the optimum table contact phase technique for handspring somersault vaults?

To obtain a high score in vaulting the gymnast must perform a vault with a high difficulty value whilst incurring minimal deductions. Each vault is given a difficulty value based on its complexity; vaults with more rotations about the longitudinal and transverse axes in the post-flight have higher difficulty values. Deductions are made for technical faults in the pre-flight, table contact, post-flight and landing phases of the vault. A specific deduction is made for lack of height in the post-flight; "the gymnast must demonstrate a distinct rise in the height of his body after push off from the table" (FIG, 2009b).

Hence, an optimal vaulting performance will be one in which post-flight rotation and height are maximised. Optimisation of the simulation model will be used to determine whether the gymnast's performance can be improved through changes in table contact phase technique.

2. What is the optimal body configuration at table contact to maximise vaulting performance, for given pre-flight conditions?

The gymnast's pre-flight angular momentum and centre of mass trajectory are determined during the approach and vaulting board contact phases of the vault, and therefore are limited by the speed with which the gymnast approaches the vaulting table and the vaulting board technique. The gymnast's body configuration at table contact is not so limited as the gymnast can change configuration during the pre-flight phase. The simulation model will be used to determine the optimal body configuration at table contact to maximise vaulting performance, where maximal performance will again be considered to be when post-flight rotation and height are maximised.

3. How much does performance depend upon technique during the table contact phase and how much does performance depend on initial conditions?

The mechanics of the table contact phase is dependent on both the technique during the table contact phase and the initial table contact conditions. The relative importance of these factors is, however, not clear. Is it within a gymnast's capability to radically alter the performance of a vault during the table contact phase through technique modifications or is the performance of the vault largely pre-determined by the performance in preceding phases? The computer simulation model will allow the relative effects of technique and initial conditions on performance to be ascertained.

4. For an optimal performance, how does the angular momentum about the gymnast's centre of mass change?

The gymnast will have angular momentum about the centre of mass on contact with the vaulting table. During the table contact phase of the vault, the gymnast interacts with the vaulting table and, therefore, the angular momentum about the centre of mass may change. It is generally accepted that angular momentum is reduced during the table contact phase of a vault (Prassas et al., 2006), but it is unclear if this is the case for an optimal performance. The computer simulation model will allow the changes in angular momentum during the table contact phase of the vault to be quantified, facilitating answering this question.

1.4 Thesis Organisation

The outline of the remainder of the thesis is as follows:

Chapter 2 provides a critical review of coaching and research literature on the biomechanics of gymnastics vaulting. The reviewed literature includes coaching publications, experimental research studies and theoretical research studies. The review highlights questions that remain unanswered about the table contact phase of vaulting and also identifies limitations of the previous research.

Chapter 3 describes the method used to collect performance data from an elite level gymnast performing two different vaults. The use of a three-dimensional chain model to determine the kinematics of the vaulting performances is explained and the results presented.

Chapter 4 presents the development of simulation models of vaulting. This includes a novel way to model the interaction between the gymnast and the vaulting table, which is implemented in both angle-driven and torque-driven simulation models. The models allow for movement within the shoulder joint, sliding of the hands relative to the table, deformation of the vaulting table surface and slight rotation of the vaulting table.

Chapter 5 describes the methods used to determine the strength, flexibility and anthropometric parameters of the gymnast. These parameters are required as inputs to both the angle-driven and the torque-driven simulation models. An explanation of the methods used to determine the inertial parameters of the vaulting table is also given.

Chapter 6 outlines the method used to determine the vaulting model system parameters using an angle-driven model. The subsequent evaluation of the system parameters, using independent trials, is presented. The method of evaluation of a torque-driven model is also described and the results of this evaluation discussed.

Chapter 7 applies the torque-driven simulation model to answer the research questions. Vaulting performance is optimised, through modifications to the table contact phase technique and modifications to the gymnast's body configuration at table contact. The results of the optimisations are presented and analysed.

Chapter 8 provides a summary of the thesis. This includes a discussion of the methods used and the results obtained. Potential areas for improvement are identified along with future applications of the vaulting model.

Chapter 2

Literature Review

2.1 Chapter Overview

The review of the literature is divided into two sections. Firstly, a description of vaulting is given, including vaulting apparatus and common vaulting techniques. This is followed by a detailed review of vaulting based coaching and research literature.

2.2 Vaulting Background

Vaulting is common to both men's and women's artistic gymnastics. This section will describe the vaulting apparatus, vaulting in general and common vaulting techniques.

2.2.1 Vaulting Apparatus

The vaulting apparatus consists of the runway, the vaulting board, the vaulting table and the landing mat. Vaulting in both men's and women's artistic gymnastics was traditionally performed over a vaulting horse (Figure 2.1a) with the major difference between the men's and women's events being the orientation of the horse with respect to the approach. The vaulting horse was orientated with the long axis in line with the approach for the men's event and with the long axis perpendicular to the approach for the women's event. The vaulting apparatus was changed in 2001 when the Fédération Internationale de Gymnastique (FIG) approved a new apparatus; the vaulting table (Figure 2.1b). The vaulting table is used in the same orientation for both the men's and the women's events, but at different heights: 1.35 m for the men's event and 1.25 m for the women's event. The vaulting table has similar elastic and dynamic characteristics to the vaulting horse (Knoll and Krug, 2002). The main differences between the two apparatus are the effective contact area, which is greater for the vaulting table, and the angle of the contact area, which is inclined for the vaulting table compared to horizontal for the vaulting horse.

(a) (b)

Figure 2.1. The vaulting apparatus: (a) vaulting horse (Robbinssports.com, 2009), (b) vaulting table (GYMmedia.com, 2005).

2.2.2 Description of Vaulting

To perform a vault, the gymnast runs along the runway, jumps off the vaulting board, briefly contacts the vaulting table with the hands and becomes airborne, before landing on the landing mat. This can be broken down into six successive phases: approach, vaulting board contact, pre-flight, table contact, post-flight and landing. To perform a vault successfully the gymnast must complete all of these phases.

The *approach* phase consists of the run-up and hurdle step. The purpose of the run-up is to generate horizontal momentum in a controlled manner. The hurdle step is "the transitional phase between the run-up and the board contact" (Hay, 1993) and allows adjustment of the gymnast's body configuration to that required at contact with the vaulting board, while maintaining the horizontal momentum gained during the run-up.

During the *vaulting board contact* phase the gymnast contacts the vaulting board. The purpose of the vaulting board contact phase is to alter the gymnast's approach momentum so that the required combination of linear and angular momenta for the vault being performed is obtained. This is achieved by compression of the vaulting board by the gymnast. The subsequent reaction force, which is applied by the vaulting board to the gymnast, results in changes to the linear and angular momenta of the gymnast, and the gymnast becomes airborne.

The *pre-flight* phase involves the flight of the gymnast onto the vaulting table. During

this phase of the vault air resistance is considered to be negligible and therefore the only external force that affects the gymnast is gravity. As a result, the trajectory of the gymnast's centre of mass during the pre-flight phase is parabolic and the motion is governed by the gymnast's linear and angular momenta at take-off from the vaulting board as well as by body configuration.

The *table contact* phase of the vault begins when the gymnast's hands come into contact with the vaulting table. The table contact phase allows the pre-flight momentum to be altered so that the linear and angular momenta required for the post-flight are obtained. The change in momentum is effected by the interaction between the gymnast and the vaulting table. The gymnast will exert a force of varying magnitude and direction on the vaulting table. The reaction force, being applied by the vaulting table to the gymnast, results in changes to the linear and angular momenta of the gymnast.

The *post-flight* phase consists of the flight of the gymnast away from the vaulting table. During the post-flight phase the gymnast often changes body configuration to control both somersault and twist. The post-flight phase is similar to the pre-flight phase in that gravity is the only external force that affects the gymnast and thus the trajectory of the gymnast's centre of mass during the post-flight phase is again parabolic.

The final phase of the vault is the *landing* phase. During this phase of the vault the linear and angular momenta of the gymnast are reduced such that the body is brought to rest in a controlled manner to end the performance.

2.2.3 Vaulting Techniques

There are four fundamental vaulting techniques when classified according to their entry and table contact characteristics: front handspring vaults, vaults with 1/4 to 1/2 turn in pre-flight (known as Kasamatsu or Tsukahara vaults), round-off entry vaults (known as Yurchenko vaults) and direct vaults (Figures 2.2, 2.3, 2.4 and 2.5 respectively). The difficulty of these base vaults can be increased by the addition of twists during the pre-flight and/or the addition of twists and/or somersaults during the post-flight.

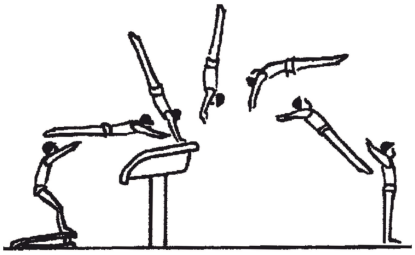

Figure 2.2. Handspring vault (adapted from the Code of Points, FIG (2009b)).

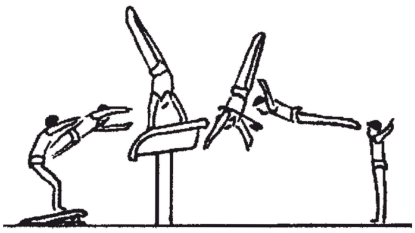

Figure 2.3. Vault with 1/4 to 1/2 turn in pre-flight (adapted from the Code of Points, FIG (2009b)).

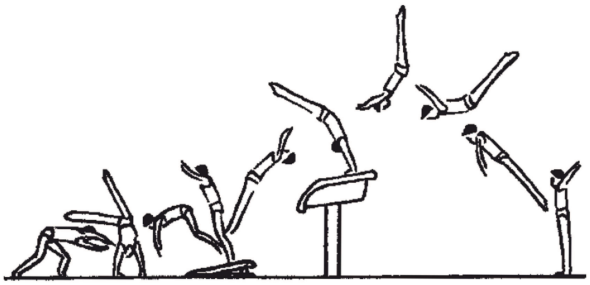

Figure 2.4. Round-off entry vault (adapted from the Code of Points, FIG (2009b)).

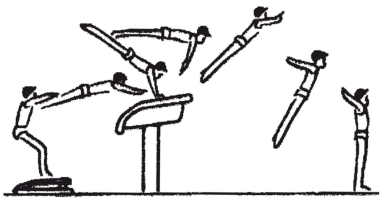

Figure 2.5. Direct vault (in this case a Hecht) (adapted from the Code of Points, FIG (2009b)).

2.3 Coaching and Research Literature

Coaching and research literature on the biomechanics of gymnastics vaulting, and in particular the table contact phase of the vault, will be reviewed. The findings of the review will be presented firstly, in terms of the mechanics of the table contact phase, based on coaching publications and experimental research studies and secondly, in terms of simulation of the table contact phase, based on theoretical research studies.

2.3.1 Vaulting Coaching Publications and Experimental Research

There are numerous coaching publications and experimental research studies on vaulting. Coaching publications are, in general, based on experience and observation with some application of science. Experimental research studies are based on performance analysis, where data are collected and analysed and results inferred. The review of these literature sources will concentrate on suggestions and findings pertinent to the table contact phase.

Within the coaching literature, there is no general consensus about the importance of the table contact phase. Prassas and Giankellis (2002) stated that "the gymnast can do little to affect the rotational and translational requirements of most vaults during the contact phase" and moreover, Still (1990) stated that "most gymnasts could do the whole vault and land on their feet without ever touching the horse". On the other hand, Smith (1982) and Boone (1976) suggest that gymnast's can change the angular momentum of their body and increase their vertical velocity during the table contact phase of the vault. Furthermore, as the coaching literature is primarily based on vaulting using the vaulting horse, the applicability of the literature to current vaulting using the table is questionable. This leaves questions such as "How important is the table contact phase of the vault?" and "Is it within a gymnast's capability to change the performance of a vault during the table contact phase?" unanswered.

The mechanics of the table contact phase is dependent on the initial table contact conditions and the technique during the table contact phase. The initial table contact conditions are, however, interdependent which makes analysis difficult. Similarly, aspects of contact phase technique cannot be considered in isolation. A summary of suggestions regarding conditions at vaulting table touchdown and contact phase technique is presented below.

2.3.1.1 Touchdown Angle

It is generally accepted that the orientation of the gymnast at vaulting table touchdown, otherwise known as touchdown angle, will appreciably influence performance of the vault. The touchdown angle is "essential to proper execution of the skill" (George, 1980). Takei et al. (1996) confirmed this, finding the body angle at touchdown of the horse to be lower for higher scoring handspring full turn vaults.

Murray (1979) and Hunn (1978) both suggested that the optimum touchdown angle depends on the post-flight requirements of the vault. This is supported by research studies which reported touchdown angles of 36° to 51° (angle between the horizontal and the line joining the centres of mass of the legs and arms) for handspring vaults (Dainis, 1979), and 16° to 20° (angle between the horizontal and the line joining the centre of mass and the fingers) for handspring double somersault vaults (Cormie et al., 2004). Furthermore, the optimum touchdown angle will depend on the type of vault performed: for a direct vault the pre-flight rotation of the body has to be stopped and reversed, which will require a lower touchdown angle than that required for a continuous rotation vault, where post-flight rotation is continued in the same direction as pre-flight rotation. For example, the mean touchdown angle reported by Yeadon et al. (1998) of 1° (angle between the horizontal and the line through the trunk) for the Hecht, a direct vault is considerably lower than the angles reported for handspring type vaults. This leads to the question "Can the table touchdown angle for a particular vault be optimised?"

2.3.1.2 Horizontal Velocity

The linear velocities of the gymnast at touchdown will also influence vaulting performance. Boone (1976) and George (1980) both advocate high horizontal touchdown velocities, while Prassas and Giankellis (2002) suggest that the horizontal velocity will be dependent on the difficulty and type of vault to be performed, stating that the horizontal velocity "may be inversely related to the complexity of the pre-vaulting table movement" and will be lower in vaults where the gymnast's rotation reverses during post-flight.

Takei (1991) compared high and low scoring handspring somersault vaults, finding horizontal mass centre touchdown velocities to be 5.52 and 5.08 $\mathrm{m\,s^{-1}}$ respectively. The horizontal velocities of the two groups were significantly different ($p \leq 0.001$), showing that higher horizontal touchdown velocities were associated with better performance,

which supports the suggestion of Boone (1976) and George (1980).

Mass centre horizontal touchdown velocities of 5.52 and 3.71 $\mathrm{m\,s^{-1}}$ have been reported for handspring somersault and layout Yurchenko vaults respectively (Takei, 1991; Kwon et al., 1990). That is, the Yurchenko vault, with the more complex pre-vaulting table movement, was found to have a considerably lower horizontal touchdown velocity than the handspring double somersault vault. This is in agreement with the suggestion of Prassas and Giankellis (2002).

Yeadon et al. (1998) compared Hecht vaults to handspring somersault vaults, finding the horizontal mass centre touchdown velocities to be 5.56 ± 0.36 and 5.31 ± 0.32 $\mathrm{m\,s^{-1}}$ respectively. The Hecht vaults, in which the gymnast's rotation reverses during post-flight, had higher horizontal touchdown velocities than the handspring somersault vaults. This is in contrast with the suggestion of Prassas and Giankellis (2002). Thus, the question "Is there a relationship between horizontal touchdown velocity and the difficulty and type of vault to be performed and if so, what is this relationship?" remains unanswered.

2.3.1.3 Vertical Velocity

The vertical component of the linear velocity is also important. Smith (1982) suggested that at touchdown, the linear velocity of the gymnast's centre of mass should be directed upwards rather than downwards as "the vertical component of the momentum will assist in elevation of the post-flight". Takei and Kim (1990) and Cormie et al. (2004) confirmed the suggestion of Smith (1982), reporting vertical mass centre velocities at touchdown of 2.36 and 2.82 $\mathrm{m\,s^{-1}}$ (upwards) for handspring somersault and handspring double somersault vaults respectively. This leads to the question "Should the vertical touchdown velocity be maximised or is there an optimal ratio of horizontal to vertical touchdown velocity for a particular vault?"

2.3.1.4 Angular Velocity

There are few suggestions within the coaching literature on favourable angular velocities at table touchdown. Nevertheless, it is reasonable to expect that the required angular velocity will be dependent on the type of vault to be performed, and that lower angular velocities at table touchdown will be required for vaults in which the direction of rotation is reversed during the table contact phase. Experimental studies confirm this sugges-

tion reporting angular velocities at horse touchdown of 3.4 and 7.4 rad s^{-1} for Hecht and handspring somersault vaults respectively (Yeadon et al., 1998). This leads to the question "Is there an optimum angular velocity at touchdown for a particular vault?"

2.3.1.5 Length of Table Contact

Experimental studies of elite level gymnasts show there is variability in the duration of the table contact phase, with contact times between 0.16 and 0.25 seconds reported (Bajin, 1978; Cormie et al., 2004; Kwon et al., 1990; Takei, 1990; Takei and Kim, 1990; Takei et al., 2000). Although it is generally accepted that the duration of the table contact phase should be short, there is not general agreement about the reasoning behind a short contact time.

In terms of mechanics, Boone (1976) suggested that the contact time should be minimised to maximise 'vertical lift' from the table. 'Vertical lift' is the result of the change in vertical momentum that occurs during the table contact phase, and is dependent on the magnitude of the vertical forces exerted by the gymnast against the table, and the time during which these forces act. As the change in vertical momentum is the integral of vertical force over time, George (1980) suggested that intuitively vertical momentum would be maximised by maximising both the vertical force and the contact time. This is not, however, the case in reality as the change in vertical momentum that occurs during the table contact phase is also be dependent on the gymnast's technique and body configuration during this phase.

In terms of physiology, a reason for a short contact time is that energy can only be stored in the muscles for a finite length of time, of the order of 0.15 s, after which time the stored energy rapidly dissipates (Smith, 1982). Smith (1982) suggests that the table contact phase should therefore be shorter than this length of time, so that the energy stored in the muscles of the upper body during the compression phase of the support can be released during the repulsion phase. Questions such as "Why is a short contact time favourable?" and "Is there a limit on how short the contact time can be while remaining effective?" still remain unanswered.

2.3.1.6 Table Take-off Angle

Another parameter affecting performance during the table contact phase is the orientation of the gymnast at take-off from the table, otherwise known as take-off angle. Within the coaching literature it is generally accepted that the gymnast should leave the vaulting table before the centre of mass reaches the vertical, that is, before the centre of mass is above the hands. Although experimental studies generally confirm this (Takei et al., 1996; Irwin et al., 2004; Irwin and Kerwin, 2009), both Dainis (1979) and Takei (1990) observed successful vaults with take-off substantially past the vertical. This raises the question "How important is it to leave the vaulting table before reaching the vertical?"

2.3.1.7 Momentum at Table Take-off

Table take-off momentum is determined by the gymnast's momentum at table touchdown and the changes in momentum that occur while in contact with the table. Experimental studies have shown that during the table contact phase of the vault, the horizontal component of linear momentum decreases while the vertical component increases. For example, Cormie et al. (2004) reported mass centre velocity changes during the table contact phase of -1.54 and 0.93 $\mathrm{m\,s^{-1}}$ in the horizontal and vertical directions respectively.

It is also generally accepted within the literature, that angular momentum is reduced during the table contact phase, with small reductions being preferable (Prassas et al., 2006). This raises questions such as "Can the linear take-off momentum be optimised for a given vault?" and "Is it within a gymnast's capability to increase angular momentum during the table contact phase?"

2.3.1.8 Technique

The gymnast's technique will also influence the effectiveness of the table contact phase. Body configuration throughout the table contact, and in particular that of the upper limbs, will affect the performance. There is, however, disagreement regarding the technique that should be used. Various techniques are suggested in the coaching literature such as opening the shoulders by increasing the angle between the trunk and the arms (Smith, 1982), elevating the shoulder girdle (George, 1980) and pushing through the wrists (Murray, 1979). Furthermore, while most publications agree that there should be no changes in elbow angle throughout the table contact phase and that changes in upper limb configuration should only occur at the wrists and shoulders, Smith (1982) suggests

that for some vaults the arms should be straightened during table contact. This raises questions such as "Which, if any, of these techniques is optimal?"

2.3.1.9 Apparatus

Finally the vaulting apparatus must also be considered. During the transitional period from the vaulting horse to the vaulting table some recommendations and observations about vaulting with the new apparatus were made. Introduction of the vaulting table increased the effective area for hand contact by approximately 40% compared to the vaulting horse. Sands and McNeal (2002) suggest that the larger, flatter surface area of the table will "make Yurchenko style vaults considerably easier" and will also "allow the gymnast to place her hands more unevenly" in vaults with 1/4 to 1/2 turn in pre-flight. The design of the old vaulting horse allowed female gymnasts to place their hands on the forward side of the vaulting horse, in effect 'blocking' or reducing horizontal momentum. The larger, flatter surface area of the vaulting table does not facilitate 'blocking' and "requires the gymnast to rely more on hand-surface friction" to control horizontal momentum (Sands and McNeal, 2002).

Irwin et al. (2004) conducted a preliminary study to examine changes to kinematic variables of the handspring somersault vault after the introduction of the new vaulting table. The study found "good agreement between the horse and table for all kinematic variables, which reflects little change in technique". Irwin and Kerwin (2009) followed this study with an analysis of changes in handspring somersault vault technique resulting from the introduction of the new apparatus. The study found differences in shoulder angle and strike angle (centre of mass to contact point) at vault take-off, as well as differences in vertical velocity and average angular velocity during vault contact. This study highlighted that the introduction of the vaulting table has to a degree changed vaulting technique and that "further investigation of current competitive performances on the table is needed" Irwin and Kerwin (2009).

2.3.1.10 Limitations of Coaching Publications and Experimental Research

Within the coaching publications and experimental research literature the authors have concentrated on similar aspects of the vault, successively analysing different vaults. In effect, the literature often answers similar questions, leaving many questions unanswered. Furthermore, as the majority of the coaching publications were published in the late

nineties, their applicability to current-day vaulting will, to some degree, be limited. The level of athletic ability and the difficulty of vaults performed has increased considerably since that time and the apparatus has also changed substantially. Analysis of current vaulting performance is required to verify the suggestions and findings.

2.3.2 Theoretical Research

A number of theoretical research studies have been conducted on the biomechanics of gymnastics vaulting. These studies have concentrated on handspring (Dainis, 1980a,b, 1981; Gervais, 1994), Yurchenko (Koh and Jennings, 2003; Koh et al., 2003a,b; Koh and Jennings, 2007) and Hecht (Sprigings and Yeadon, 1997; King et al., 1999; King and Yeadon, 2005) vaults respectively. The review of these research studies will concentrate on simulation of the table contact phase.

2.3.2.1 Handspring

Dainis (1980a,b, 1981) developed a model of the handspring vault to gain insight into the mechanics of this vault. The three-segment model assumed that the horse contact phase of the vault comprised two distinct phases: compression and repulsion. The model allowed for shortening of the gymnast during compression, to represent elbow flexion and/or shoulder girdle depression, and subsequent lengthening of the gymnast during repulsion.

The main findings of this study were that the initial distance of the vaulting board from the horse and the board take-off velocity were found to be the principal variables affecting the outcome of the vault, and that the force exerted by the performer during the repulsion phase has only a minimal effect on the post-flight characteristics. In effect, "the maximum potential of the vault is essentially determined at board take-off and enhancements during the various phases can do little to enhance it" (Dainis, 1980b). However, it was noted that if the tangential component of the force exerted by the gymnast was different, the result would be an increase/decrease in post-flight rotation. This would suggest that the gymnast can, to a certain degree, influence post-flight performance during the table contact phase, which seems to be in contradiction to the author's conclusions.

Limitations of this study relate to assumptions that were made in the generation of the model. Firstly, the body angle was defined as the mean of the trunk and leg angles

as “these angles were always quite similar”. This in effect reduced the system to a two-segment model with just arm and body segments. Secondly, it was assumed that at the end of the compression phase the angular velocity of the body was equal to the angular velocity of the centre of mass about the contact point i.e. it was assumed that the gymnast rotated as a rigid segment at this time. This limits the applicability of the model to vaults in which the body configuration changes during the table contact phase. Thirdly, the forces exerted on the gymnast by the horse, although functions of time, were assumed to be “constant average forces acting for the duration of the repulsion phase”. This assumption limits the accuracy of the model as the force time history, is not correct.

An angle-driven model of the handspring somersault vault was developed by Gervais (1994) to enable predictions of optimal vaulting performance to be made. Mathematical equations, based on a five-segment gymnast model described the horse contact phase of the vault. Optimisations of vaulting performance were based on maximising the points awarded by the judges for the vault, by varying the gymnast’s configuration during the horse contact phase and the length of the horse contact phase.

Results of the study indicated that compared to a “typical high-level performance”, an optimal handspring somersault vault will have a shorter contact time, greater post-flight amplitude, fewer form violations, greater take-off velocities and a greater change in linear momentum. The optimal vault also had a longer post-flight time and greater post-flight angular momentum, which together necessitated the gymnast tuck less tightly to land without over-rotation. In Gervais’s opinion, the optimal technique was feasible as the joint displacements and their rates of change were constrained such that they were dependent on the performer’s present capabilities. A limitation however, is that the timing of the relative segmental movements was not constrained and therefore there was still the potential to produce joint torques beyond the capability of the gymnast.

A further major limitation of this study was that simulation began with the gymnast in contact with the vaulting horse, eliminating touchdown. This is not a full representation of the horse contact phase as the impact of the gymnast with the vaulting horse was not considered. Substantial changes in linear and angular momentum can occur as a result of an impact, therefore touchdown should be considered when simulating the table contact phase of vaulting.

2.3.2.2 Yurchenko

Simulation studies of the Yurchenko vault have been based on a five-segment model of the gymnast (Koh and Jennings, 2003; Koh et al., 2003a,b; Koh and Jennings, 2007). These studies were completed to provide an understanding of the mechanics of the Yurchenko vault, and to enable predictions of optimal vaulting performance to be made.

The main emphasis of these studies was identifying the technique required to optimise performance of the Yurchenko vault. The definition of optimal performance was based on maximising the points awarded by the judges for the vault. Performance was optimised by varying the joint angles and joint angular velocities at horse impact, and the duration of the contact phase.

Compared to the "best trial performance", a simulated optimal Yurchenko layout vault was found to have greater post-flight amplitude and better form during post-flight. According to Koh et al. (2003b) this was achieved through a larger angular velocity at impact, an increased vault touchdown angle (where touchdown angle is defined as the angle between the line from the centre of mass to the contact point and the horizontal), an increase in angular momentum during the horse contact phase and a higher vertical take-off velocity from the horse.

Koh et al. (2003b) stated that angular momentum could be increased during the horse contact phase if the line of the reaction force passed posteriorly to the gymnast's centre of mass. In such a case, the reaction force would produce a turning effect that would increase the angular momentum. However, in contrast, experimental studies of Yurchenko vaults show a decrease in angular momentum during the horse contact phase (Kwon et al., 1990). The question "Can angular momentum be increased during the table contact phase of the vault?" remains unanswered.

For the optimal vault, Koh et al. (2003a) found peak torques about the wrist and shoulder joints, during the horse contact phase, of approximately 100 Nm and 125 Nm respectively. The torque about the wrist joint is necessary to support the weight of the gymnast and to effect an extension-flexion action, while the torque about the shoulder joint is also necessary to support the weight of the gymnast as well as to reduce the shoulder angle. The magnitude of these torques "would suggest that the impact action is not passive" (Koh et al., 2003a), as the required joint torque is greater than that required to just overcome the centripetal torque. As the joint torques were not dependent on the joint

angular velocities, questions about the capability of a gymnast to generate these torques remain unanswered.

Finally, to contact the vaulting horse at the required angle and with the required angular momentum to produce the optimal performance, modifications to the pre-flight performance were necessary. Koh and Jennings (2007) showed that by varying either the segment angular velocities or the segment angular orientations during pre-flight, the optimal vault could be obtained, noting that varying the segment angular orientations would be more feasible. However, the effect of the modifications to the pre-flight on the required joint torques was not considered in this study, so questions about the capability of a gymnast to perform the optimal vault remain.

Within each of these studies, simulation of the vault commenced with the gymnast in contact with the vaulting horse and ended just before landing. Therefore the main limitation of these studies is that touchdown is not modelled, over simplifying the horse contact phase. A second limitation of these studies is that the maximum joint torques were determined from kinematic data using an inverse-dynamics approach. Computing the joint torques in this way resulted in maximum joint torque values that were independent of the joint angular velocity. Joint torques are dependent on joint angular velocity (Hill, 1938) and therefore the method used did not accurately represent the capabilities of the muscles surrounding the joint.

2.3.2.3 Hecht

Sprigings and Yeadon (1997) and King et al. (1999) developed two-segment models of the Hecht vault to gain insight into the reversal of rotation during the horse contact phase of the vault, and to determine the optimum pre-flight conditions for the vault. In each of these studies, the Hecht vault was modelled from vaulting board take-off through to landing.

The main finding of Sprigings and Yeadon (1997) was that "with a suitable pre-flight trajectory the majority of the reversal of rotation is a consequence of the impact with the horse rather than the result of any muscular torques exerted by the gymnast around the shoulder joints". This finding suggests that while the gymnast can actively contribute to the vault during the table contact phase through shoulder extension, success will be largely pre-determined by the pre-flight characteristics. The results of the study by

King et al. (1999) support this, finding that "most of the backwards rotation required to perform the Hecht vault comes from the correct pre-flight".

King et al. (1999) went further and also analysed the effect on performance of varying the pre-flight parameters. Increasing the horizontal touchdown velocity was found to increase post-flight height, distance and backwards rotation, whereas increasing the vertical touchdown velocity was found to also increase the post-flight height, but decrease the backwards rotation. Furthermore, King et al. (1999) found that reversal of rotation was facilitated by a low angular momentum and low body angle at touchdown.

The main limitation of the studies of Sprigings and Yeadon (1997) and King et al. (1999) was that the impact with the vaulting horse was modelled as an inelastic contact, i.e. the velocity of the hands dropped to zero instantaneously upon contact. This representation of the table contact phase is inaccurate as it results in a very short contact time and, therefore, the impulsive reaction forces between the gymnast and the horse are unrealistically large. Furthermore, modelling the impact as an inelastic contact results in overestimation of the energy losses. This follows from the coefficient of restitution being zero for an inelastic impact, which results in maximum energy loss. Conversely for an viscoelastic impact, as occurs in reality, the energy loss would be less. Another limitation of the studies is that the internally generated shoulder torque was constrained to be zero during the table contact phase, in effect eliminating the contribution of muscle-generated shoulder torques. King et al. (1999) acknowledged these limitations stating "the main simplifications of the model occur during the contact phase, where it is assumed there is no shoulder torque during horse contact and that the impact with the horse is non-elastic".

In another study by King and Yeadon (2005) a five-segment model of the Hecht vault was developed to further investigate the factors that influence performance of the vault. The vault was again modelled from vaulting board take-off to landing. Within this model an attempt was made to account for the viscoelastic properties of the shoulder joint and of the hand/vaulting horse interface during the horse contact phase through the use of massless non-linear springs. In this study an attempt was also made to account for muscular torques about the shoulder joint, contributed by the gymnast during the horse contact phase, through the use of a torque generator.

The results of the study indicated that although a simple model of vaulting can be used

to understand some of the basic principles of vaulting, a more complex model is required to accurately simulate the movement. King and Yeadon (2005) also found that while appropriate initial kinematics are essential, other factors have a substantial influence on performance. For example, translational movement at the shoulder joint during the table contact phase must be included to avoid substantial energy losses. Similarly elasticity of the hand/horse interface is required to allow the gymnast to stay in contact with the horse for a reasonable length of time.

The study by King and Yeadon (2005) also found that sub-maximal shoulder torque was required for an optimal performance which suggests that "the ability of the gymnast to produce shoulder torque may not limit performance in the Hecht vault". This may be because the angle between the shoulder and the trunk decreases rapidly during the table contact phase, under which conditions only relatively small torques can be produced. This raises the question "In vaults where there is not rapid opening/closing of the shoulder joint, does the ability of the gymnast to produce shoulder joint torque limit performance?"

Although King and Yeadon (2005) overcame many of the previously listed problems associated with modelling the table contact phase, the model still had limitations. For example, the model did not have a rigid hand segment or wrist joint and there were no active forces to resist movement at the shoulder joint. However, as the model matched recorded performances reasonably well, King and Yeadon concluded that "it is likely that any omissions from the model have only a small effect on performance".

2.4 Chapter Summary

Coaching and research literature on the biomechanics of gymnastics vaulting, and in particular the table contact phase of the vault was reviewed. While the coaching publications and experimental research studies reviewed provided some insight into the mechanics of vaulting, they left many questions about the table contact phase unanswered. Furthermore, within the literature there was no general consensus about the importance of the table contact phase. While some sources advocated that vaulting performance is largely determined prior to the table contact phase (Prassas and Giankellis, 2002; Still, 1990), other sources suggested that the gymnast has the ability to influence the performance of the vault during the table contact phase (Smith, 1982; Boone, 1976).

Theoretical research studies, that used simulation models to investigate the mechanics of gymnastics vaulting, were also reviewed. While the theoretical research studies provided some insight into the mechanics of the movement, they generally over-simplified the table contact phase and therefore this phase of the vault is still not well understood. A simulation model of vaulting that accurately represents the table contact phase has the potential to provide better understanding of this particular phase of the vault and to answer questions that previously could not be addressed. Furthermore all of the vaulting simulation studies assumed a horizontal vaulting horse rather than an inclined vaulting table. A simulation study based on the vaulting table will not only be more applicable to current vaulting but will also allow findings from previous studies to be verified or refuted for the new apparatus.

Chapter 3

Kinematic Data Collection

3.1 Chapter Overview

Kinematic data of vaulting were collected from an elite level gymnast. This chapter gives a description of the protocol used to collect the data and also explains the processing and analysis of the data.

3.2 Data Collection

An optoelectronic motion capture system (Vicon, Oxford Metrics Group), situated within the National Gymnastics Performance and Research Centre at Loughborough University, was used to collect kinematic vaulting data of an elite male gymnast (21 years, 69.9 kg, 1.732 m). The gymnast performed two different vaults: a handspring forward with salto forward stretched (layout) as shown in Figure 3.1, and a handspring forward with double salto forward tucked (Roche) as shown in Figure 3.2.

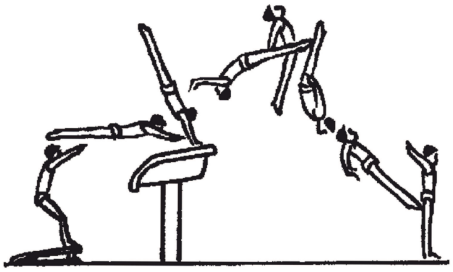

Figure 3.1. Handspring forward with salto forward stretched (layout) (FIG, 2009b).

Figure 3.2. Handspring forward with double salto forward tucked (Roche) (FIG, 2009b).

3.2.1 Data Collection Set-up

18 Vicon MX13 cameras, sampling at a frequency of 480 Hz, were used to track the motion of markers attached to the gymnast and the vaulting table during vaulting performances. The cameras were positioned and focused to give a capture volume that encompassed the vaulting board, the vaulting table and the landing mat (Figure 3.3). The capture volume was wand calibrated, and the calibration error was found to be $\pm$ 0.5 mm (variation in measured distance between two wand markers).

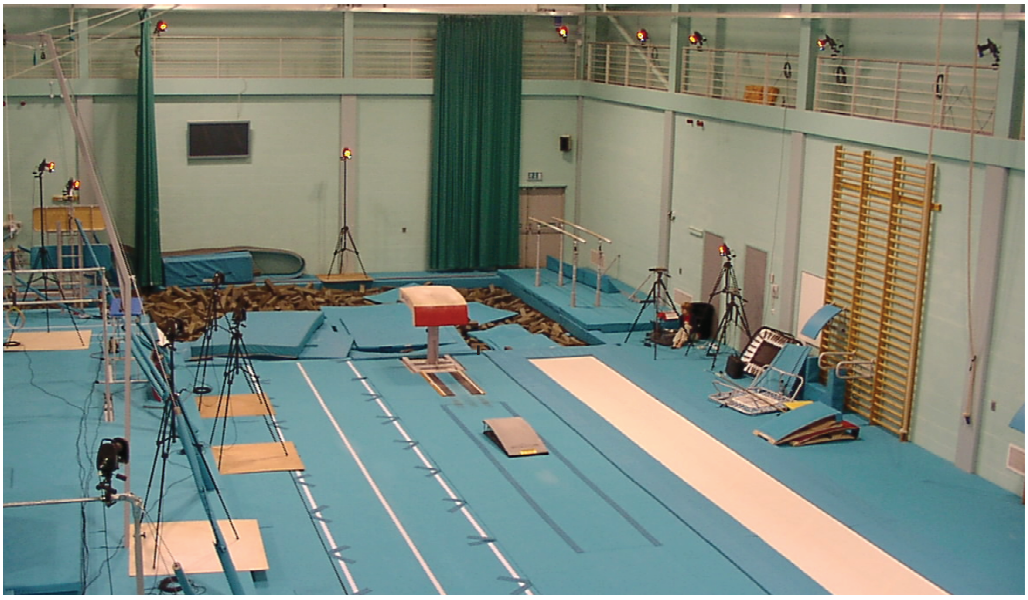

Figure 3.3. A view of the experimental set-up.

58 spherical markers, of 25 mm diameter, were attached to the gymnast. An additional 42 spherical markers, of 15 mm diameter, were attached to the vaulting table and the floor under the vaulting table. The marker placement on the gymnast and the vaulting table is shown in Figure 3.4.

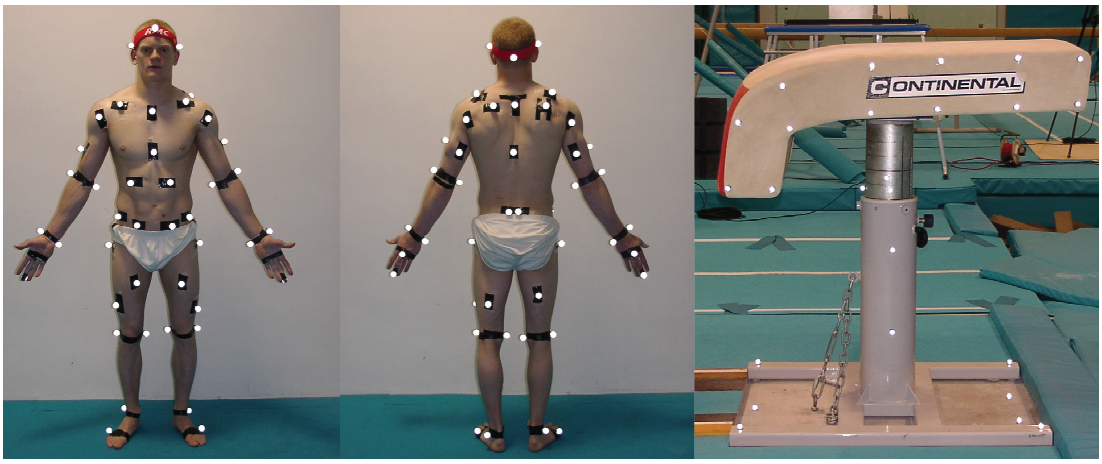

Figure 3.4. Marker placement on the gymnast and on the vaulting table.

In addition a high speed camera (Phantom v4.1), sampling at a frequency of 960 Hz, was positioned perpendicular to the vaulting runway and focused to capture hand contact with the vaulting table. The camera was triggered such that the hand contact occurred approximately in the middle of the data capture. A schematic of the experimental set-up showing the positions of the cameras is given in Figure 3.5.

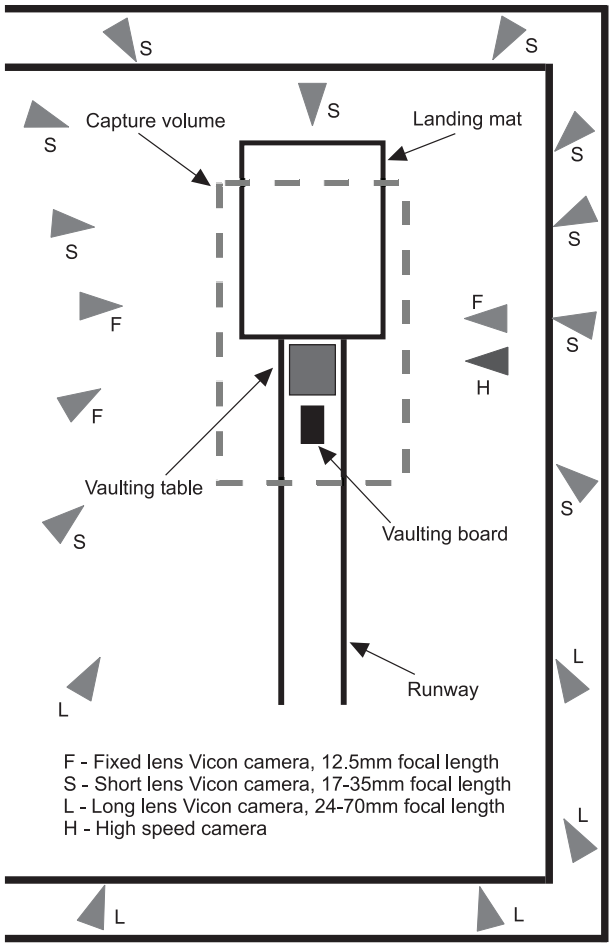

Figure 3.5. Schematic of experimental set-up.

3.2.2 Data Collection Protocol

The data collection procedures were explained to the gymnast in accordance with the Loughborough University ethical guidelines and informed consent forms were signed (Appendix A). The gymnast performed a warm-up, similar to that performed at a training session, and was then asked to perform repetitions of each vault until six successful trials had been captured. A trial was considered to be successful if the equipment was triggered correctly and the gymnast landed the vault on the feet on the landing mat. An international Brevet judge assessed the performances such that the successful trials could be ranked in terms of performance.

3.3 Data Analysis

The kinematic data collected using the Vicon motion capture system were processed using a chain model, to determine the motion of both the gymnast and the table during each vaulting trial. This method of data analysis is explained below.

3.3.1 Chain Model

There are a number of methods to determine the poses (position and orientation) of body segments from marker positions. Traditional methods of determining the poses involve sequentially calculating the pose of each segment. When using these methods, skin movement artefacts and marker occlusions can give rise to problems such as variable segment length and/or apparent joint dislocations (non-anatomical displacements at the joints). The global optimisation method which imposes joint constraints has been shown to reduce these problems (Lu and O'Connor, 1999; Roux et al., 2002; Begon et al., 2008).

The global optimisation method involves "determining the optimal pose of a multi-link model for each data frame such that the overall differences between the measured and model determined marker coordinates are minimised throughout all the body segments" (Lu and O'Connor, 1999). The multi-link (chain) model is defined by a number of degrees of freedom, which represent the relative movements of the rigid segments, and a number of parameters, which represent the lengths of the segments. Global optimisation solves for the degrees of freedom such that the overall distance between the measured marker coordinates and the model determined marker coordinates is minimised. As the global optimisation problem results in a non-linear system of equations, an iterative optimisation method (Newton-Gauss non-linear least square algorithm) is used to solve the equations.

A three-dimensional chain model and global optimisation procedure, similar to that used by Begon et al. (2008), was used to determine the kinematics of the table contact phase of each of the vaulting trials (Appendix B). The model comprised 13 rigid bodies corresponding to the following segments: head + upper trunk, lower trunk, left thigh, right thigh, left shank, right shank, left arm, right arm, left palm, right palm, left fingers, right fingers and table. Within the model the motions of the left and right limbs were assumed to be symmetrical. Fourteen degrees of freedom q_i, nine parameters p_i, and two constraints $f(q_i)$, characterised the model, as depicted in Figure 3.6.

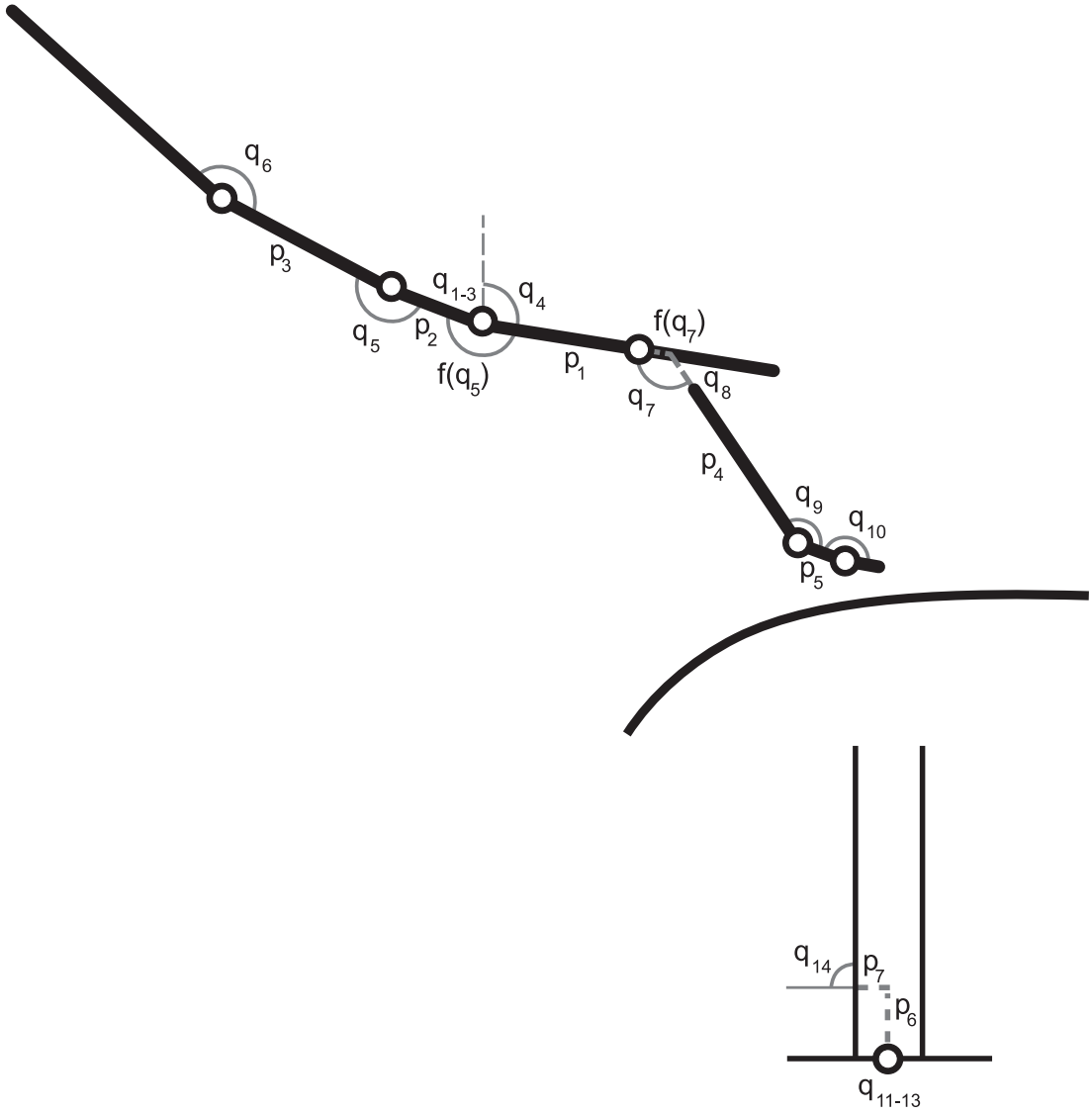

Figure 3.6. Chain model definition for vaulting. Degrees of freedom: q_{1-3} position of gymnast, q_4 orientation angle, q_5 hip angle, q_6 knee angle, q_7 shoulder angle, q_8 shoulder retraction/protraction, q_9 wrist angle, q_{10} knuckle angle, q_{11-13} table position and q_{14} table angle. Constraints: trunk angle $f(q_5)$ and glenohumeral position $f(q_7)$. Parameters: p_1 head + upper trunk length, p_2 lower trunk length, p_3 thigh length, p_4 arm length, p_5 palm length, p_{6-7} distance from base of table to table centre of rotation, p_8 shoulder half width and p_9 hip half width. Note: shoulder half width p_8, and hip half width p_9 are not shown in this schematic as they perpendicular to the plane shown.

3.3.2 Details of Chain Model Definition

The chain model described above was defined after observation and preliminary analysis of the contact phase of vaulting. The following sections provide justification for the structure of the chain model and give details of specific features of the model.

3.3.2.1 Trunk Representation

Preliminary analysis highlighted that for handspring entry vaults a single segment trunk was not sufficient to accurately represent the motion. Therefore two segments were used to represent the trunk: a head + upper trunk segment and a lower trunk segment, while the angle between the two segments was defined as the trunk angle. The orientation of the head + upper trunk segment was based on the orientation of the upper trunk i.e. the head was assumed to have the same orientation as the upper trunk.

During the contact phase of the vault, the gymnasts exhibited trunk angles ranging from small amounts of spinal flexion to small amounts of spinal hyper-extension. Within this range of motion, an approximately linear relationship was found between trunk angle and hip angle. Thus, within the chain model, hip extension/flexion was represented by the hip degree of freedom q_5, while trunk flexion/extension was modelled as a function of hip angle $f(q_5)$ as shown in Figure 3.6. The resulting function constrained the trunk angle to be the same as the hip angle. This representation of trunk flexion/extension is similar to that used by Yeadon (1990b).

3.3.2.2 Shoulder Representation

The shoulder is a complex joint comprising the scapula, the clavicle and the humerus. The components of the shoulder move simultaneously, allowing a large range of motion. Movements of particular interest for vaulting are shoulder flexion and extension and shoulder retraction and protraction.

The humerus joins the shoulder girdle at the glenohumeral joint. When the shoulder is flexed the scapula is elevated, rotated upward and abducted, resulting in elevation of the glenohumeral joint (Floyd, 2007). Within the chain model arm flexion and extension was represented by the shoulder extension/flexion degree of freedom q_7, while the resulting glenohumeral joint movement was modelled as a function of the shoulder angle $f(q_7)$ as shown in Figure 3.6. This representation of glenohumeral joint movement as a

function of shoulder angle is similar to that used by Begon et al. (2008) when modelling straddled movements on high bar and that used by Hiley et al. (2009) when modelling the undersomersault on parallel bars.

A dynamic calibration trial, in which the gymnast completed flexion-extension movements from the anatomical position, was used to determine the relationship between shoulder angle and glenohumeral joint position (defined relative to the top of the upper trunk). A cubic polynomial was fitted, and resulted in good agreement between the polynomial and the experimental data as seen in Figure 3.7.

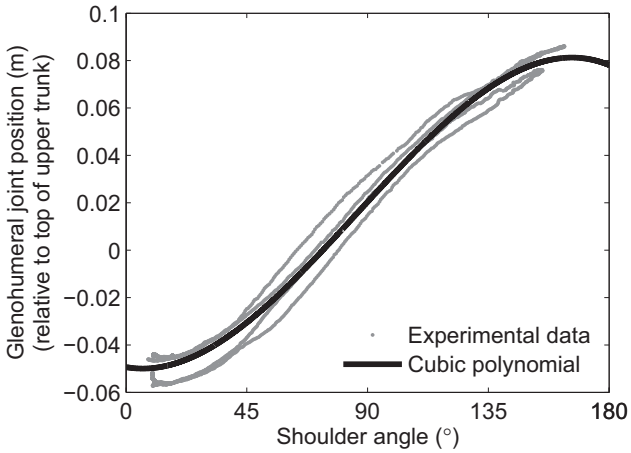

Figure 3.7. Glenohumeral joint position as a function of shoulder angle.

The root mean square error (RMSE) between the cubic polynomial and the experimental data was 0.005 m, which indicates the curve is a good fit to the data. A benefit of using a cubic polynomial is that it exhibited a minimum near 0° and a maximum near 180° which is realistic, in that symmetry about 0° and 180° might be expected.

Shoulder retraction and protraction also occur during the contact phase of vaulting. Shoulder retraction/protraction was represented by motion of the arm relative to the trunk in the direction of the arm q_8.

3.3.2.3 Arm Representation

Preliminary analysis highlighted that for the two handspring entry vaults there was a maximum variation in elbow angle during the contact phase of approximately 12°. It was therefore considered reasonable to model the arm as a rigid segment. The mean length of the arm during the contact phase of the vault was determined for each vaulting type, and was input to the model as the length of the arm segment p_4.

3.3.2.4 Hand Representation

Analysis of the high speed video showed that contact with the vaulting table was initially made with the fingers and then with the palm of the hand. Furthermore, the palm of the hand also lost contact with the table before the fingers during take-off from the vaulting table. If the hands were represented by a single segment the centre of pressure would be incorrect when the palms were not in contact with the table. The hands were therefore modelled using two segments: palm and fingers. Finger extension and flexion was represented by the finger degree of freedom q_{10}.

3.3.2.5 Table Representation

When the gymnast contacts the vaulting table the impact causes the table to tilt backwards and then the table oscillates. The oscillation of the table was represented by the table degree of freedom q_{14}. The position of the centre of rotation of the table was defined by the parameters p_6 and p_7 as shown in Figure 3.6, and was determined by finding the point about which the markers on the table rotated.

3.3.3 Chain Model Implementation

Static and dynamic calibration trials were used to determine the centres of rotation of adjoining segments and also to define local reference frames associated with each segment. This allowed the model parameters p_i, and the marker locations with respect to the segment reference frames to be determined. The static calibration trial was conducted with the gymnast in the anatomical position, while dynamic calibration trials were conducted for the hip and shoulder and involved flexion-extension/abduction-adduction combined movements from the anatomical position, in line with the recommendation of Camomilla et al. (2006).

To determine the centre of rotation of the ball and socket joints of the shoulder and hip, a functional method was used. Functional methods identify the joint centre as the centre of rotation of adjacent segments (Camomilla et al., 2006). The functional method used was the symmetrical centre of rotation estimation (SCoRE) method (Ehrig et al., 2006). This method involves determining the coordinates of the joint centre such that its position remains constant relative to both of the adjoining segments. The SCoRE method was chosen as it has been shown to be an accurate method of determining spherical joint centres (Ehrig et al., 2006; Monnet et al., 2007).

The centre of rotation of the hinge joints of the knee and the wrist were determined as the midpoint of medial and lateral markers. The location of the knuckle centre of rotation was defined as the offset position of the knuckle marker. The top of the upper trunk was determined as the midpoint of markers on the sternum and the C7 vertebrae, and the bottom of the upper trunk was defined relative to the top of the upper trunk according to anthropometric measurements. The head + upper trunk segment and the lower trunk segment were assumed to meet at the bottom of the upper trunk.

The chain model, which was implemented using the HuMAnS toolbox (Wieber et al., 2006), was applied to the three best trials of each vault to determine the kinematics during the table contact phase. The model was run from 0.1 s prior to table contact through to 0.1 s after table take-off, during which time the assumptions made within the model, in terms of the degrees of freedom, were considered to be valid.

The global error of reconstruction, defined as the root mean square difference between the measured and the model-determined marker positions, was also calculated to check the accuracy of the model. The global errors of reconstruction were 38.9 $\pm$ 1.1 mm and 38.1 $\pm$ 1.5 mm for the layout and Roche vaults respectively. Analysis of the errors indicated that the markers on the fingers and hands were inflating the errors. Without the hand markers the errors of reconstruction were 26.2 $\pm$ 1.5 mm and 27.5 $\pm$ 0.6 mm for the layout and Roche vaults respectively. This suggests that while the chain model matches most of the data well, it is not such a good fit to the hands. Analysis of the high speed video showed that the hands were often adducted during the contact phase of the vault, which the model did not allow for and is the probable reason for the higher error. Adduction of the hands is not, however, expected to significantly affect the kinematics of the table contact phase and therefore the model is an acceptable compromise between accuracy and simplicity. Furthermore the reconstruction errors are also similar to those found by Begon et al. (2008) during different gymnastics skills and are therefore considered to be acceptable.

The kinematic data determined using the chain model were interpolated by fitting quintic splines (Wood and Jennings, 1979). This allowed complete time histories to be obtained, such that the kinematics could be determined at any time during the performances. In addition to interpolation the process also smoothed the data. In order to determine the level of smoothing, a psuedo data set was generated by averaging the data values from the frames adjacent to each original data point. The difference between the psuedo

data point and the original data point gave an estimate of the error in that data point (Yeadon and King, 2002). In order to obtain a balance between removing noise and over-smoothing, local and global errors were each given a weighting of 50%.

3.4 Results

A three-dimensional chain model was used to determine the kinematics of the gymnast and the table during the table contact phase of the three best layout vaults and the three best Roche vaults. The data were subsequently interpolated using a quintic spline. Figure 3.8 and Figure 3.9 give an example of the splined results obtained for a layout vault. The dashed lines indicate the times of table contact and take-off respectively.

The gymnast's horizontal and vertical centre of mass velocities at table contact were slightly above the ranges reported in the literature for elite male gymnasts performing handspring somersault vaults using the vaulting table: reported horizontal velocities (4.04 - 4.78 $\mathrm{m\,s^{-1}}$), reported vertical velocities (2.36 - 2.82 $\mathrm{m\,s^{-1}}$) (Cormie et al., 2004; Irwin et al., 2004). The gymnast's horizontal centre of mass velocity decreased substantially while in contact with the vaulting table, while the gymnast's vertical centre of mass velocity at take-off was similar to that at table contact as shown in Figure 3.8.

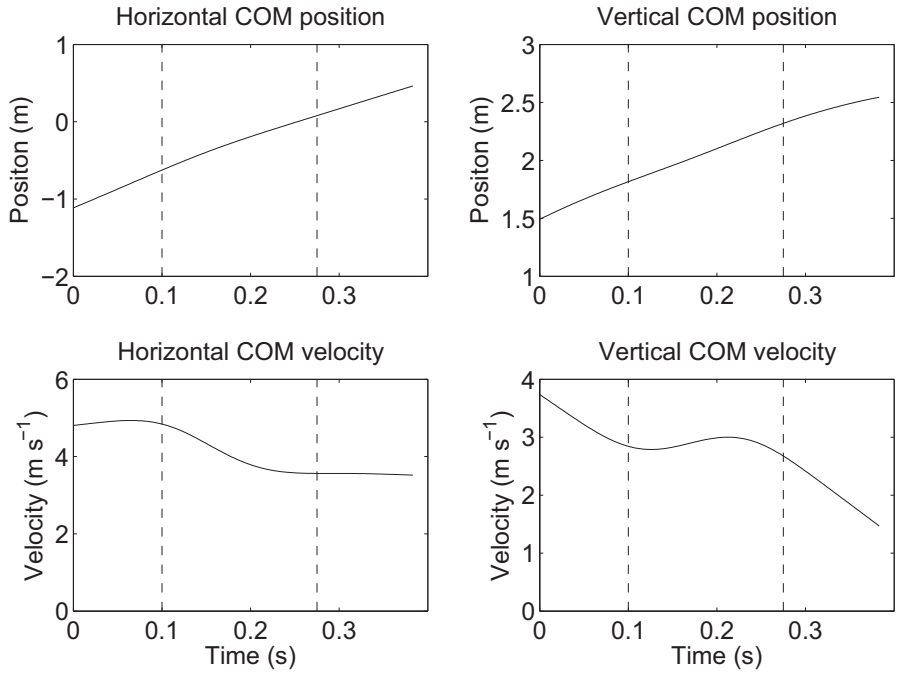

Figure 3.8. Example of centre of mass position and velocity time histories. The dashed lines indicate the times of table contact and take-off respectively. Centre of mass position relative to the front edge of the table at floor level.

Figure 3.9 shows substantial changes in wrist, shoulder and hip angles during the table contact phase and less substantial changes in knee angle. Oscillation of the table during the table contact phase can also be seen.

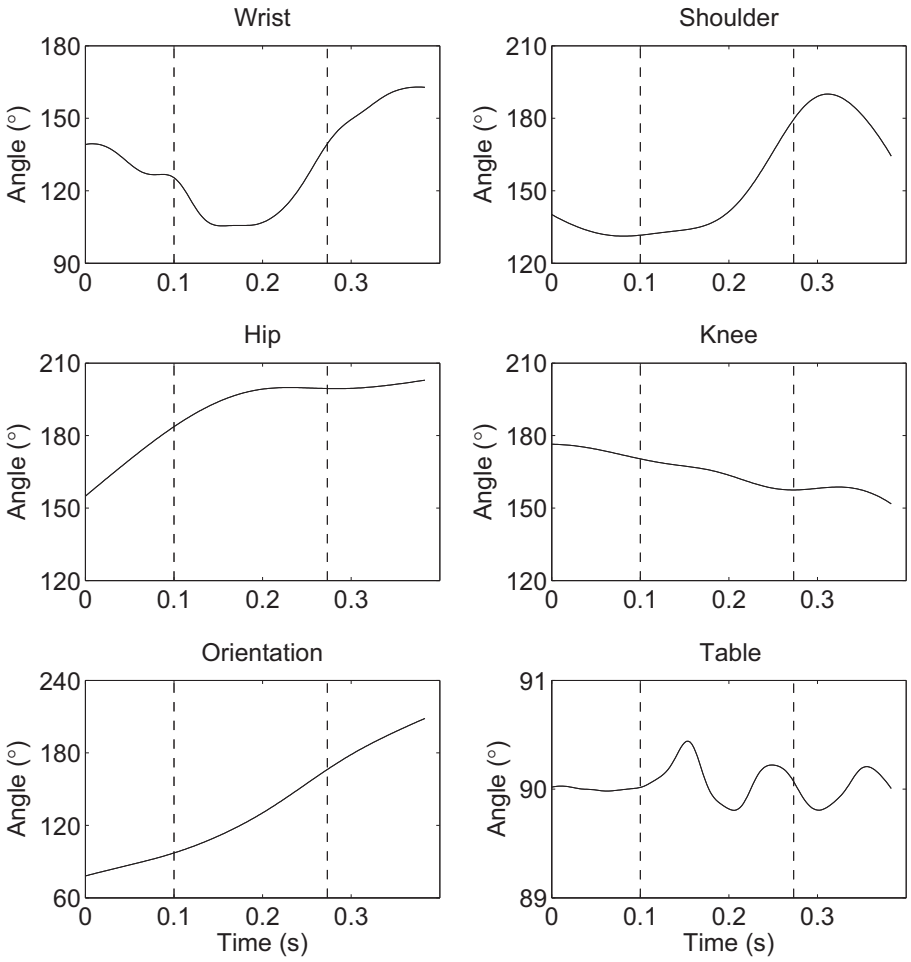

Figure 3.9. Example of angle time histories. The dashed lines indicate the times of table contact and take-off respectively.

3.5 Chapter Summary

Performance data were collected from an elite level gymnast using a Vicon optoelectronic motion capture system. A chain model was shown to be suitable for determining the kinematics of the gymnast and the vaulting table during the contact phase of the vault. Kinematic data were obtained and the results presented.

Chapter 4

Simulation Model Development

4.1 Chapter Overview

Angle-driven and torque-driven computer simulation models of vaulting were developed. The models comprised a gymnast and a vaulting table and simulated the interaction between these two bodies during the table contact phase of the vault. This chapter describes how the models were formulated and details specific features of the models.

4.2 Gymnast Representation

The gymnast was modelled in planar form using seven rigid segments to represent the fingers, the palms, the arms, the head + upper trunk, the lower trunk, the thighs and the shanks (Figure 4.1). Each of the rigid segments had mass, length and moment of inertia, such that they represented the body segments of the gymnast. The motions of the left and right limbs were considered to be symmetrical during the table contact phase and therefore the inertial properties of these segments represent the combined limbs. Details of the inertial parameter determination are given in Section 5.4. The following features were used within the gymnast model and are shown in Figure 4.1:

- The trunk angle (angle between the upper and lower trunk segments) was modelled as a function of the hip angle (as detailed in Section 3.3.2.1).
- A damped linear spring was used to represent shoulder retraction and protraction.
- Displacement of the glenohumeral joint centre was modelled as a function of the shoulder angle (as detailed in Section 3.3.2.2).
- A damped torsional spring was used to represent flexion/extension of the fingers.

The orientation of the gymnast was defined by the angle of the upper trunk to the vertical (θ_{OR}) while the joint angles were defined as shown in Figure 4.1.

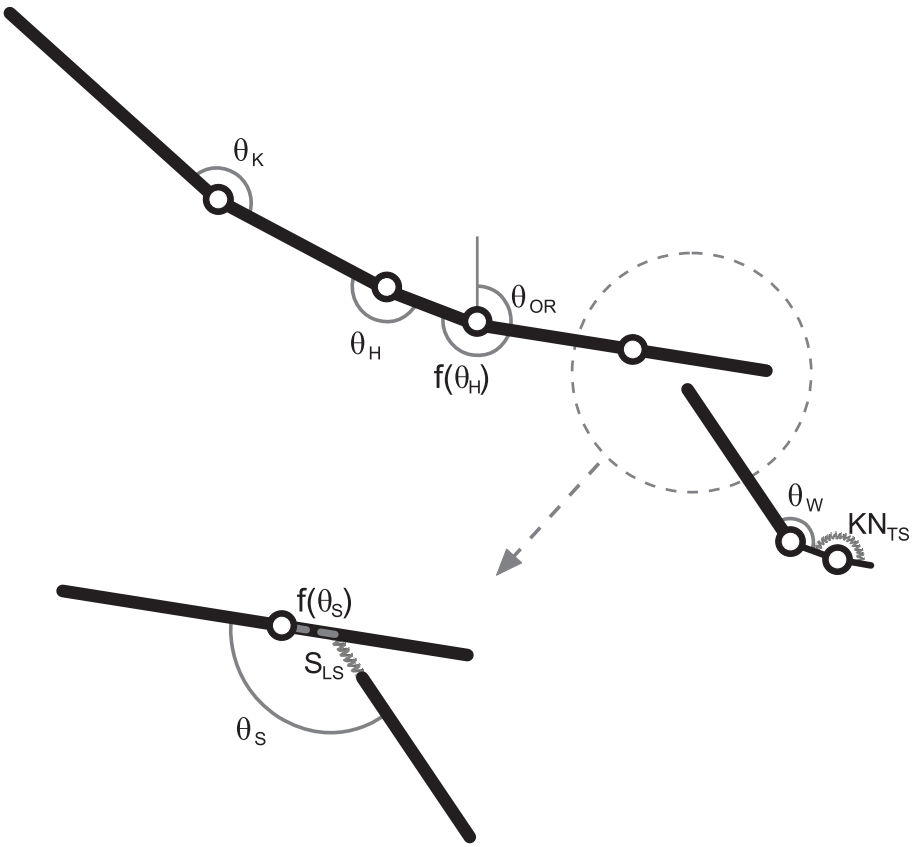

Figure 4.1. Gymnast representation in simulation models. Joint/orientation angles: knee angle θ_K, hip angle θ_H, shoulder angle θ_S, wrist angle θ_W and orientation angle θ_{OR}. Constraints: trunk angle $f(\theta_H)$ and glenohumeral position $f(\theta_S)$. Viscoelastic elements: knuckle torsional spring-damper KN_{TS} and shoulder spring-damper S_{LS}.

The gymnast representation described above was used within angle-driven and torque-driven simulation models of vaulting. Details of the specifics of these models are given in Section 4.5 and Section 4.6 respectively. Within both simulation models the gymnast interacted with a model of the vaulting table. Details of the vaulting table representation and of the interaction between the gymnast and the vaulting table are given below.

4.3 Table Representation

The table was modelled as a single rigid body with mass, dimensions and moment of inertia such that it was representative of the vaulting table. Details of the table inertial parameter determination are given in Section 5.5. The following features were used within the table model and are shown in Figure 4.2:

- The contact surface, which was represented by a plane, was defined relative to the table, based on the position that the gymnast initially contacted the vaulting table.
- A damped torsional spring allowed the table to rotate about the centre of rotation.

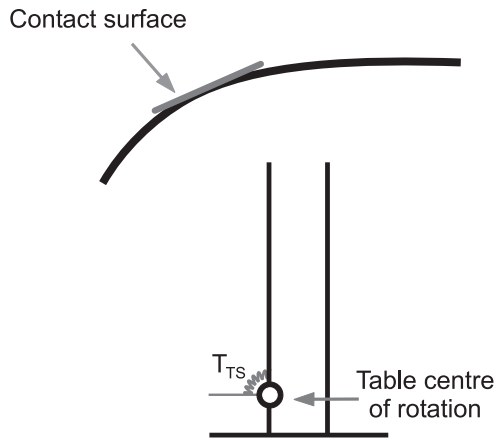

Figure 4.2. Table representation in simulation models. Viscoelastic element: table torsional spring-damper T_{TS}.

The torque produced by the torsional spring was a function of the angular displacement θ_T and angular velocity $\dot{\theta_T}$ of the table:

$$T_{TS} = -K_{\mathrm{TT}_1}\,\theta_T - K_{\mathrm{TT}_2}\,\theta_T|\theta_T| - D_{\mathrm{TT}}\,\dot{\theta_T}\,|\theta_T| \tag{4.1}$$

where T_{TS} is the torque, K_{TT_1} and K_{TT_2} are stiffness coefficients and D_{TT} is the damping coefficient. The two stiffness coefficients allowed for non-linear stiffness of the spring. The sign of the second stiffness term was dependent on the direction of the angular displacement, such that the two stiffness terms were always additive. The damping term was multiplied by the magnitude of the angular displacement, such that damping increased with displacement.

4.4 Interaction Between the Gymnast and the Table

Reaction forces between the gymnast and the vaulting table arise during the contact phase of the vault. These reaction forces and can be separated into components normal to and tangential to the table surface.

Analysis of the high speed video indicated that the gymnast's hands deformed the surface of the vaulting table in the normal direction as shown in Figure 4.3. To model the motion of the hands and compression of the table, the normal contact force was represented by spring-dampers situated at the three points of contact, the fingertip, the knuckle and the base of the palm:

$$R_{ni} = -K_{\mathrm{CS}}\,n_i - D_{\mathrm{CS}}\,\dot{n}_i\,|n_i| \quad (\text{for } i = 1, 3) \tag{4.2}$$

where R_{ni} is the normal force, n_i is the displacement in the direction normal to the contact surface, $\dot{n}_i$ is the first derivative of n_i, K_{CS} and D_{CS} are the stiffness and damping

coefficients of the table surface respectively and i represents the three points of contact on the hand. Since the gymnast's hands approach the table with a non-zero velocity the damping was a function of the displacement of the hands to avoid force discontinuities.

Analysis of the high speed video indicated that when the gymnast contacts the vaulting table the hands initially slide tangentially along the surface, pause in a stationary position and then slide again in the tangential direction before take-off as shown in Figure 4.3. The force acting on the hands in the tangential direction is friction. When there is relative motion between the hands and the table (sliding) the force is known as dynamic friction, whereas if the hands are at rest relative to the table the force is known as static friction, a state which is referred to as stiction.

Coulomb friction, which is commonly used to model frictional forces, uses separate models for the sliding and stiction phases. The use of two separate models is difficult to implement, and therefore numerous authors have advocated the use of pseudo-Coulomb friction models to simulate human/ground interactions (Wojtyra, 2003; McLean et al., 2003; Neptune et al., 2000). A pseudo-Coulomb model is an approximation of Coulomb friction, in that instead of the stiction phase, sliding continues but with a small velocity. This representation of frictional forces has a number of shortcomings (Bauchau and Ju, 2006). Primarily it alters the physical behaviour of the system as it does not allow stiction to occur.

To allow for both sliding and stiction within the model, and the associated change in the number of degrees of freedom, a two-state contact model was developed. Details of this contact model are given below.

When the gymnast is in contact with the table, and the hands are moving relative to the table in the tangential direction, the frictional force is modelled as dynamic friction:

$$R_{ti} = \mu\, R_{ni} \quad (\text{for } i = 1, 3) \tag{4.3}$$

where R_{ti} is the tangential force acting on the hands, μ is the coefficient of friction, R_{ni} is the normal force acting on the hands at a given contact point and i again represents the three points of contact on the hand. The tangential force acts in the opposite direction to the relative velocity of the hands.

When the relative velocity goes to zero a constraint is added, such that there is no relative velocity in the tangential direction. During this phase, the force required to keep the

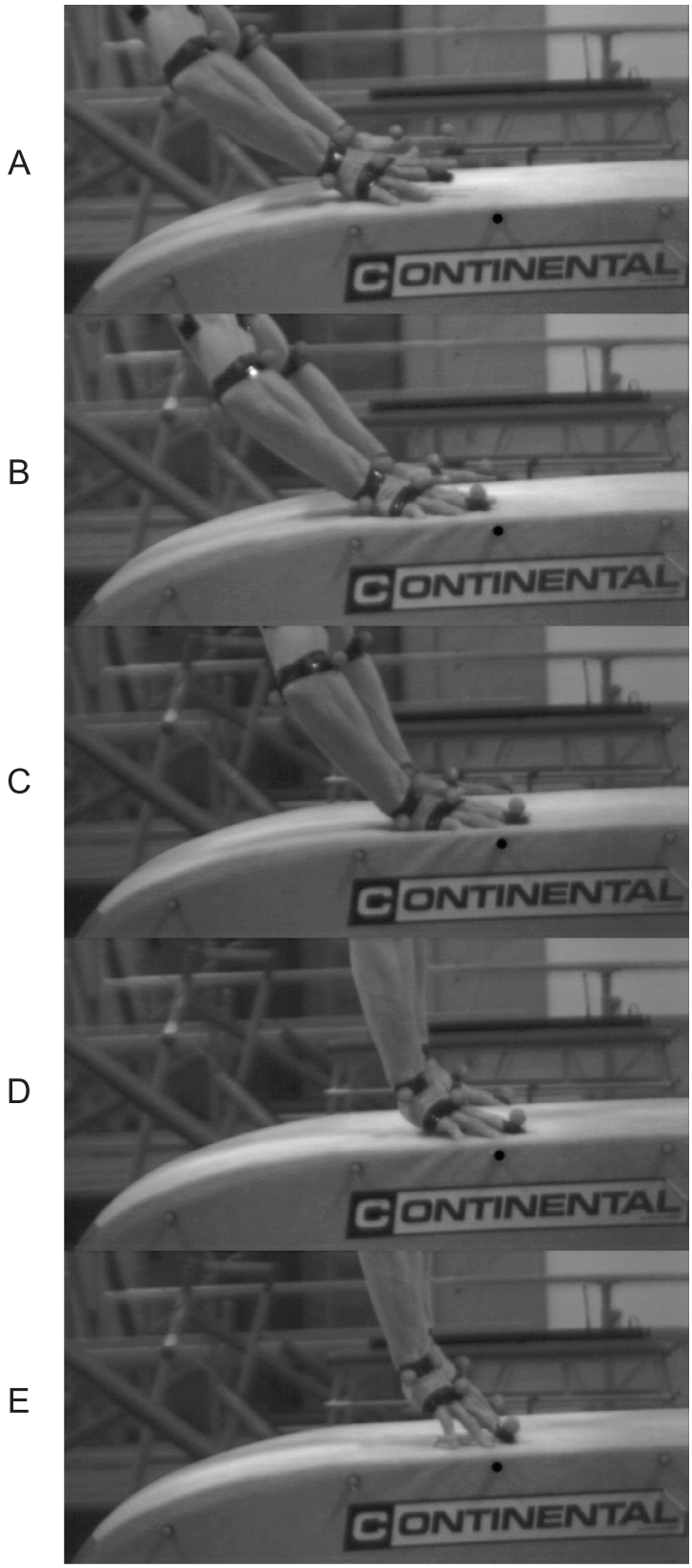

Figure 4.3. Table contact phase. Note the position of the marker on the finger relative to the marker on the table (indicated in black). A - contact, B - hands sliding forwards, C - stiction of hands, maximum depression of contact surface, D - loss of palm contact, E - finger sliding backwards

hands stationary, known as the auxiliary force, is determined. When the auxiliary force becomes greater than the limiting frictional force, the constraint is removed and the hands once again slide.

Figure 4.4 shows the structure of the contact model. Switching from sliding to stiction is governed by the tangential velocity of the fingers, whilst switching from stiction to sliding is governed by the limiting friction. When the total normal force acting on the hands goes to zero the gymnast leaves the table and begins the post-flight phase.

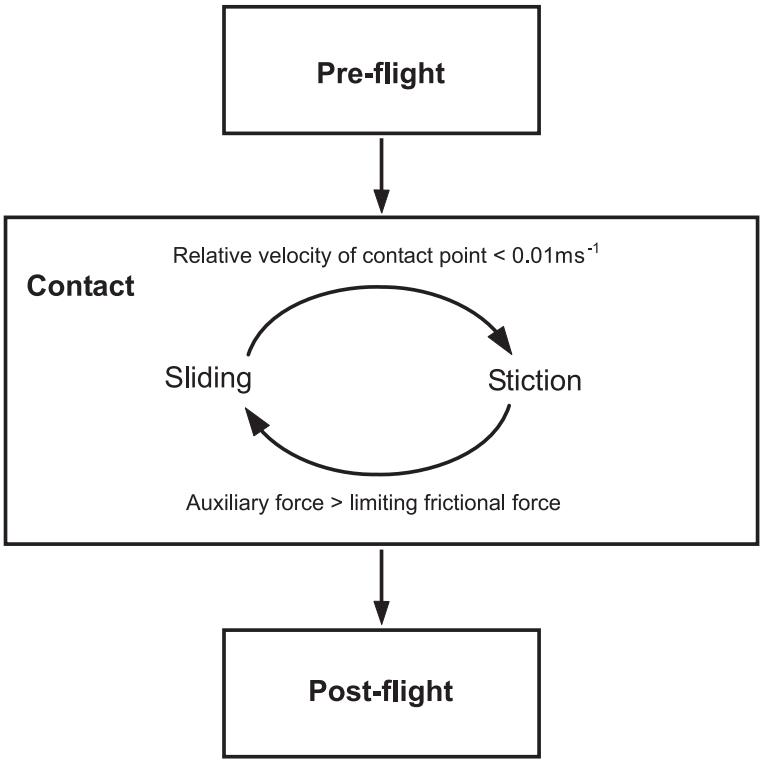

Figure 4.4. Structure of the sliding / stiction procedure.

4.5 Angle-Driven Simulation Model

The gymnast, table and contact phase representations previously described, were used within a gymnast-specific angle-driven simulation model. The model was driven with joint angle time histories obtained from recorded performances, and hence the technique was very close to that actually used. Thus the angle-driven model was well suited to determining model parameters that could not be measured directly.

The angle-driven model was used with known initial conditions and joint angle time histories to determine the viscoelastic parameters of the shoulder, knuckle, contact surface and table springs and also the coefficient of friction between the gymnast's hands and

the contact surface. The inputs to the angle-driven model were the initial conditions just prior to table contact, including the horizontal and vertical positions and velocities of the gymnast's centre of mass (COM), and the orientation and angular velocity of the head + upper trunk segment. Throughout the simulation the movement of the gymnast was driven by joint angle time histories obtained from the kinematic motion analysis (Section 3.3). The output of the model included time histories of the orientation and angular velocity of the head + upper trunk segment, the gymnast's COM velocities, displacements of the hand and shoulder, and angular displacements of the table. The model parameters were determined using an optimisation routine that minimised the difference between simulations and recorded performances as detailed in Chapter 6.

4.6 Torque-Driven Simulation Model

Within a torque-driven model, the technique is determined by torques produced at the joints, thus torque-driven models are well suited to understanding the mechanics of a movement. A gymnast-specific torque-driven simulation model was developed using the gymnast, table and contact phase representations previously described in order to gain an understanding of the mechanics of the contact phase of vaulting. Extensor and flexor torque generators acted at the wrist, shoulder, hip and knee joints as shown in Figure 4.5. Details of the structure of the torque generators are given in Section 4.6.1.

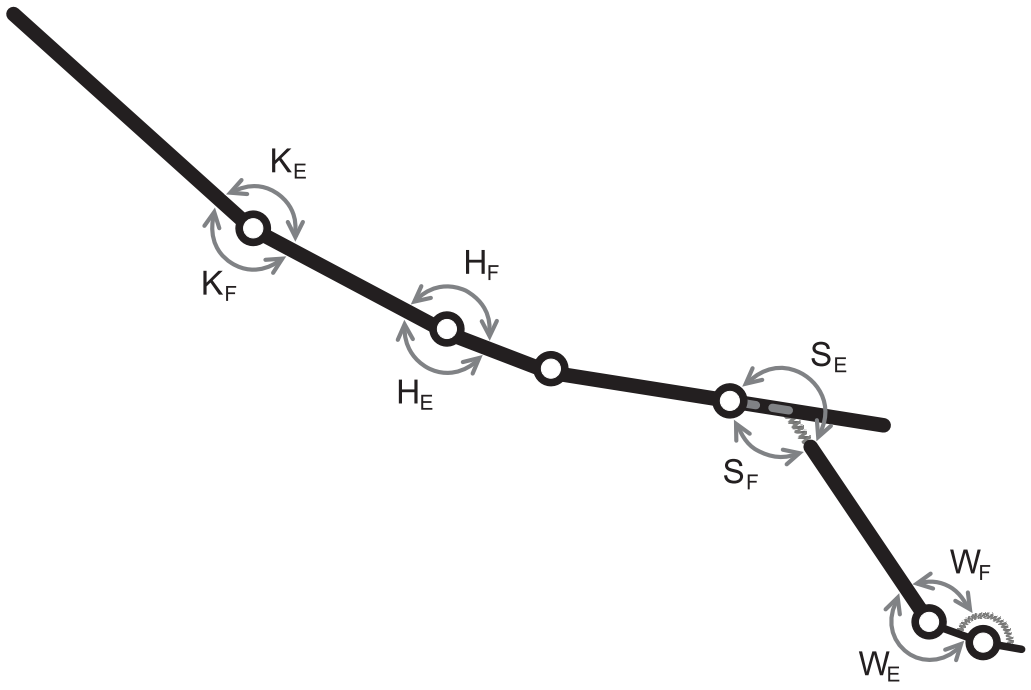

Figure 4.5. Torque-driven gymnast representation. Nomenclature: W wrist, S shoulder, H hip, K knee, F flexor torque generator and E extensor torque generator.

In addition to the active torque generators, passive torque elements were included at the wrist, shoulder and hip joints. The passive torque elements produced restorative torques at the extremes of the joints range of motion. Passive torques are produced by the presence and deformation of the tendons, ligaments, inactive muscle, skin, joint capsules and bones that make up a joint (Hatze, 1997; Esteki and Mansour, 1996), and are independent of muscle activation (Anderson et al., 2007). The passive torque elements were determined by flexibility testing of the gymnast as detailed in Section 5.3.

The torque-driven model used known initial conditions, and was driven with activation profiles that specified the level of activation of each of the torque generators. Details of the activation profiles are given below in Section 4.6.2. The initial conditions were specified just prior to table contact and included the horizontal and vertical positions and velocities of the gymnast's COM, the angular velocity of the head + upper trunk segment and the configuration of the gymnast. Throughout the simulation the movement of the gymnast was driven by the activation levels of the torque generators. The output of the model included time histories of the gymnast's COM velocities, orientation and joint angle time histories, and the whole-body angular momentum at take-off.

4.6.1 Torque Generators

Each torque generator was modelled as a muscle-tendon complex with a contractile component (CON) to represent the properties of the muscle, and a series elastic component (SEC) to represent the properties of the tendon and aponeurosis. Figure 4.6 is a representation of the muscle-tendon complex where θ is the joint angle, θ_{CON} is the contractile component angle and θ_{SEC} is the series elastic component angle. Case 1 represents knee and hip extension and shoulder and wrist flexion, while Case 2 represents knee and hip flexion and shoulder and wrist extension.

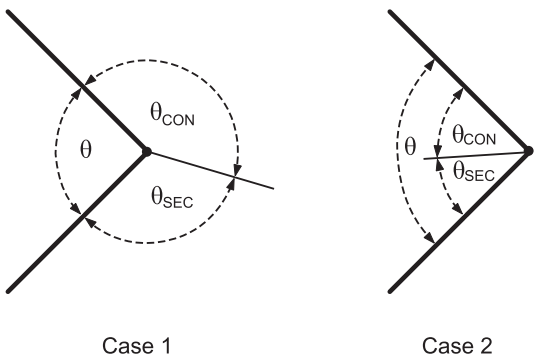

Figure 4.6. The muscle-tendon complex consisting of a contractile component and a series elastic component.

The relationships between joint angle, contractile component angle and series elastic component angle are:

$$\text{Case 1:} \quad \theta = \theta_{CON} + \theta_{SEC} \tag{4.4}$$

$$\text{Case 2:} \quad \theta = 2\pi - \theta_{CON} - \theta_{SEC} \tag{4.5}$$

As the components are in series, the series elastic component torque T_{SEC} is equal to the torque produced by the contractile component T_{CON}. The torque production properties of the contractile component depend on the contractile component angle and angular velocity, and were determined by strength measurements of the gymnast as detailed in Section 5.2. Thus to drive the model using torque generators, the contractile component angle and angular velocity for each torque generator need to be determined at each time step. This process is described below.

At the beginning of the simulation (time = 0) it was assumed that the contractile component angular velocity $\dot{\theta}_{CON}$ was equal to that of the joint ($\dot{\theta}$). An iteration was performed to determine the value of θ_{CON} for which T_{CON} was equal to T_{SEC}, using Equations 4.4 and 4.5 and the relationship between series elastic component stiffness k_{SEC} (as determined in Section 5.2.2.4) and torque T_{SEC}:

$$T_{SEC} = k_{SEC}\, \theta_{SEC} \tag{4.6}$$

In subsequent time steps, θ_{CON} was defined by assuming constant velocity:

$$\theta_{CON_{new}} = \theta_{CON} + \dot{\theta}_{CON}\, dt \tag{4.7}$$

θ_{SEC} was then determined using Equations 4.4 and 4.5, and subsequently T_{SEC} was determined using Equation 4.6. Finally, T_{CON} was equated to T_{SEC} to determine $\dot{\theta}_{CON}$.

4.6.2 Activation Profiles

The torque generators used within the torque-driven model represent the maximal voluntary torque that the gymnast can produce. To determine the applied torque this maximal torque was multiplied by a muscle activation level:

$$Tq(t) = A(t)\; Tq_{\text{max. voluntary}} \tag{4.8}$$

where $Tq(t)$ is the torque at time t, $A(t)$ is the muscle activation level at time t, and $Tq_{\text{max. voluntary}}$ is the maximal voluntary torque.

When the muscle was relaxed, the activation level was 0.0, whereas when the muscle was fully activated the activation level was 1.0. A quintic function, which has zero velocity and acceleration at the end points (Yeadon and Hiley, 2000), was used to ramp up / down the activation level:

$$A(t) = a_i + (a_f - a_i)\left(\frac{t - t_i}{t_f - t_i}\right)^3 \left(6\left(\frac{t - t_i}{t_f - t_i}\right)^2 - 15\left(\frac{t - t_i}{t_f - t_i}\right) + 10\right) \tag{4.9}$$

where $A(t)$ is the activation level at time t, a_i is the initial activation level at time t_i and a_f is the final activation level at time t_f. This function was chosen as it resulted in a smooth activation profile.

An example of an activation profile, representing a torque generator ramping up and down during a simulation, is given in Figure 4.7. Some torque generators had this profile while others ramped down and then up during a simulation. Seven parameters were required to define the curve as listed in Table 4.1.

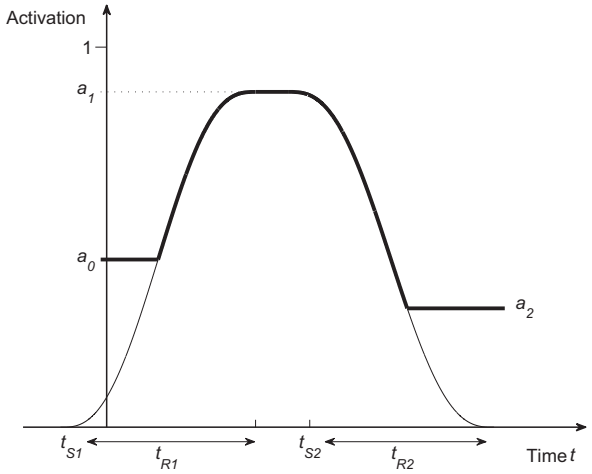

Figure 4.7. Example of a torque generator activation profile (bold line indicates the activation profile).

Table 4.1. Parameters defining activation profile

Parameter	Definition
a_0	Pre-impact activation level
a_1	Maximal / minimal activation level
a_2	Final activation level
t_{S1}	Start time of first ramp
t_{R1}	Ramp time of first ramp
t_{S2}	Start time of second ramp
t_{R2}	Ramp time of second ramp

4.7 Equations of Motion

To formulate the equations of motion for both the angle-driven and the torque-driven models, the Autolev^{TM} software package (Version 3.4) was used. Autolev^{TM} makes use of Kane's method to derive the equations of motion. Kane's method is based on determining partial velocity and partial angular velocity vectors, which are then used to determine generalised active and inertia forces, from which the dynamic equations of motion of the system are defined (Yamaguchi, 2006).

In order for Autolev^{TM} to produce the equations of motion, the user must generate a command file in which:

- The relative positions and orientations of each segment within the system are defined.
- The internal and external forces acting on the system are expressed.

Autolev^{TM} command files were generated in this way for the angle-driven and torque-driven models (Appendix C). When run, the command files produced Fortran programs, which made use of a Kutta-Merson numerical integration algorithm to determine the solution to the equations of motion. The Fortran programs were customised to allow for the different phases of the vault as explained in Section 4.4, and to incorporate the torque generators as explained in Section 4.6.1 and Section 4.6.2.

4.8 Chapter Summary

Planar angle-driven and torque-driven simulation models of a gymnast vaulting were developed using Autolev^{TM}. The models simulate the interaction between a multi-segment gymnast and the vaulting table during the contact phase of the vault. The models utilize a two-state contact phase representation to allow the gymnast's hands to slide tangentially to and/or remain stationary relative to the table surface, during the table contact phase. The models also allow for movement within the shoulder joint, deformation of the vaulting table surface and slight rotation of the vaulting table.

Chapter 5

Parameter Determination

5.1 Chapter Overview

In this section an explanation of the protocol for determining gymnast-specific parameters is given. These parameters, such as strength, flexibility and segmental inertias are required as inputs to both the angle-driven and the torque-driven simulation models described in Chapter 4. The use of gymnast-specific strength and flexibility parameters ensures that the models do not produce movements that exceed the capabilities of the gymnast, while determination of the segmental inertia parameters ensures that the relative size of the model segments accurately represents the gymnast. An explanation of the methods used to determine the inertial parameters of the vaulting table is also given.

5.2 Strength Parameters

Gymnast-specific strength parameters for the knee, hip, shoulder and wrist joints were determined from maximum voluntary joint torque measurements obtained on an isovelocity dynamometer. An explanation of the protocol used to collect, process and analyse the joint torque data is given below.

5.2.1 Joint Torque Measurement Protocol

A Con-trex multi-joint isovelocity dynamometer (CMV AG, Switzerland) was used to measure maximal isometric and isovelocity joint torques. The movements considered were flexion and extension of the knee, hip, shoulder and wrist. Bilateral symmetry was assumed and therefore measurements were only taken from one side of the body.

The dynamometer set-ups for the knee, hip, shoulder and wrist joints are shown in Figure 5.1, Figure 5.2, Figure 5.3, and Figure 5.4 respectively. The gymnast sat/lay on the dynamometer and the crank arm position was adjusted so that the gymnast's joint centre was aligned with the centre of rotation of the crank, and the axis of rotation of

the joint coincided with the axis of rotation of the crank. The gymnast was then firmly strapped to the dynamometer.

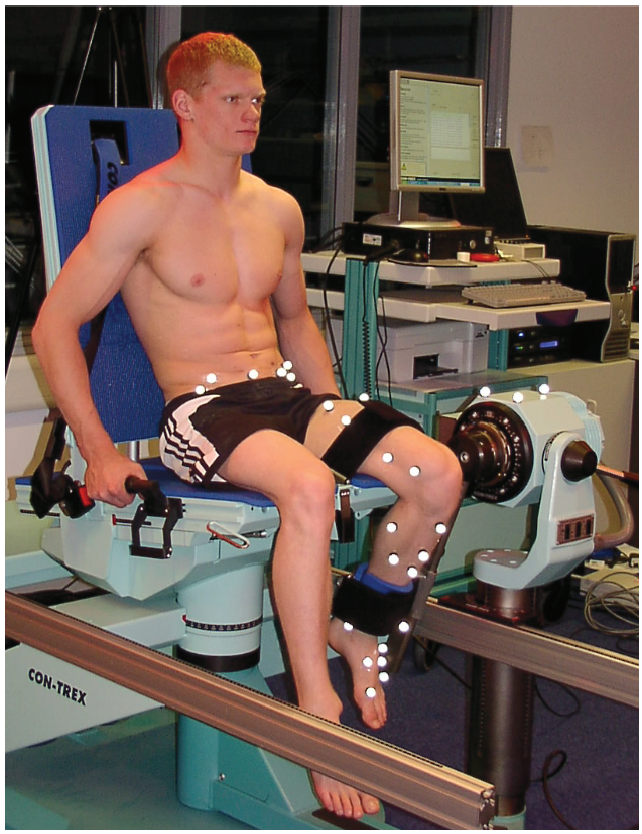

Figure 5.1. Dynamometer set-up to obtain knee torque measurements.

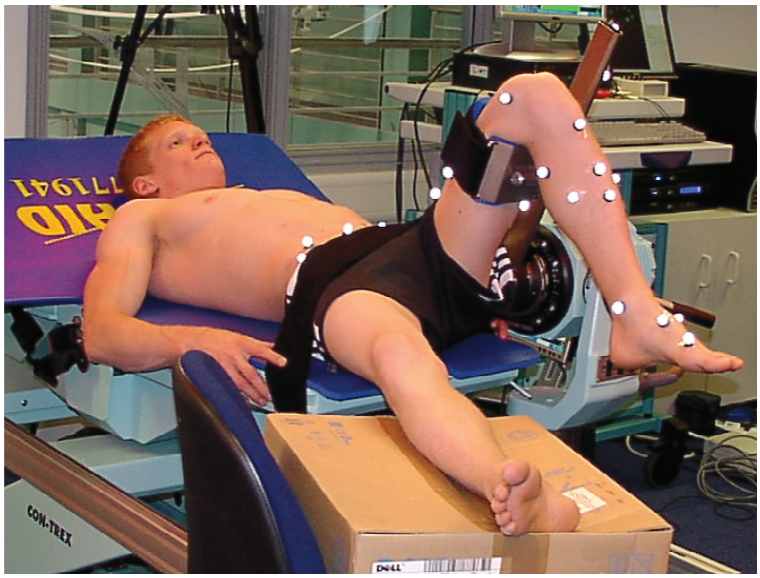

Figure 5.2. Dynamometer set-up to obtain hip torque measurements.

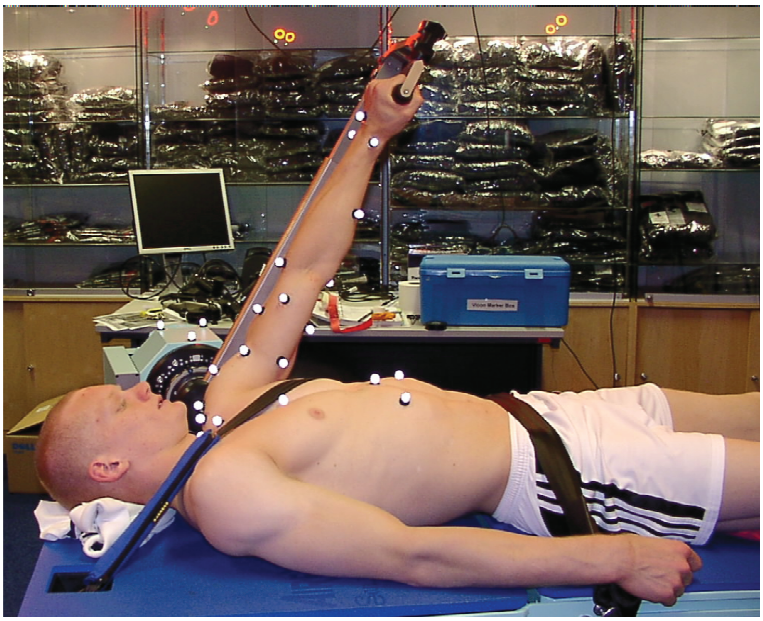

Figure 5.3. Dynamometer set-up to obtain shoulder torque measurements.

Figure 5.4. Dynamometer set-up to obtain wrist torque measurements.

Dynamometer data of torque, crank angle and crank angular velocity were collected at a sampling rate of 512 Hz. Nine Vicon cameras (MX13), sampling at a frequency of 500 Hz, were also used to track the position of markers attached to the gymnast and the isovelocity dynamometer during the trials. The Vicon data were used to determine the joint angle throughout the trials as there is inaccuracy in assuming the dynamometer crank angle and the joint angle are the same (Herzog, 1988; Deslandes et al., 2008). The dynamometer outputs (torque, crank angle and crank angular velocity) were also

collected as analogue signals in the Vicon system so that the two data sets could be synchronised.

The following procedure was followed for each joint movement. Following a short warm-up, joint torques were measured during maximal isometric contractions, at seven to twelve joint angles covering the range of motion that the gymnast felt comfortable producing joint torques over. Due to the large range of motion at the shoulder, the range of motion for this joint was limited to that expected in vaulting performances (joint angles between 60° and 180°). Joint torques were also measured during isovelocity trials, conducted at five angular velocities from $30^\circ\,s^{-1}$ to a maximum of $400^\circ\,s^{-1}$. The isovelocity trials consisted of a number of repetitions of an eccentric - concentric cycle, where the repetition is used to provide the pre-activation necessary to ensure the middle contractions were maximal (King and Yeadon, 2002).

For each joint movement a calibration trial was also carried out, during which the subject was asked to relax while the crank arm was moved through the range of motion. The torque measured during this trial is the passive torque due to gravity (weight of the system and the limb) and also due to passive elements (tendons and ligaments). The Contrex dynamometer software removed the passive torque component from the measured torque during each isometric and isovelocity trial, so that the resulting torque was the active torque exerted by the gymnast.

In addition to the joint torque trials, other trials were also recorded using the Vicon system. These included static and dynamic calibration trials, for use in determining the joint kinematics, and maximum joint velocity measurements. The static calibration trial was conducted with the gymnast in the anatomical position, while the dynamic calibration trials were conducted to determine the centres of rotation of the hip and shoulder, and involved flexion-extension/abduction-adduction combined movements from the anatomical position in line with the recommendation of Camomilla et al. (2006). Details of the methods used to determine the joint centres are given in Section 3.3.3. The maximum joint velocity measurements were taken from trials in which the gymnast was asked to flex and extend each joint as quickly as possible, with flexion and extension being two separate measurements.

5.2.2 Data Processing

5.2.2.1 Determination of Joint Angle

The marker position data collected using the Vicon system were used in conjunction with simple chain models to determine the kinematics of the gymnast. The chain models were applied to the isometric and isovelocity trials, and also the maximum joint velocity trials, to determine the angles and angular velocities of the joint being considered. The definition of the gymnast model (degrees of freedom, parameters and constraints) was the same as that in the chain model of vaulting (Section 3.3) to ensure consistency.

5.2.2.2 Synchronisation of Dynamometer and Kinematic Data

The kinematic data and the analogue torque signal, collected using the Vicon system, were synchronised. However the analogue torque was measured in volts. To determine the corresponding joint torques, the analogue torque signal and the dynamometer torque were synchronised as outlined below.

As the dynamometer and kinematic data both contained noise a residual analysis was performed, as described by Winter (1990), to determine an appropriate cut-off frequency for filtering the data. The data were subsequently smoothed using an 8 Hz, 4^{th} order, zero lag, low pass Butterworth filter. As the Vicon system sampled at a different frequency to the dynamometer (500 Hz compared to 512 Hz) the kinematic data and analogue torque data were interpolated to obtain data points every 1/512 seconds. To determine the common point in time a Matlab function, which determined the correlation between the analogue torque signal and the dynamometer torque for different time offsets, was written. The synchronisation offset was identified as the offset for which the correlation between the analogue torque signal and the dynamometer torque was maximum. Output files with synchronised joint torque, joint angle and joint angular velocity were then written.

5.2.2.3 Determination of Isometric and Isovelocity Data

For each isometric trial the maximum torque and corresponding joint angle were determined. For the isovelocity trials, the isovelocity periods were identified, and the single maximal eccentric and concentric periods selected, as outlined below.

It was assumed that when the crank had constant velocity the joint also had constant

velocity. Although this assumption may introduce some error, the torques associated with joint accelerations are minimal compared to the active torques being exerted (Lewis, 2009, personal communication), and therefore the assumption is reasonable. Thus the isovelocity periods of the trial correspond to the sections in which the crank angular velocity is constant, that can be seen as the flat sections in Figure 5.5, which is an example of the data obtained during an isovelocity knee extension trial. The corresponding torque throughout each isovelocity period was averaged, and the single maximal eccentric period and single maximal concentric period were identified. The torques during these periods were then interpolated to give torque values at 1° intervals.

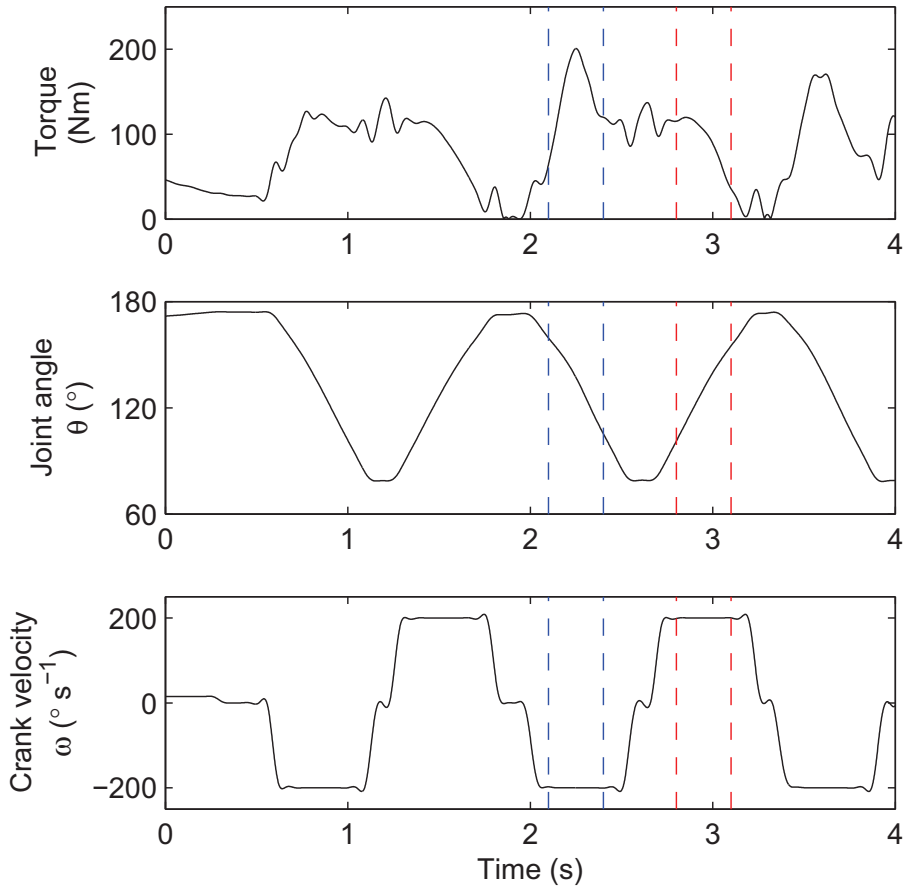

Figure 5.5. Experimental data from a single knee extension isovelocity trial showing torque, joint angle and crank angular velocity. The regions between the dashed lines are the selected maximal eccentric (blue lines) and concentric (red lines) contractions.

5.2.2.4 Converting Joint Angle to Contractile Component Angle

The joint torque measurement trials determined the maximum voluntary torque produced at certain joint angles and certain joint angular velocities. For subsequent use in the muscle-tendon complex, as described in Section 4.6.1, it was necessary to convert

the joint angles and angular velocities into contractile component angles and angular velocities. King and Yeadon (2002) found that the joint angular velocity is approximately equal (or opposite and equal) to the contractile component angular velocity during periods of isovelocity, while the joint angle can be related to the contractile component angle as described below.

The torque measured using the dynamometer is the torque generated by the muscles, which are known as the contractile component. As the tendon and aponeurosis, which are known as the elastic component, are in series with the contractile component, the torque in the elastic component is also equal to the measured torque. The series elastic component angle can be determined using Equation 4.6, which relates the torque in the elastic component to the stiffness of the elastic component. The contractile component angle can then be determined based on geometric relationships between joint angle, series elastic component angle and contractile component angle (Equations 4.4 and 4.5). The stiffness of each series elastic component was required to use these equations to transform the data from a joint basis to a contractile component basis.

Determining Series Elastic Component Stiffness

Each joint movement has a corresponding series elastic component stiffness. The stiffness of each series elastic component was estimated based on the properties of the muscle groups contributing to the joint movement. The muscle groups chosen were those with major contributions to the movements: knee extension - rectus femoris, vastus lateralis, vastus intermedius and vastus medialis, knee flexion - biceps femoris, hamstrings and gastrocnemius, hip extension - gluteus maximus and hamstrings, hip flexion - psoas major and rectus femoris, shoulder extension - teres major, latissimus dorsi and posterior deltoid, shoulder flexion - pectoralis major and anterior deltoid, wrist extension - extensor carpi ulnaris, extensor carpi radialis brevis and extensor carpi radialis longus, wrist flexion - flexor carpi radialis and flexor carpi ulnaris.

The geometric relation between the series elastic component length L_{SEC} and the muscle architecture parameters of a muscle group is defined as (Pierrynowski, 1995):

$$L_{SEC} = L_b + L_t - L_f\, cos(\alpha) \tag{5.1}$$

where L_{SEC} is the length of the series elastic component, L_b is the muscle belly length, L_t is the tendon length, L_f is the muscle fibre length and α is the pennation angle. L_{SEC} was calculated for each muscle group based on architectural parameters found in

the literature (Pierrynowski, 1995; Langenderfer et al., 2004; Lieber et al., 1990), scaled to the gymnast where possible.

It was assumed that the series elastic component was stretched by 5% during maximal isometric contractions (Finni and Komi, 2002). The corresponding change in series elastic component angle $\Delta\theta_{SEC}$ was calculated as follows:

$$\Delta\theta_{SEC} = \frac{0.05\, L_{SEC}}{d} \tag{5.2}$$

where d is the moment arm. The moment arms of the selected muscle groups were also based on values in the literature (Jacobs et al., 1996; Duda et al., 1996; Bassett et al., 1990; Loren et al., 1996).

Since the muscles contributing to a joint movement act in parallel, the series elastic stiffness value k_{SEC} of a joint movement was assumed to be the sum of the stiffness values of the contributing muscles for that movement:

$$k_{SEC} = \sum_{i=1}^{n} k_i \tag{5.3}$$

where n is the number of muscles considered and k_i is the stiffness of an individual muscle, which is given by:

$$k_i = \frac{T_i}{(\Delta\theta_{SEC})_i} \tag{5.4}$$

where T_i is the maximum torque generated by an individual muscle and $(\Delta\theta_{SEC})_i$ is the change in θ_{SEC} for an individual muscle.

The maximum torque generated by an individual muscle was calculated by estimating its contribution to the maximum isometric torque of the whole muscle group:

$$T_i = T_{iso}\frac{d_i\, PCSA_i}{\sum_{i=1}^{n}(d_i\, PCSA_i)} \tag{5.5}$$

where T_{iso} is the maximum isometric torque, d_i is the moment arm for an individual muscle, $PCSA_i$ is the physical cross sectional area for an individual muscle and n again is the number of muscles considered.

Equations 5.1 - 5.5 were combined to determine the series elastic stiffness value for each series elastic component. The resulting values are listed in Table 5.1. Details of the architectural parameters and moment arms used, and the contributions from each muscle group are given in Appendix D.

Table 5.1. Calculated series elastic component stiffness values

Joint action	k_{SEC} (Nm rad^{-1})
Knee extension	805
Knee flexion	173
Hip extension	1004
Hip flexion	306
Shoulder extension	1988
Shoulder flexion	1574
Wrist extension	25
Wrist flexion	37

5.2.3 Determination of Joint Torque Parameters

The processed joint torque measurement data gave the maximum voluntary torque produced at certain contractile component angles and certain contractile component angular velocities. To express the torque generated by a particular movement at a joint, as a function of contractile component angle and contractile component angular velocity, such that it could be used within the torque-driven model, torque surfaces were fitted to the data. The torque surfaces were defined based on the relationships between torque and angular velocity, differential activation and angular velocity, and torque and angle as detailed below.

5.2.3.1 Tetanic torque - angular velocity relationship in muscle

Two hyperbolic functions, one for each of the concentric and eccentric phases, were used to express the relationship between tetanic torque (maximum torque at full activation) and contractile component angular velocity (Yeadon et al., 2006). In the concentric phase, the relationship between torque, T, and angular velocity, ω, was represented by a rotational equivalent of the classic hyperbola of Hill (1938):

$$T = \frac{C}{(\omega_c + \omega)} - T_C \quad \text{for } \omega \geq 0 \tag{5.6}$$

where

$$T_C = \frac{T_0\,\omega_C}{\omega_{max}}, \quad C = T_C\,(\omega_{max} + \omega_C)$$

In the eccentric phase the relationship between torque and angular velocity was represented by an inverted rectangular hyperbola:

$$T = \frac{E}{(\omega_E - \omega)} + T_{max} \quad \text{for } \omega < 0 \tag{5.7}$$

where

$$\omega_E = \frac{(T_{max} - T_0)}{k\,T_0} \frac{\omega_{max}\,\omega_C}{(\omega_{max} + \omega_C)}, \quad E = -(T_{max} - T_0)\,\omega_E$$

and k is the ratio of the slopes of the eccentric and concentric phases. k was set at 4.3, the theoretical value predicted by Huxley (1957) in his original model.

Four parameters define the hyperbolas as shown in Figure 5.6: the maximum torque in the eccentric phase T_{max}, the isometric torque T_0, the maximum angular velocity above which torque cannot be produced ω_{max}, and the angular velocity of the vertical asymptote of the concentric hyperbola ω_C.

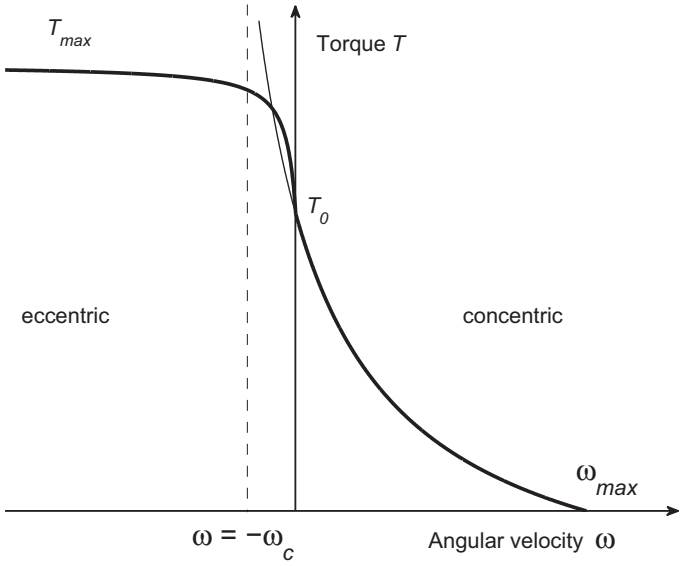

Figure 5.6. The four-parameter tetanic torque / angular velocity function. Parameters: T_{max} - maximum torque in the eccentric phase, T_0 - isometric torque, ω_{max} - maximum angular velocity above which torque cannot be produced, ω_C - angular velocity of the vertical asymptote of the concentric hyperbola.

5.2.3.2 Differential activation - velocity relationship

Due to neural inhibition, full activation is not achieved in voluntary eccentric contractions (Westing et al., 1991). To account for the difference between tetanic torque and maximum voluntary torque, Yeadon et al. (2006) proposed a three parameter differential activation function, in which the activation, rises from a plateau a_{min} in the eccentric region, to a maximum a_{max} in the concentric region. Yeadon et al.'s differential activation function requires the use of the quadratic formula to solve for the activation, which

is cumbersome. Forrester et al. (2010) therefore proposed a similar sigmoid function, in which the activation is directly defined:

$$a = a_{min} + \frac{(a_{max} - a_{min})}{\left[1 + \exp\left(\frac{-(\omega - \omega_1)}{\omega_r}\right)\right]} \tag{5.8}$$

where the maximum activation level, a_{max}, was assumed to be equal to 1.0.

Three parameters define the sigmoid function as shown in Figure 5.7: the low plateau level a_{min}, the midpoint of the curve ω_1 and the effective interval over which the activation increases, which is equal to $10\omega_r$.

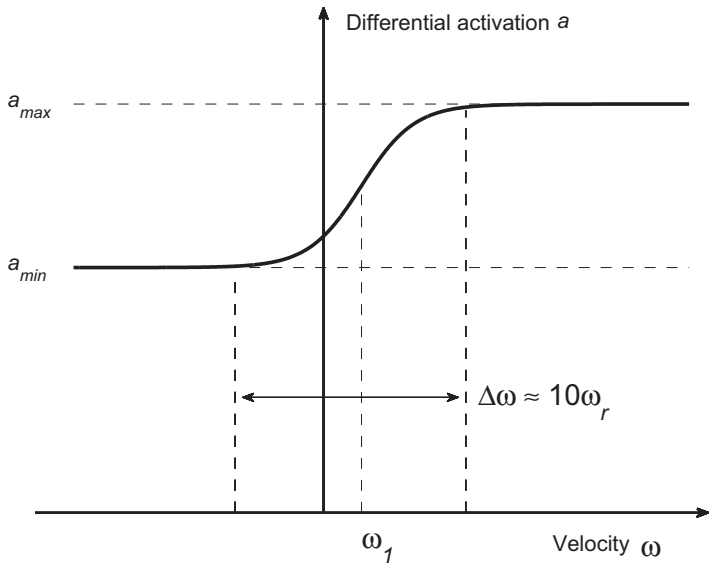

Figure 5.7. The three-parameter differential activation function. Parameters: a_{max} - maximum activation level, assumed to be 1.0, a_{min} - low plateau level, ω_1 - midpoint of the curve, $10\omega_r$ - effective interval over which the activation increases.

5.2.3.3 Torque - angle relationship in muscle

The relationship between torque and contractile component angle was based on a rotational equivalent of the muscle force - length relationship. A bell shaped curve was used to represent the torque - angle relationship (Audu and Davy, 1985):

$$T_a = \exp\left[\frac{-(\theta_{opt} - \theta)^2}{2\,r^2}\right] \tag{5.9}$$

Two parameters define the curve as shown in Figure 5.8: the width r of the curve, and the optimum angle θ_{opt} for torque production.

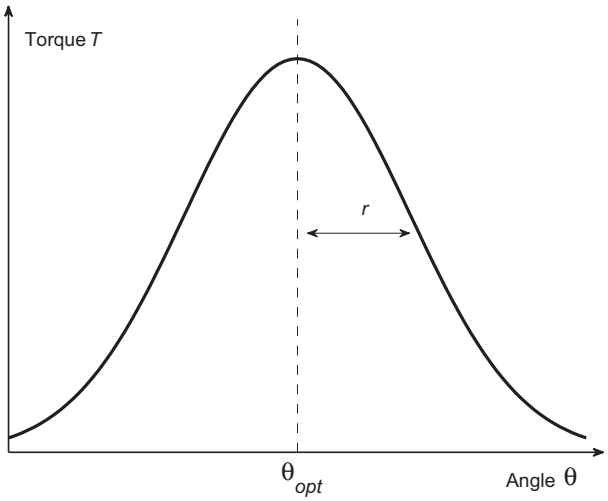

Figure 5.8. The two-parameter torque / angle function. Parameters: r - width of the curve, θ_{opt} - optimum angle for torque production.

5.2.3.4 Torque - angle - angular velocity profiles

Maximum voluntary torque was defined as the product of the tetanic torque - angular velocity, torque - angle and differential activation - angular velocity functions:

$$T = T(\omega)\, T_a(\theta)\, a(\omega) \tag{5.10}$$

This nine parameter function was used to determine a torque profile for each joint movement considered using a simulated annealing algorithm (Corana et al., 1987). The nine parameters were determined by minimising the global difference between the torque profile and the experimental torque data using a weighted root mean square score function (wRMSD). The score function was weighted as the torque data were expected to have one-sided errors due to some submaximal efforts by the gymnast (Forrester et al., 2010) (i.e. the gymnast could achieve anywhere up to their actual maximum but could not exceed it).

The upper and lower limits for each of the nine parameters were estimated from the literature and/or experimental measures and are given in Table 5.2. In particular, the two torque - angle parameters were initially estimated by fitting the torque - angle function (Equation 5.9) to only the isometric data. These two parameters were then allowed only a small amount of variation in the final fit. This method was recommended by Forrester et al. (2010).

Table 5.2. Lower and upper bounds of the nine torque profile parameters

Parameter	Lower Bound	Upper Bound	Source
T_0	0.95 $T_{0,\,expt}$	1.05 $T_{0,\,expt}$	Experimental measure from isometric trials
T_{max}	1.4 T_0		Based on Dudley et al. (1990)
ω_{max}	0.95 $\omega_{max,\,expt}$	1.25 $\omega_{max,\,expt}$	Experimental measure from maximum joint angular velocity trials
ω_C	0.15 ω_{max}	0.5 ω_{max}	Based on literature values (Scovil and Ronsky, 2006)
a_{min}	0.5	0.99	Based on Seger and
ω_r	$0°s^{-1}$	$90°s^{-1}$	Thorstensson (1994) and
ω_1	$-90°s^{-1}$	$90°s^{-1}$	Westing et al. (1991)
r	0.95 $r_{,\,isom\,fit}$	1.05 $r_{,\,isom\,fit}$	Based on values determined
θ_{opt}	0.95 $\theta_{opt,\,isom\,fit}$	1.05 $\theta_{opt,\,isom\,fit}$	during fit to isometric data

The experimentally determined maximum joint angular velocities are given in Table 5.3. The bounds on ω_{max} were set to be 95% and 125% of these values as suggested by Forrester et al. (2010). This is in recognition of possible errors in the kinematic data and the inability of the gymnast to reach a true maximum velocity during the trials.

Table 5.3. Experimentally determined maximum joint angular velocities

	Maximum joint angular velocity ($°s^{-1}$)			
	Knee	Hip	Shoulder	Wrist
Extension	1150	550	740	1870
Flexion	760	440	950	2190

The resultant parameters for each joint are given in Table 5.4. T_{max} and T_0 were doubled within the torque-driven model to represent the combined torque of two limbs.

Table 5.4. Torque - angle - angular velocity profile results

		Knee		Hip		Shoulder		Wrist	
Parameter		Ext	Flex	Ext	Flex	Ext	Flex	Ext	Flex
T_0	(Nm)	301	105	225	168	144	93	16	41
T_{max}	(Nm)	421	147	315	235	202	130	22	57
ω_{max}	$(^\circ s^{-1})$	1101	953	517	526	931	1093	2094	2085
ω_C	$(^\circ s^{-1})$	165	311	126	263	466	545	314	313
a_{min}		0.81	0.80	0.78	0.80	0.75	0.88	0.85	0.82
ω_r	$(^\circ s^{-1})$	5.7	8.6	8.0	7.5	21.8	4.6	5.7	8.0
ω_1	$(^\circ s^{-1})$	-5.7	-7.4	42.4	-5.7	-3.4	-7.4	-8.6	-9.2
r	$(^\circ)$	29.2	63.6	60.7	69.9	104.9	73.9	79.6	98.0
θ_{opt}	$(^\circ)$	234	121	241	138	123	309	91	218
wRMSD	(Nm)	49	17	19	29	29	5	1	8
wRMSD % of T_{max}	(%)	12	12	6	12	14	4	5	14

An example of the nine parameter function fitted to the data obtained for shoulder flexion is presented in Figure 5.9.

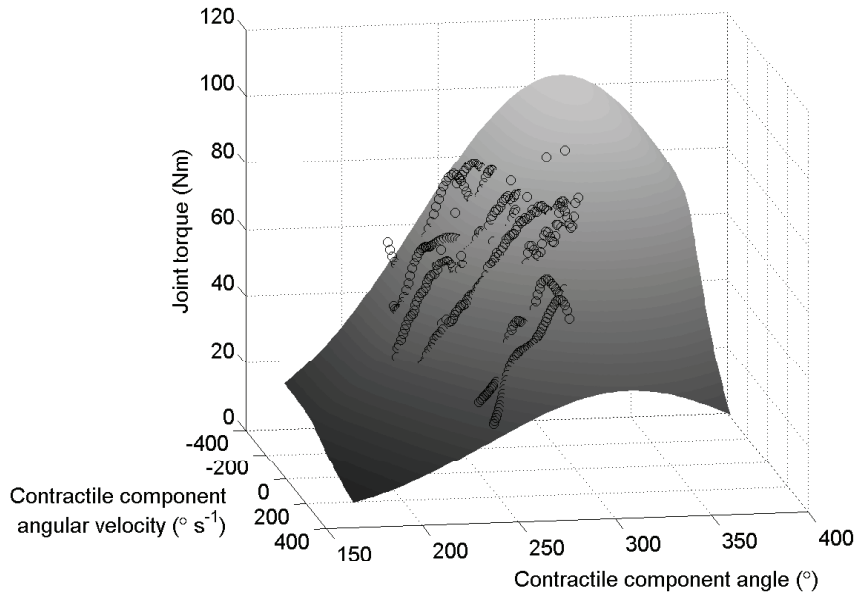

Figure 5.9. Surface fit to torque data for shoulder flexion. The open circles represent the data points.

5.3 Flexibility Parameters

Gymnast-specific flexibility parameters for the shoulder, wrist and hip joints were determined from passive joint torque measurements obtained on an isovelocity dynamometer. An explanation of the protocol used to collect, process and analyse the flexibility data is given below.

5.3.1 Passive Joint Torque Measurement Protocol

The Con-trex multi-joint isovelocity dynamometer, used to measure active joint torques, was also used to measure passive joint torques. Passive joint torque measurements were taken for shoulder flexion, wrist extension and hip extension. These movements were chosen as during vaulting performances the joints may be near the end of the range of motion, in the directions considered. The procedure outlined below was followed for each movement.

The dynamometer was set-up as shown in Figure 5.10 for the shoulder flexibility measurements. The dynamometer set-ups for the hip and wrist joints were the same as those used during strength measurements (Figure 5.2 and Figure 5.4) respectively.

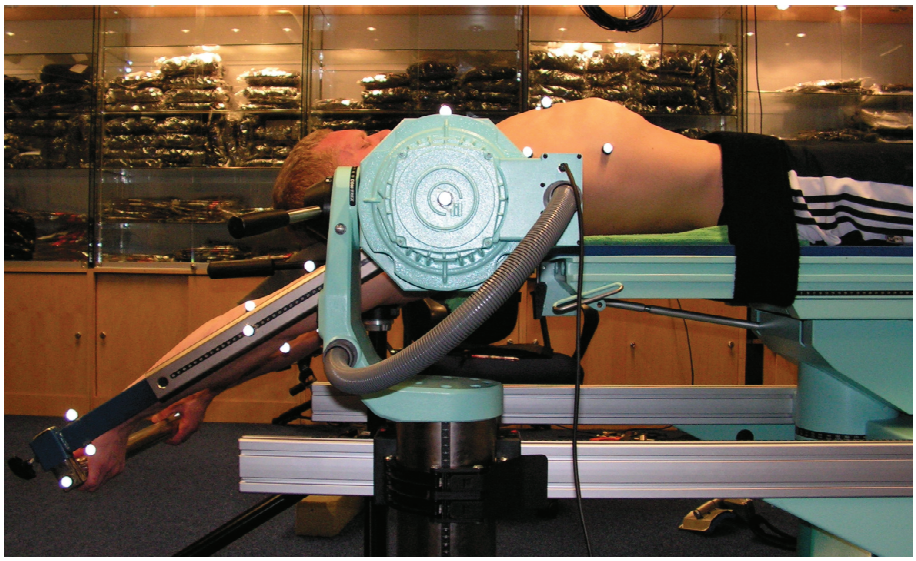

Figure 5.10. Dynamometer set-up to obtain passive shoulder torque measurements.

The following procedure was followed for each joint movement. Following a short warm-up, the flexibility trial was carried out. The gymnast was asked to relax while the crank angle was slowly increased; the gymnast stopped the dynamometer, or released the bar in the case of the shoulder measurement, when the joint reached the end of the full range of motion. A calibration trial was also conducted during which the crank arm

was moved through the full range of motion without the gymnast holding onto it. The torque measured during this trial was the torque due to the weight of the crank arm. The Con-trex dynamometer software removed this torque from the measured torque during each flexibility trial such that the resulting torque was the passive torque. The passive torque, however, included torque due to the weight of the gymnast's limb. This was corrected for in post-processing to determine the passive torque of the joint.

5.3.2 Data Processing

The determination of joint angles and synchronisation of the data were completed as described for the strength trials in Section 5.2.2. The torque due to the mass of the limb(s) was determined, and the torque data were corrected such that the resulting torque was the passive torque of the joint. For the wrist and hip the measured torque was doubled to represent the combined passive torque of both limbs; for the shoulder the dynamometer set-up was such that the measured torque was the combined passive torque of both limbs.

5.3.3 Determination of Passive Torque Parameters

To express the passive torque generated at a joint as a function of joint angle an exponential function was fitted to the data. Passive torque - angle relations are generally approximately exponential and have therefore been modelled using exponential equations (Riener and Edrich, 1999; Esteki and Mansour, 1996). The functions of Riener and Edrich (1999) and Esteki and Mansour (1996) were based on the classical 'double exponential function' proposed by Yoon and Mansour (1982), which takes into account both directions of movement. Within this study, each joint was only tested in one direction and therefore, a single exponential equation of the following form was fitted to the passive torque data:

$$T_{pass} = P_a \, e^{(P_b \, \theta)} \tag{5.11}$$

where T_{pass} is the passive torque, θ is the joint angle and P_a and P_b are parameters which define the shape of the function.

The two parameters were determined to give a least squares solution. The root mean square error (RMSE) between the exponential function and the experimental data was determined for each joint to evaluate the quality of the fit. The passive torque profiles obtained were also compared to literature values where available, and it was found that

the passive torque profile for the hip was in reasonable agreement with that found by Riener and Edrich (1999). The results for each joint are presented Table 5.5, while an example of the exponential function fitted to the data for the wrist is presented in Figure 5.11.

Table 5.5. Passive torque parameters

Parameter		Hip	Shoulder	Wrist
P_a	(Nm)	1.109×10^{-15}	2.219×10^{-8}	1.859×10^{6}
P_b	(-)	10.80	6.315	-6.547
RMSE	(Nm)	3.5	1.0	1.2

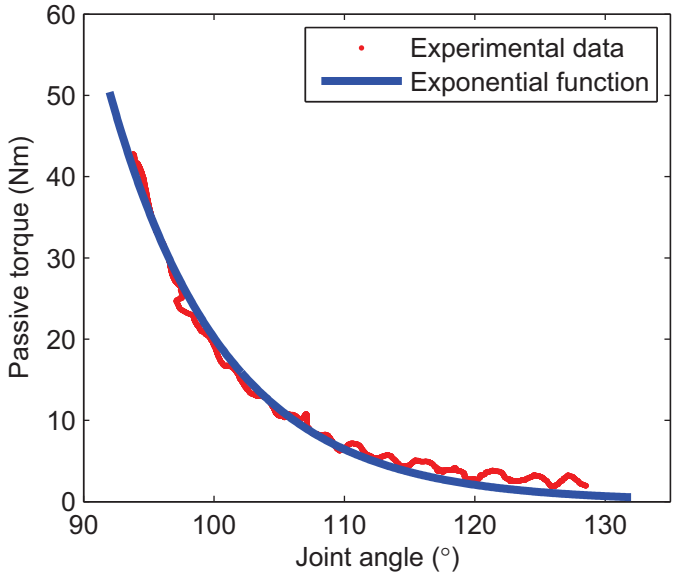

Figure 5.11. Exponential function fit to passive torque data for wrist hyper-extension.

5.4 Gymnast Inertial Parameters

Gymnast-specific segmental inertial parameters were determined from 95 anthropometric measurements using the geometric inertia model of Yeadon (1990a). The inertia model used the segmental density values of Chandler et al. (1975) as initial estimates; these values were subsequently scaled so that there was agreement between the measured mass of the gymnast and the mass determined by the inertia model.

The inertia model of Yeadon (1990a) has 20 segments whereas the simulation models of vaulting require 7 segments, therefore some segments were combined using the Parallel Axis Theorem. The motions of the left and right limbs were considered to be symmetrical

during the table contact phase and therefore, the segmental inertia parameters given in Table 5.6 represent the combined left and right limbs.

Table 5.6. Body segment inertia parameters for gymnast model

Segment	Mass (kg)	Length (m)	CM[1] (m)	Inertia[2] ($kg\,m^2$)
Head-chest-thorax	26.15	0.633	−0.066	0.76518
Pelvis	10.26	0.210	−0.111	0.06878
Arm (layout)[3]	7.44	0.505	0.197	0.13749
Arm (Roche)[3]	7.44	0.522	0.207	0.14752
Hand	0.59	0.087	0.044	0.00064
Fingers	0.41	0.103	0.044	0.00050
Thigh	16.68	0.404	0.171	0.23893
Shank-foot	8.37	0.602	0.229	0.20983

1 CM - For the limbs, distance of the segment's mass centre from the proximal joint centre; for the head-chest-thorax, distance of the segment's mass centre from the chest-thorax joint centre; for the pelvis, distance of the segment's mass centre from the thorax-pelvis joint centre.

2 Inertia - moment of inertia about the transverse axis through the segment mass centre.

3 Values adjusted to represent straight arm.

4 Values given for the limbs represent the combined left and right limbs.

5.5 Table Inertial Parameters

The inertial parameters of the vaulting table were measured, where possible, or estimated as described. The mass of the table was measured using a force plate and the dimensions of the table were measured to check against those given in the specifications (FIG, 2009a). The centre of mass and the inertia of the table were estimated by separating the table into two components: the table-top and the base-frame (Figure 5.12a).

5.5.1 Determination of Table Centre of Mass

The table-top was suspended from a pulley and the plumb line determined. The table-top was then balanced on a beam and the equilibrium line determined. The centre of mass of the table-top was the point of intersection of the plumb line and the equilibrium line (Figure 5.12b).

The base-frame was also balanced on a beam and the equilibrium line determined. The centre of mass of the base-frame was the point of intersection of the equilibrium line and the vertical line of symmetry (Figure 5.12c).

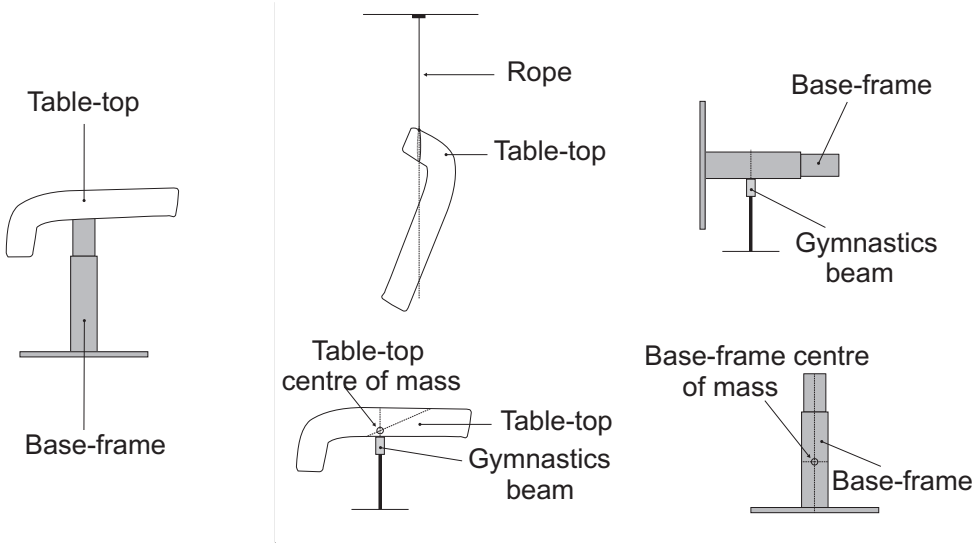

Figure 5.12. Determining centre of mass of vaulting table.

The masses of the table-top and the base-frame were each measured separately using a force plate. The method of moments was used to determine the combined centre of mass of the table, based on the relative masses and centre of mass positions of the two components.

5.5.2 Determination of Table Moment of Inertia

The moment of inertia of the table was estimated by approximating the two components as a number of cylindrical and cuboidal sections. The moments of inertia of each of these sections were determined using known relations between dimensions and inertia. Finally the parallel axis theorem was used to determine to combined moment of inertia of the whole table.

5.6 Chapter Summary

The strength and flexibility of the gymnast were determined from measurements obtained on an isovelocity dynamometer. Maximum voluntary joint torque and passive torque profiles were fitted to the data to determine the gymnast-specific strength and

flexibility parameters. The inertial parameters of the gymnast were determined from anthropometric measurements and the inertial parameters of the table were also estimated. These parameters will be used within angle-driven and torque-driven simulation models of vaulting as detailed in Chapter 6.

Chapter 6

Model Evaluation

6.1 Chapter Overview

In this section optimisation algorithms are first reviewed. The method for determining model system parameters using a genetic algorithm together with an angle-driven model of vaulting is then described. The resulting system parameters are subsequently evaluated using independent trials. The method of evaluation of a torque-driven model of vaulting is also described and the results of this evaluation are reported.

6.2 Optimisation Algorithms

Optimisation algorithms will be employed in the determination of model system parameters using an angle-driven model of vaulting, and also in the determination of muscle activation profiles, using a torque-driven model of vaulting. Both of these problems may be considered as 'hard' optimisation problems, which can be defined as those sharing the following characteristics (van Soest and Casius, 2003):

1. The objective function typically has many local optima and is non-smooth or even discontinuous;

2. The objective function is available in implicit form only, and as a result time consuming simulations must be performed for every evaluation of the objective function;

3. Even for relatively simple models, the dimension of the optimisation parameter space cannot be kept very low.

van Soest and Casius (2003) evaluated the performance of four different optimisation algorithms in solving hard problems: downhill simplex, sequential quadratic programming, simulated annealing and genetic. They found that both the simulated annealing algorithm and the genetic algorithm were capable of finding global optima in hard op-

timisation problems. The genetic algorithm was chosen for this work as it was found to converge to an optimal value faster than simulated annealing for problems similar to those posed in this work (Allen, 2009, personal communication).

6.2.1 Genetic Algorithms

A genetic algorithm is a search technique that was "invented to mimic some of the processes observed in natural evolution" such as inheritance, crossover, selection and mutation (Davis, 1991). The purpose of the genetic algorithm is to determine parameter values such that a given problem is solved. The genetic algorithm is linked to the problem by two mechanisms: encoding, where each set of parameter values is represented by a chromosome, and evaluation, where the worth of each chromosome is determined. The general scheme of a genetic algorithm is as follows (Davis, 1991):

1. Generate a random initial population of n chromosomes.
2. Evaluate the fitness of each chromosome in the population.
3. Create new chromosomes by mating the current chromosomes. Chromosomes are selected for mating based on their fitness, with the more fit chromosomes more likely to be selected. During the mating process crossover and mutation are applied; crossover recombines two chromosomes to generate two new chromosomes, while mutation randomly alters a single chromosome to produce a new chromosome.
4. Evaluate the fitness of the new chromosomes.
5. Stop if maximum number of generations is reached; if not return to 3.

Determining an adequate population size, n, is difficult. If the population size is too small the genetic algorithm may not find the best solution to the problem; if the population size is too large the genetic algorithm will take a long time to find the best solution to the problem (Harik et al., 1999). Within the present study a population size of 1000 was chosen as this led to convergence within 48 hours, which was considered to be an acceptable computation time.

6.3 Determination of System Parameters

An angle-driven model was used with joint angle time histories obtained from recorded performances (Section 3.4) to determine the model system parameters. The model sys-

tem parameters included the viscoelastic parameters of the shoulder, knuckle, contact and table springs and the coefficient of friction between the hands and the contact surface. A genetic algorithm (Carroll, 2001) varied the model system parameters in order to minimise an objective function that was based on matching simulations with recorded performances. In order to obtain a robust set of parameters that may be used generally for similar movements, Wilson et al. (2006) found that more than one performance should be used. Hence four vaulting performances were used within this work. Each vault was first matched individually to obtain an initial estimate of the parameter values, and then the four vaults were matched concurrently to determine the final parameter values.

6.3.1 Model Inputs

The inputs for the angle-driven model included the initial conditions just prior to contact with the vaulting table and joint angle time histories throughout the table contact phase (Section 3.4), body segmental inertias (Section 5.4) and the inertial parameters of the vaulting table (Section 5.5). The initial conditions comprised the horizontal and vertical positions and velocities of the centre of mass (COM) of the gymnast and the orientation angle and angular velocity of the head + upper trunk segment. These values were determined just prior to table contact from the kinematic data.

Two handspring forward with salto forward stretched (layout) vaults, L_1 and L_2, and two handspring forward with double salto forward tucked (Roche) vaults, R_1 and R_2, were selected from the vaulting trials. An international Brevet judge assessed and ranked the performances during the data collection; the vaults selected were the best and third best performance of each vault. The initial conditions for the four vaults are shown in Table 6.1.

Table 6.1. Initial conditions of four handspring entry vaults

		Vault			
Initial condition		L_1	L_2	R_1	R_2
Horizontal COM position	(m)	-0.501	-0.606	-0.345	-0.560
Vertical COM position	(m)	1.808	1.765	1.840	1.736
Horizontal COM velocity	($m\,s^{-1}$)	5.20	5.09	5.10	5.27
Vertical COM velocity	($m\,s^{-1}$)	2.80	3.00	2.71	2.95
Orientation angle	($^\circ$)	94.5	96.0	93.1	87.2
Angular velocity	($^\circ\,s^{-1}$)	212	140	286	91

6.3.2 Objective Function

To assess how well the simulations matched the performances each simulation was given a score. The score was composed of nine components: four performance components P_i, and five system components S_i, as listed below:

- P_1 - Difference in orientation angle at take-off (in degrees)
- P_2 - Percentage difference in angular velocity at take-off
- P_3 - Percentage difference in horizontal linear velocity at take-off
- P_4 - Percentage difference in vertical linear velocity at take-off
- S_1 - Root mean square (RMS) difference in the displacement of the shoulders (shoulder retraction and protraction) during contact as a percentage of the maximum displacement of the shoulders during contact
- S_2 - RMS difference in the angular displacement of the table during contact as a percentage of the maximum angular displacement of the table during contact
- S_3 - Average percentage difference in maximum normal displacement of the three contact points (fingertip, knuckle and base of the palm) during contact
- S_4 - Percentage difference in maximum tangential displacement of the fingertip during contact
- S_5 - Percentage difference in contact time

Apart from contact time the components were determined over the common contact period, i.e. the take-off time was determined to be either the take-off time of the recorded performance or the simulated take-off time, based on whichever occurred first. This ensured that comparisons of the contact phase could reasonably be made.

The overall score of the simulation was calculated by taking the RMS of the nine components. The performance and system categories were each given a 50% weighting and within each category the components were equally weighted, where 1°, was considered comparable to a 1% difference in other measures (Yeadon and King, 2002). Thus the score function that was minimised was:

$$\text{Score} = \sqrt{\left(\frac{P_1^2 + P_2^2 + P_3^2 + P_4^2}{8}\right) + \left(\frac{S_1^2 + S_2^2 + S_3^2 + S_4^2 + S_5^2}{10}\right)} \qquad (6.1)$$

When the four vaults were matched concurrently using a common parameter set (referred to as combined matching), the overall score was the mean of the overall scores for each of the four vaults.

6.3.3 Results

When each vault was matched individually the genetic algorithm converged to a solution within 150 generations. The simulations matched the performances well with overall scores of 9.7% (L_1), 11.2% (L_2), 8.9% (R_1) and 9.0% (R_2). Table 6.2 shows the parameters determined from the individual matching with the associated scores. These results provided an initial estimate of the parameter bounds for the combined optimisation.

Table 6.2. Parameters determined from individual matching with associated scores

Parameter		Vault L_1	L_2	R_1	R_2
K_{CS}	($N\,m^{-1}$)	138700	153100	68060	64850
D_{CS}	($Ns\,m^{-2}$)	147.7	173.1	92.28	176.9
K_{KT}	($Nm\,rad^{-1}$)	319.3	193.6	438.8	50.10
D_{KT}	($Nms\,rad^{-1}$)	8.872	6.655	9.512	4.500
K_{SH}	($N\,m^{-1}$)	10270	11080	23530	18200
D_{SH}	($Ns\,m^{-1}$)	418.4	613.1	1354	463.3
K_{TT_1}	($Nm\,rad^{-1}$)	190200	203200	155000	174300
K_{TT_2}	($Nm\,rad^{-2}$)	10930000	12940000	8724000	6375000
D_{TT}	($Nms\,rad^{-2}$)	126.6	86.5	110.5	83.19
μ		0.7988	0.6938	0.6946	1.063
Score					
Overall	(%)	9.7	11.2	8.9	9.0
Performance	(%)	4.0	3.4	4.8	3.3
System	(%)	13.1	15.5	11.6	12.3

Nomenclature: K - stiffness, D - damping, μ - coefficient of friction, CS - contact surface element, KT - knuckle torsional element, SH - shoulder element, TT - table torsional element.

When the four vaults were matched concurrently, the genetic algorithm again converged to a solution within 150 generations. Reasonable agreement was found between the simulations and the performances with an overall score of 16.8% resulting from scores of 13.9% (L_1), 17.2% (L_2), 20.8% (R_1) and 15.4% (R_2). Table 6.3 shows the parameters determined from the combined matching with the associated scores.

Table 6.3. Parameters determined from combined matching with associated scores

Parameter		
K_{CS}	($N\,m^{-1}$)	105100
D_{CS}	($Ns\,m^{-2}$)	19.04
K_{KT}	($Nm\,rad^{-1}$)	181.3
D_{KT}	($Nms\,rad^{-1}$)	6.141
K_{SH}	($N\,m^{-1}$)	14760
D_{SH}	($Ns\,m^{-1}$)	602.8
K_{TT_1}	($Nm\,rad^{-1}$)	170000
K_{TT_2}	($Nm\,rad^{-2}$)	12280000
D_{TT}	($Nms\,rad^{-2}$)	477.3
μ		0.8326
Score		
Mean Overall	(%)	16.8
Mean Performance	(%)	4.7
Mean System	(%)	23.2

Nomenclature: K - stiffness, D - damping, μ - coefficient of friction, CS - contact surface element, KT - knuckle torsional element, SH - shoulder element, TT - table torsional element.

The mean performance scores were 3.9% and 4.7% for the single and the combined optimisations respectively, which shows that the simulation model was capable of replicating performance at take-off from the table. Furthermore, the simulation model produced performances in which key contact phase features were similar to those seen in the recorded performances, namely:

- The movement of the arm replicated shoulder retraction during the initial part of the contact phase and shoulder protraction during the latter part of the contact phase.
- The fingertip, knuckle and base of the palm all deformed the table in the normal direction.
- The hands initially slid tangentially relative to the table, then remained stationary, and finally began to slide again in the opposite direction before take-off.
- The table oscillated with appropriate amplitude and frequency.

The mean system scores were 13.1% and 23.2% for the single and the combined optimisations respectively. Larger discrepancies were, however, expected for the system components of the score as there were inaccuracies associated with determining the reference values for these components. For example in the recorded performances the gymnast's left and right hands did not contact the vault at exactly the same time and therefore the values of contact time and hand displacement were estimated based on the average of the two hands.

The system components were included in the score function to ensure that key features of the contact phase were replicated. Despite the larger errors observed in the system components of the score the key contact phase features were similar to those seen in the recorded performances, and thus the larger errors were considered acceptable.

6.4 Evaluation of Angle-Driven Model

To ensure that the simulation model produced realistic human movements, and to ascertain if the parameter set obtained from the combined matching could be used generally for handspring entry vaults, an evaluation of the model was conducted. Two additional vaults were used to evaluate the angle-driven model: a layout vault, L_3, and a Roche vault, R_3. These vaults were considered to be the second best performance of each vault. The initial conditions for these two vaults are given in Table 6.4.

Table 6.4. Initial conditions of two additional handspring entry vaults

		Vault	
Initial condition		L_3	R_3
Horizontal COM position	(m)	-0.635	-0.686
Vertical COM position	(m)	1.810	1.725
Horizontal COM velocity	($m\,s^{-1}$)	4.85	4.74
Vertical COM velocity	($m\,s^{-1}$)	2.85	3.03
Orientation angle	($^\circ$)	96.6	93.0
Angular velocity	($^\circ\,s^{-1}$)	228	123

The two additional vaults were each simulated using the system parameters determined from the combined matching procedure (Table 6.3) and the associated score for each vault was determined using Equation 6.1. Reasonable agreement was found between the simulations and the performances with overall scores of 16.8% (L_3) and 17.3% (R_3)

respectively, as shown in Table 6.5.

Table 6.5. Scores determined from evaluation of the angle-driven model

		Vault	
Score		L_3	R_3
Overall	(%)	16.8	17.3
Performance	(%)	3.6	4.9
System	(%)	23.5	24.0

The overall scores for the additional two vaults fell within the range of scores for the previous four vaults from the combined matching. Moreover, the performance scores were again low, 3.6% and 4.9% respectively, which showed that the combined matching parameter set could be used generally for handspring entry vaults.

Visual representations of the table contact phase during the recorded performances and the evaluation simulations are given for vaults L_3 and R_3 in Figure 6.1 and Figure 6.2 respectively, and show the close agreement between the recorded and simulated performances.

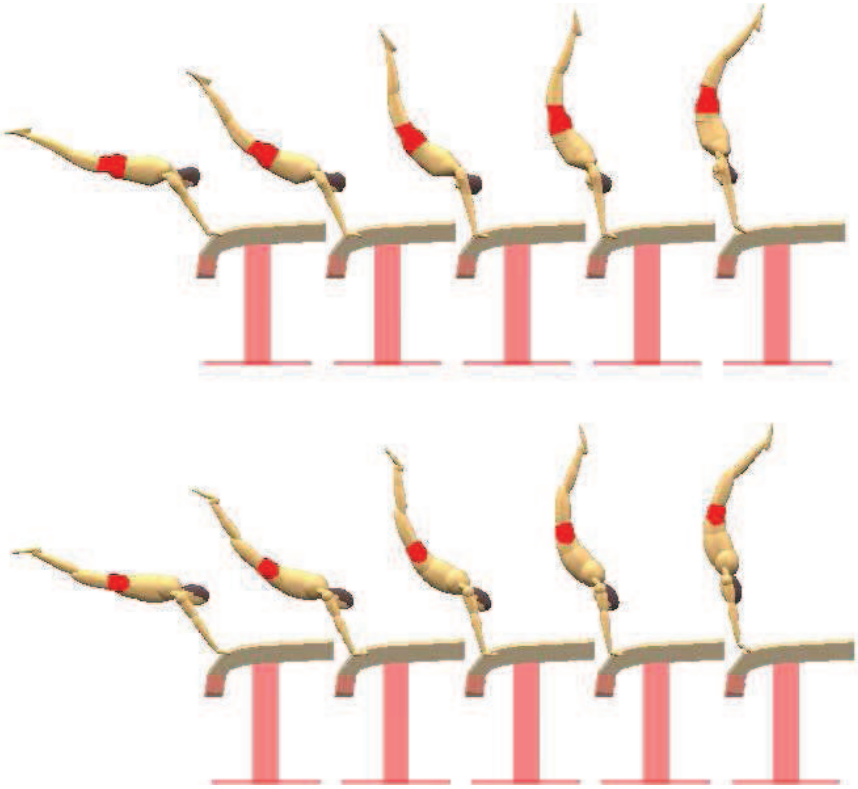

Figure 6.1. Comparison of L_3 table contact phase: recorded performance (upper) and angle-driven simulation using combined matching system parameters (lower).

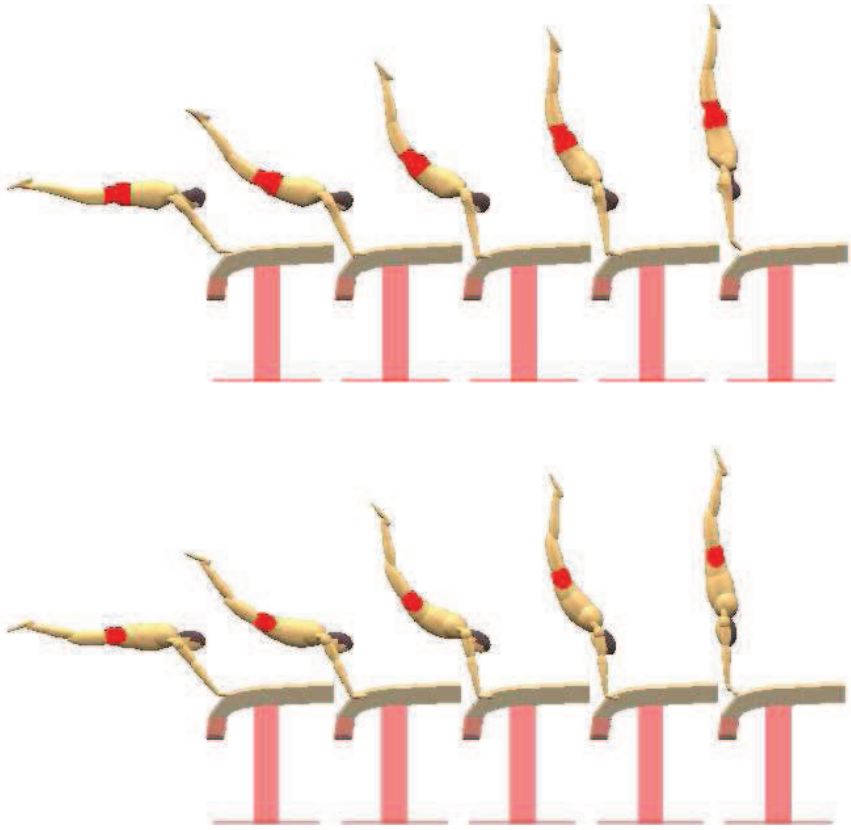

Figure 6.2. Comparison of R_3 table contact phase: recorded performance (upper) and angle-driven simulation using combined matching system parameters (lower).

6.5 Evaluation of Torque-Driven Model

The torque-driven vaulting model was also evaluated to ensure that it produced realistic movements. The model was driven with extensor and flexor torque generators at the wrist, shoulder, hip and knee joints. A genetic algorithm (Carroll, 2001) varied the torque generator activation profiles plus three initial conditions to minimise an objective function that was based on matching simulations with recorded performances. The six vaults used with the angle-driven model were each evaluated individually.

6.5.1 Model Variables

6.5.1.1 Activation Profiles

The levels of activation of the torque generators were defined by activation profiles as outlined in Section 4.6.2. The extensor torques at each joint were assumed to ramp down and then up, conversely the flexor torques at each joint were assumed to ramp up and then down (as shown in Figure 6.3). These assumptions were based on the torques generated about each joint in the angle-driven simulations. The activation profiles could,

however, remain at the initial activation level or only ramp in one direction, if the start time of the first or second ramp, respectively, was delayed. Therefore the assumptions of profile shape allowed suitable flexibility.

Each activation profile was defined by seven parameters as detailed in Section 4.6.2. The lower and upper bound of each of the activation parameters were set based upon information from the literature as outlined below.

It has been demonstrated that the muscles of the legs are activated before a landing (Yeadon et al., 2010). As the table contact phase is essentially a landing on the hands, it was expected that the muscles of the arms would have similar characteristics. For any joint, if only the extensors or only the flexors were active prior to the contact, the joint angle would change rapidly. Co-contraction of the extensors and flexors enables the muscles to be active without large joint accelerations. Since the gymnast changes configuration during the pre-flight there may be a non-zero net joint torque at the instant of impact. Thus, the pre-impact activation level a_0 was allowed to be within the range 0.2-0.5. As there is non-zero activation prior to impact, the first muscle activation ramp may also start prior to impact. The bounds of the start time of the first ramp t_{S1}, were therefore set to 100 ms before and 200 ms after impact.

It has been observed that for voluntary muscle contractions, the time required to ramp from zero to maximal activation is of the order of 70 ms (Freund and Budingen, 1978). It is reasonable to expect that the time required to ramp from maximal to zero activation will be similar and therefore, the lower bound for the ramping durations t_{R1} and t_{R2} was set at 70 ms. There is no theoretical upper limit for the ramping duration but it was set at 300 ms, within which time the whole contact phase would have been completed.

Without any constraints, the pre-impact activation levels could fall outside the set limits. For example, if the activation was ramping quickly and the start time of the first ramp was prior to contact, there was the possibility that the parameters would be such that the activation level was outside the pre-impact activation bounds. The start time of the first ramp t_{S1} was therefore constrained such that the pre-impact activation fell within the bounds. The start time of the second ramp t_{S2} was constrained such that it occurred after the end of the first ramp to avoid rapid changes in activation level. The activation parameters and associated bounds are summarised in Table 6.6.

Table 6.6. Lower and upper bounds of the activation parameters

Parameter	Definition	Lower bound	Upper bound
	Extensors		
a_0	Pre-impact activation level	0.2	0.5
a_1	Minimal activation level	0	a_0
a_2	Final activation level	a_1	1
t_{S1}	Start time of first ramp (s)	-0.1*	0.2
t_{R1}	Ramp time of first ramp (s)	0.07	0.3
t_{S2}	Start time of second ramp (s)	$t_{S1} + t_{R1}$	$t_{S1} + t_{R1} + 0.2$
t_{R2}	Ramp time of second ramp (s)	0.07	0.3
	Flexors		
a_0	Pre-impact activation level	0.2	0.5
a_1	Maximal activation level	a_0	1
a_2	Final activation level	0	a_1
t_{S1}	Start time of first ramp (s)	-0.1*	0.2
t_{R1}	Ramp time of first ramp (s)	0.07	0.3
t_{S2}	Start time of second ramp (s)	$t_{S1} + t_{R1}$	$t_{S1} + t_{R1} + 0.2$
t_{R2}	Ramp time of second ramp (s)	0.07	0.3

* Start time subject to pre-impact activation level constraints.

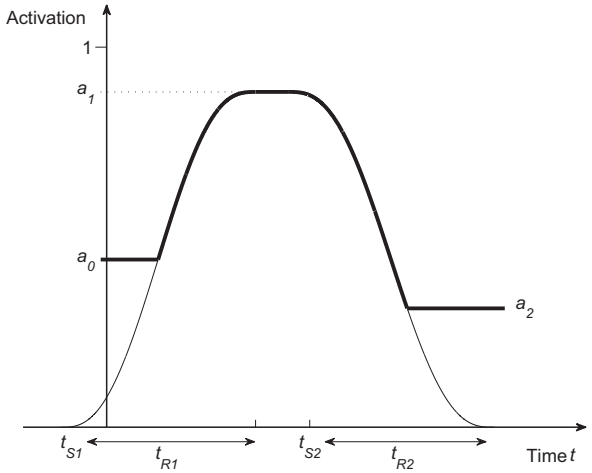

Figure 6.3. Example of a flexor torque generator activation profile ramping up and then down (bold line indicates the activation profile).

6.5.1.2 Initial Conditions

The horizontal and vertical velocities of the gymnast's centre of mass, and the angular velocity of the head + upper trunk segment were allowed to vary from the measured values by $\pm 0.1\ \mathrm{m\,s^{-1}}$ and $\pm 0.5\ \mathrm{rad\,s^{-1}}$ respectively. The small amounts of variation were allowed in order to compensate for errors due to model assumptions and reconstruction errors in the kinematic data.

6.5.2 Model Inputs

The inputs to the torque-driven model included the horizontal and vertical position of the gymnast's centre of mass just prior to contact with the vaulting table and the gymnast's initial configuration and joint angular velocities, all of which were determined from the kinematic data (Section 3.4). The inputs also included the body segmental inertias (Section 5.4), and the inertial parameters of the vaulting table (Section 5.5).

The model system parameters were set to those determined during the combined matching (Table 6.3) apart from the damping parameter of the contact spring. This parameter was increased to prevent the hands from 'bouncing' during the initial part of the table contact phase.

During the angle-driven simulations the wrist angle was driven using kinematic data from the recorded performances, and thus the orientation of the palm was fixed. In the torque-driven simulations the wrist angle was one of the degrees of freedom. Reaction forces generated by the contact spring could, therefore, change the wrist angle and rotate the palm segment. As the damping of the contact spring was low, the wrist angle oscillated which led to the hands 'bouncing'. Hence an increase in the contact spring damping parameter was necessary during the torque-driven simulations.

6.5.3 Objective Function

To assess how well the simulations matched the recorded performances each simulation was given a score. The score was composed of 12 components: four performance components P_i, and eight configuration components C_i, as listed below.

- P_1 - Difference in orientation angle at take-off (in degrees)
- P_2 - Percentage difference in angular momentum at take-off
- P_3 - Percentage difference in horizontal linear velocity at take-off
- P_4 - Percentage difference in vertical linear velocity at take-off
- C_1 - RMS difference in the wrist angle during contact (in degrees)
- C_2 - RMS difference in the shoulder angle during contact (in degrees)
- C_3 - RMS difference in the hip angle during contact (in degrees)
- C_4 - RMS difference in the knee angle during contact (in degrees)
- C_5 - Difference in the wrist angle at take-off (in degrees)
- C_6 - Difference in the shoulder angle at take-off (in degrees)
- C_7 - Difference in the hip angle at take-off (in degrees)
- C_8 - Difference in the knee angle at take-off (in degrees)

For the recorded performances the angular momentum at take-off was determined by using the angle-driven model to simulate the post-flight. Angular momentum is conserved when the gymnast is in flight, and thus should remain constant during the post-flight. Initial conditions at the time of take-off were determined from the kinematic data and the model was driven with joint angle time histories for the first 100 ms of post-flight. The mean angular momentum over this period was then determined. An average value was taken to reduce the error in the angular momentum value due to inaccuracies in the kinematic data.

The overall score was calculated by taking the RMS of the 12 components. The performance and configuration categories were each given a 50% weighting and within each category the components were equally weighted, where 1°, was again considered comparable to a 1% difference in other measures. Thus the score function that was minimised was:

$$\text{Score} = \sqrt{\left(\frac{P_1^2 + P_2^2 + P_3^2 + P_4^2}{8}\right) + \left(\frac{C_1^2 + C_2^2 + C_3^2 + C_4^2 + C_5^2 + C_6^2 + C_7^2 + C_8^2}{16}\right)} \tag{6.2}$$

6.5.3.1 Penalties

Where necessary, the model incurred penalties if the joint angles exceeded the gymnast's anatomical limits. A penalty equivalent to 1 percentage point was incurred for each degree that the joint angle exceeded the limits given in Table 6.7.

Table 6.7. Limits of range of motion of the joints

Joint	Lower angle limit (°)	Upper angle limit (°)
Wrist	95	n/a
Shoulder	n/a	200
Hip	n/a	210
Knee	n/a	180

The joint angle limits of the wrist, shoulder and hip were based on the maximum angle reached during flexibility trials (Section 5.3), while the joint angle limit of the knee was based on anatomical constraints. Limits were only in place if the model was likely to violate them, hence the one sided limits at each joint.

The joint angle penalties were in place not only during the table contact phase but also during the first 100 ms of post-flight. This ensured that the torque generator activation profiles, determined from matching the contact phase, did not produce joint torques that would cause the joint angles to exceed their anatomical limits during either the table contact phase or the subsequent post-flight.

6.5.4 Results

When each vault was matched using the torque-driven model the genetic algorithm converged to a solution within 200 generations. The simulations matched the layout performances particularly well, with overall scores of 2.8% (L_1), 2.6% (L_2) and 2.1% (L_3), however the simulations did not match the Roche performances quite so well, with overall scores of 10.3% (R_1), 5.4% (R_2) and 10.0% (R_3). Table 6.8 shows the differences between the simulations and recorded performances for each of the vaults. Penalties were not incurred in any of the simulations.

Table 6.8. Differences between performances and matched torque-driven simulations

	Vault					
Score Component	L_1	L_2	L_3	R_1	R_2	R_3
P_1 (°)	-1.4	-1.5	-1.4	-2.9	-3.2	-4.9
P_2 (%)	4.1	1.5	1.3	11.7	1.7	8.8
P_3 (%)	-4.9	2.4	3.1	16.7	4.7	15.7
P_4 (%)	-2.9	0.2	1.2	-18.1	-12.3	-19.5
C_1 (°)	2.4	8.0	3.1	4.4	4.5	7.1
C_2 (°)	2.9	3.3	4.4	6.4	3.6	4.1
C_3 (°)	1.1	1.6	1.4	7.1	1.7	2.2
C_4 (°)	1.6	2.7	1.7	3.9	4.7	2.3
C_5 (°)	-0.9	0.1	-0.1	0.9	3.0	3.0
C_6 (°)	0.3	-0.5	-1.5	2.1	-4.0	-2.1
C_7 (°)	1.1	-1.1	-1.1	-8.2	-2.9	-7.0
C_8 (°)	0.9	1.2	0.8	-1.5	-0.3	1.2
Overall (%)	2.8	2.6	2.1	10.3	5.4	10.0
Performance (%)	3.6	1.6	1.9	13.7	6.8	13.5
Configuration (%)	1.6	3.3	2.2	5.0	3.4	4.2

For components $P_1 - P_4$ and $C_5 - C_8$ a positive value indicates that the simulated value was higher than the recorded value and conversely a negative indicates that the simulated value was lower than the recorded value.

Visual representations of the table contact phase during the recorded performances and the matched torque-driven simulations are given for vaults L_2 and R_3 in Figure 6.4 and Figure 6.5 respectively. These two performances were chosen as they are representative of the matches for the two different vaults. Close agreement can be seen between the recorded and simulated performances of the layout vault, while some discrepancies can be seen between the recorded and simulated performances of the Roche vault. The simulation results presented above will be analysed and discussed in the following sections.

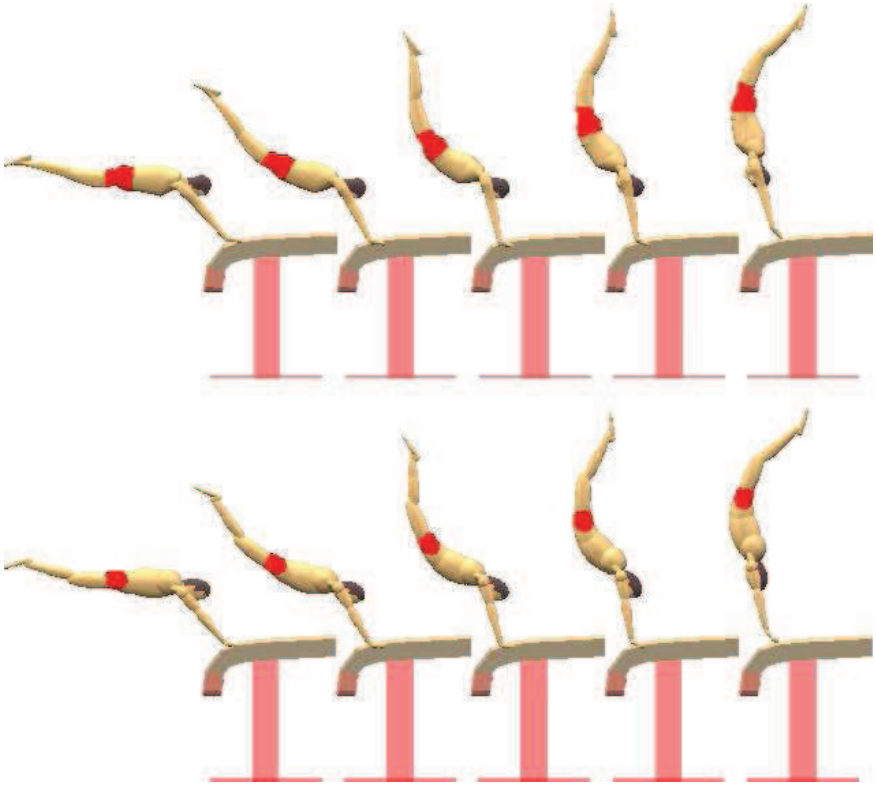

Figure 6.4. Comparison of L_2 table contact phase: performance (upper) and torque-driven simulation (lower).

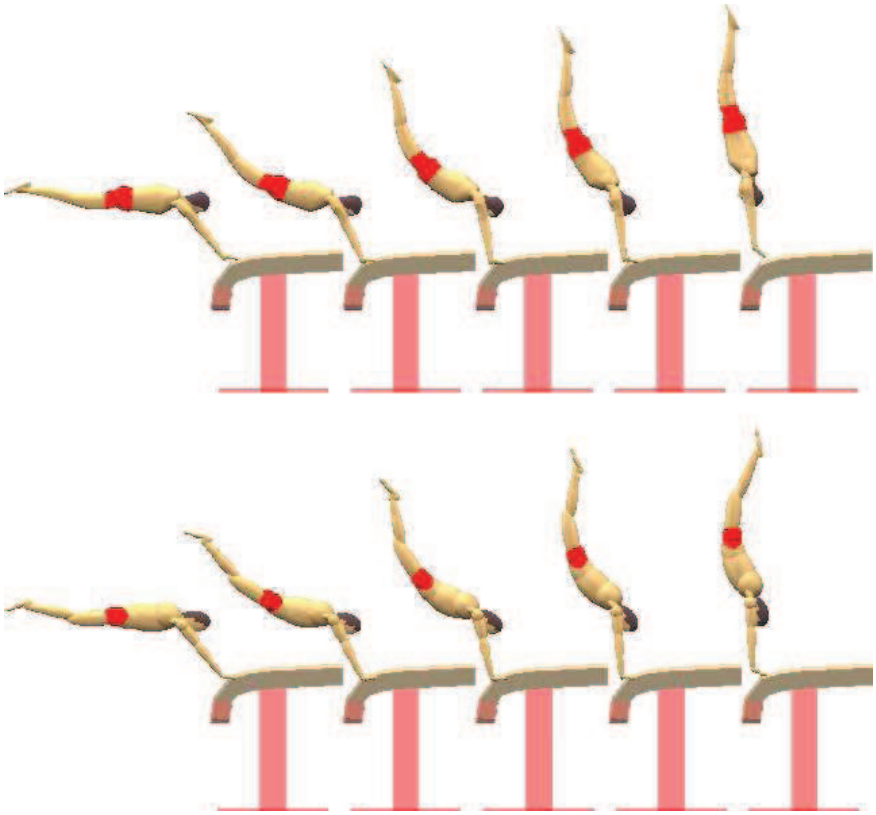

Figure 6.5. Comparison of R_3 table contact phase: performance (upper) and torque-driven simulation (lower).

6.5.4.1 Performance

The values of the performance indicators that were considered in the matching process are provided for the recorded and simulated performances of vaults L_2 and R_3 in Table 6.9. The overall close agreement between the performance and simulation values for the layout vault indicates that the simulation model was capable of adequately replicating the take-off performance of this vault. In contrast, for the Roche vault the agreement between the performance and simulation values of the linear velocity and angular momentum at take-off was not as good. This suggests that an aspect of the gymnast's technique when performing the Roche vault may not be accurately represented by the simulation model.

Table 6.9. Table take-off conditions of performances and torque-driven simulations

	L_2		R_3	
	Performance	Simulation	Performance	Simulation
Orientation (°)	162	164	151	156
Angular momentum ($\mathrm{kg\,m^2 s^{-1}}$)	99.5	100.9	82.5	89.7
Horizontal velocity ($\mathrm{m\,s^{-1}}$)	3.43	3.51	3.20	3.70
Vertical velocity ($\mathrm{m\,s^{-1}}$)	2.92	2.93	3.70	2.98

The data in Table 6.9 shows that, in terms of take-off conditions there were two main differences between the vaults: the angular momentum at take-off and the vertical velocity at take-off. In the Roche performance, the angular momentum at take-off was 21% lower than that in the layout performance but the vertical velocity was 27% higher. This suggests that when performing the Roche vault the gymnast used a technique that favoured gaining height in the post-flight at the expense of angular momentum. Possible differences in technique that could have led to the poorer agreement of the simulated and recorded take-off performances of the Roche vaults will be discussed in more detail in Section 6.5.5.1.

6.5.4.2 Joint Angles

The simulated joint angles of each of the joints considered in the matching process are compared to those from the recorded performances for vaults L_2 and R_3 in Figure 6.6 and Figure 6.7 respectively. For both vaults there was not a clear trend for the simulation joint angles to match performance joint angles more closely at one joint than another. This indicates that no individual torque generator was consistently incapable of providing the requisite torques for the simulation to match the performance data.

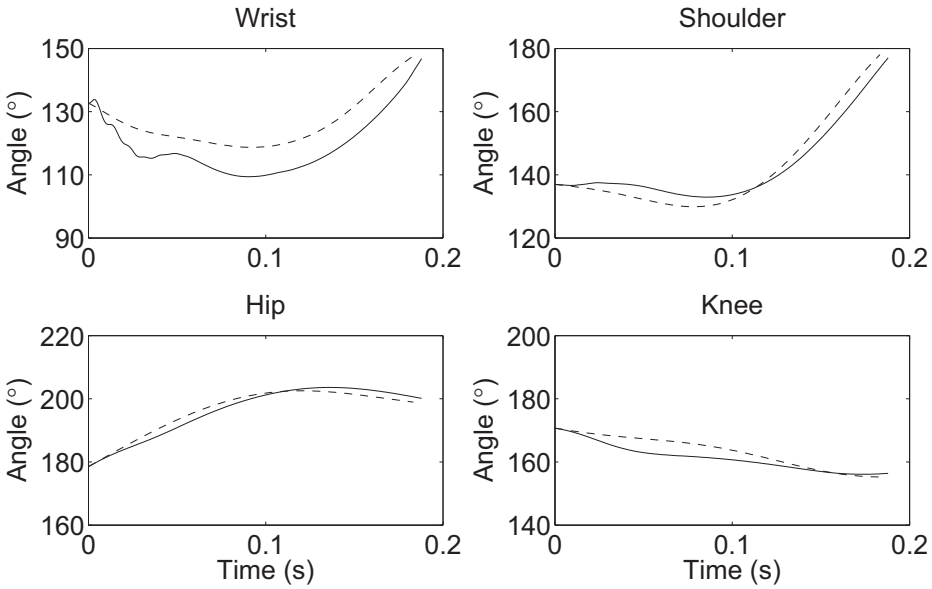

Figure 6.6. Comparison of joint angle time histories for L_2: performance (dashed lines) and matched simulation (solid lines).

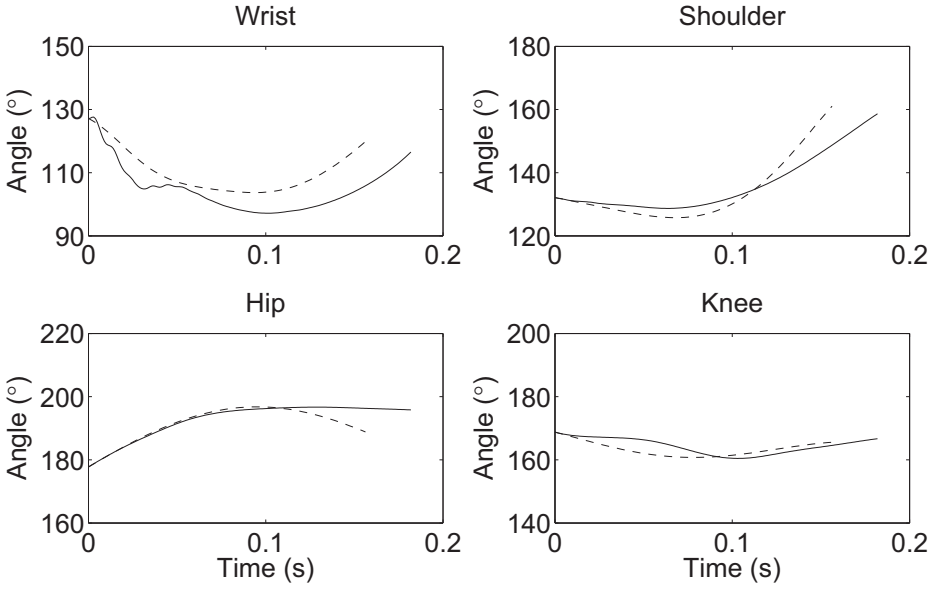

Figure 6.7. Comparison of joint angle time histories for R_3: performance (dashed lines) and matched simulation (solid lines).

The overall close agreement between the performance and simulation joint angles for the layout vault indicates that the torque generators included in the model were strong enough to match the performance torques for this vault. In contrast, for the Roche vault the shape of the joint angle time histories from the simulation were similar to those of the recorded performance, but the simulated wrist, shoulder and hip joint angles lagged behind the performance joint angles during the second half of the contact phase. Possible reasons for the difference in agreement of the simulated and performance joint angle time histories for the Roche vault will be discussed in more detail in Section 6.5.5.2.

6.5.4.3 Joint Torque Activation Profiles

The muscle activation profiles of the eight torque generators for vaults L_2 and R_3 are shown in Figure 6.8 and Figure 6.9 respectively. The activation time histories of the layout vault show high activation of the wrist and shoulder flexors during the majority of the contact phase, and co-contraction in the hip and knee throughout the contact phase. The activation time histories of the shoulder and the knee were similar for the Roche vault, but the wrist and hip activation time histories were dissimilar.

The wrist activation profile shown in Figure 6.9 for the Roche vault R_3 was, however, atypical for Roche vaults: the typical activation profile had high activation of the wrist flexors during the majority of the contact phase, more like that found for the layout vault. The high activation of the wrist and shoulder flexors allowed the gymnast to resist the tendency for these joint angles to decrease.

The hip activation profiles are markedly different between the vaults, with higher activation of the flexors for the Roche vault than for the layout vault. This was expected due to the different post-flight requirements of the two vaults. As shown in Figure 6.4 and Figure 6.5, when performing the vaults the gymnast's body becomes arched during the initial part of the contact phase. The body then remains arched when performing the layout vault but straightens during the final part of the contact phase when performing the Roche vault. The high activation of the hip flexors, throughout the table contact phase of the Roche vault, allowed the gymnast to straighten the body in the latter part of the table contact phase in preparation for the tucked somersaults that were performed during the post-flight.

The flexor torque generators of the shoulder and wrist in the layout vault and the shoulder

and hip in the Roche vault, ramped up quickly from the initial activation levels, and were maximally activated for the some of the contact phase. This indicates that either the gymnast was exerting maximal effort during the vaults or that the fitted maximum voluntary torque surfaces (Section 5.2.3.4) were sub-maximal. The duration of the table contact phase was short, between 150 ms and 200 ms, and therefore it is not unreasonable to expect that gymnast could exert a maximal or near maximal effort for this length of time.

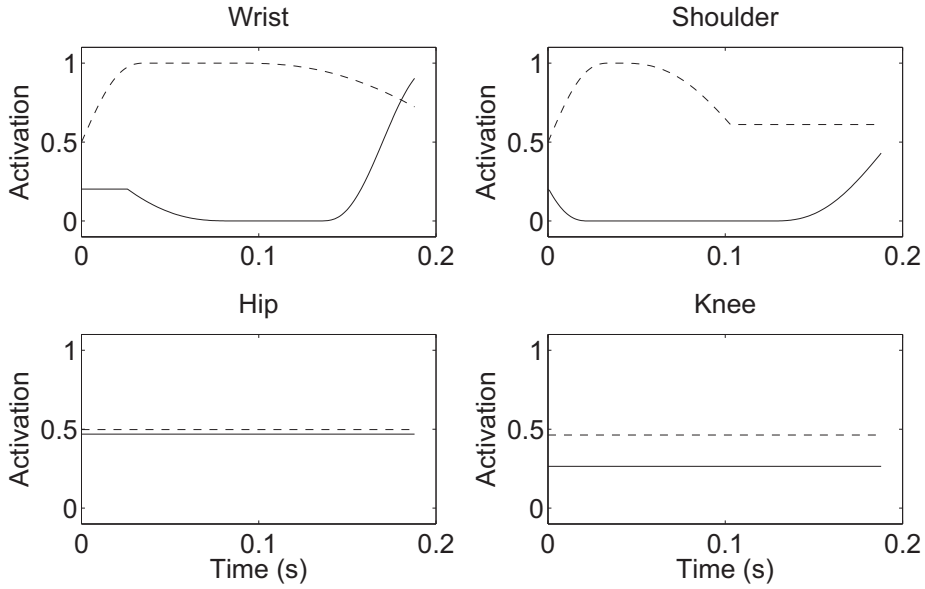

Figure 6.8. Extensor (solid lines) and flexor (dashed lines) torque generator activation profiles for a matched simulation of L_2.

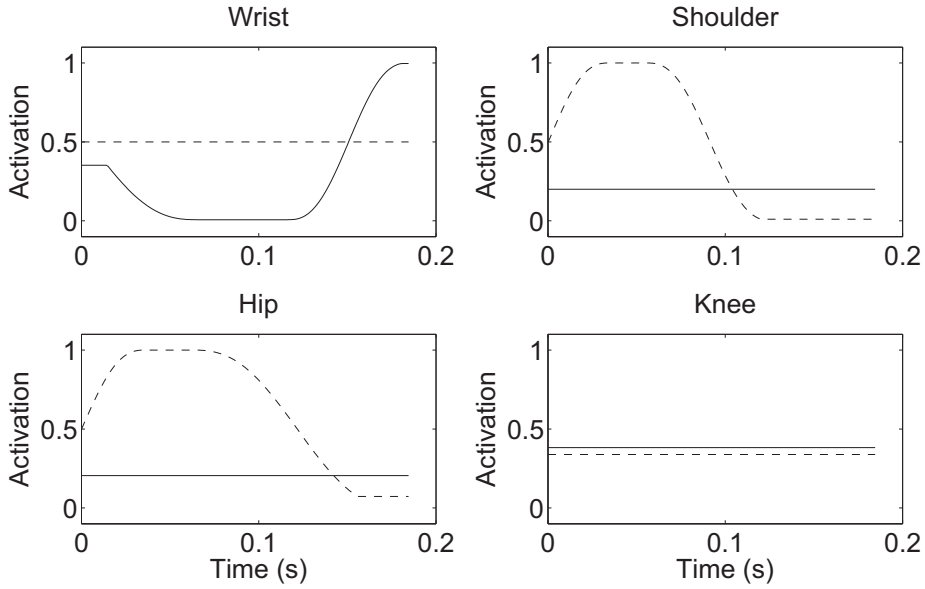

Figure 6.9. Extensor (solid lines) and flexor (dashed lines) torque generator activation profiles for a matched simulation of R_3.

6.5.4.4 Joint Torques

The net joint torque time histories obtained from the torque-driven simulations for vaults L_2 and R_3 are given in Figure 6.10 and Figure 6.11 respectively. In these figures positive torques represent extension and negative torques represent flexion. While the torque profiles have a similar shape for the two different vaults, there were some differences in the magnitudes of the torques. For instance there was greater flexion torque at the shoulders in the layout vault and greater flexion torque at the hips in the Roche vault, both of which allowed the gymnast to leave the table in different configurations as seen in Figure 6.4 and Figure 6.5.

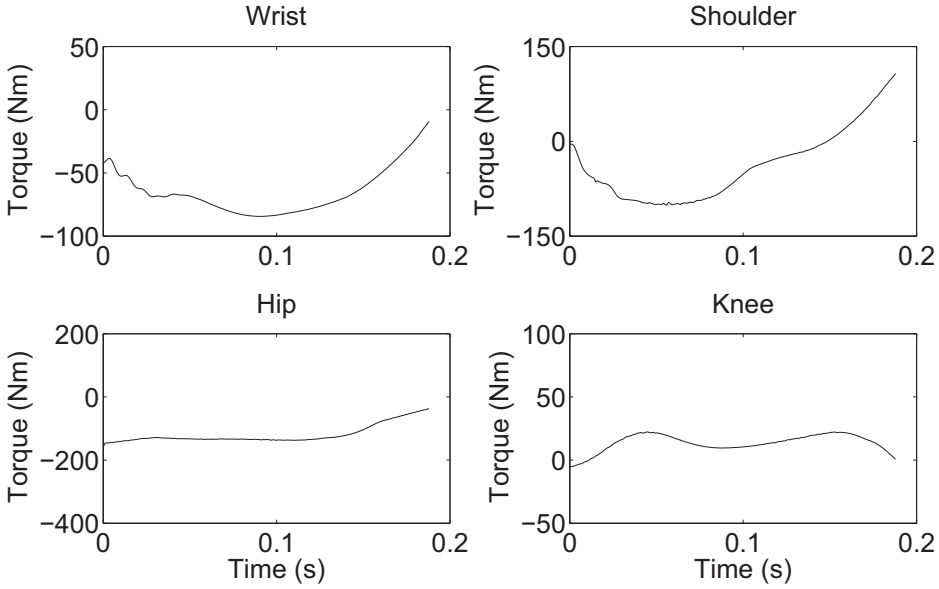

Figure 6.10. Joint torque time histories for a matched simulation of L_2.

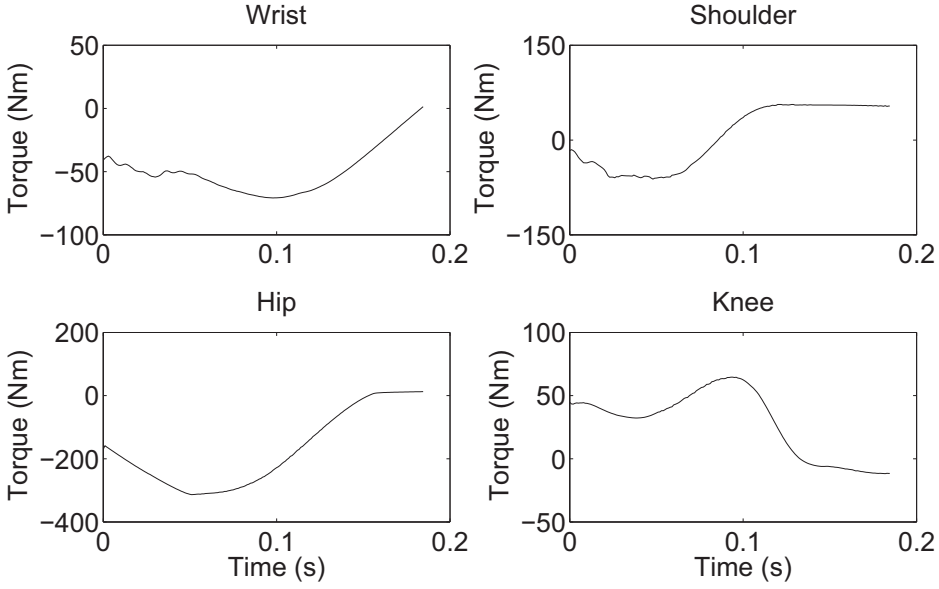

Figure 6.11. Joint torque time histories for a matched simulation of R_3.

The wrist, shoulder and hip net joint torque profiles shown above include passive torque components. Passive torques were implemented within the model to provide restorative torques at the extremes of the gymnast's range of motion. The passive torques obtained during the simulations of vaults L_2 and R_3 are shown in Figure 6.12 and Figure 6.13 respectively, where again positive torques represent extension and negative torques represent flexion. For both vaults the passive torques were at reasonable levels, and the simulations did not incur any penalties, which indicates that the wrist, shoulder and hip joints did not exceed the gymnast's range of motion.

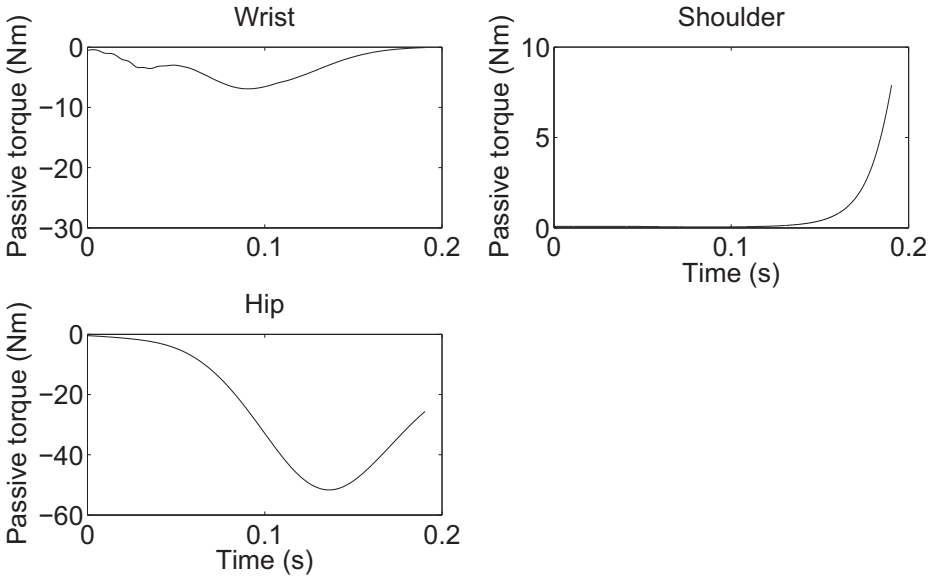

Figure 6.12. Passive joint torque time histories for a matched simulation of L_2.

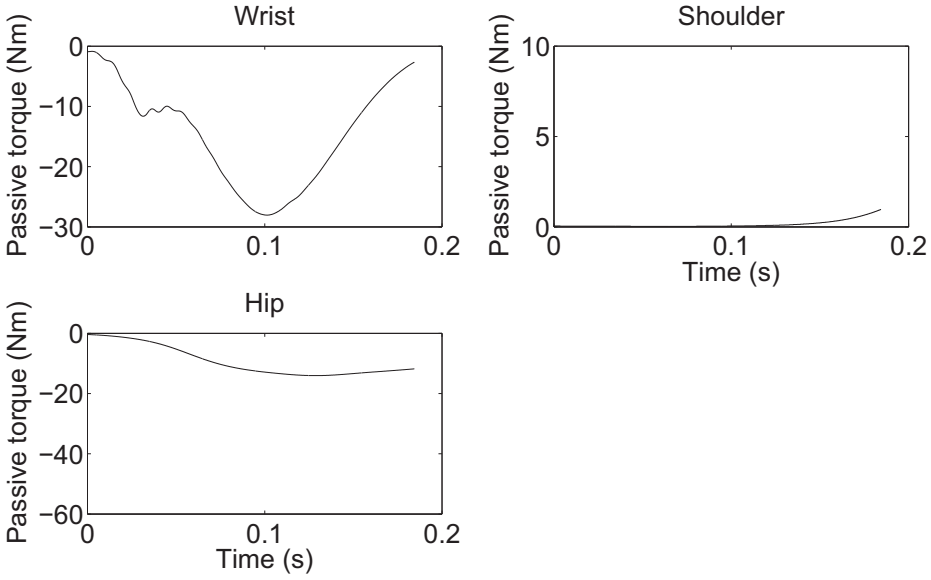

Figure 6.13. Passive joint torque time histories for a matched simulation of R_3.

6.5.5 Discussion

Evaluation of the torque-driven simulation model showed that the model adequately simulated the performance of handspring entry vaults. The simulations matched the layout performances particularly well, with a mean overall difference of 2.5% and also showed a close match to the Roche performances, with a mean overall difference 8.6%. The evaluations results are discussed in the following sections.

6.5.5.1 Take-off Performance

The model replicated the take-off performance of layout vaults particularly well, but did not match the take-off performance of Roche vaults quite so well. When performing the Roche vault the gymnast used a technique that favoured gaining height in the post-flight at the expense of angular momentum. The inferior match between recorded and simulated Roche performances, indicates that an aspect of the gymnast's technique when performing the Roche vault, may not be accurately represented by the simulation model.

For both vaults the horizontal components of the table take-off velocities achieved during recorded performances were lower than those at table contact. The vertical components of the table take-off velocities were similar to those at table contact for the layout vaults, while for Roche vaults the vertical components of the table take-off velocities were higher than those at table contact. Gravity acted on the gymnast to vertically decelerate the centre of mass throughout the vault, therefore the velocities at table take-off imply that the interaction with the vaulting table vertically accelerated and horizontally decelerated the gymnast's centre of mass during the table contact phase.

In terms of centre of mass velocities, the main difference between the two vaults, was that the Roche vault had an increase in the vertical velocity of the centre of mass during the table contact phase, while for the layout vault the vertical velocity of the centre of mass remained much the same. Aside from the external force due to the interaction with the table, the gymnast may also be able to generate internal forces to vertically accelerate the centre of mass. A flexor torque at the shoulder will increase the shoulder angle, and in turn raise the centre of mass, while protraction of the shoulder during the latter part of the contact phase, when the gymnast is in an inverted position, will also raise the centre of mass. Thus shoulder flexion and protraction may allow the gymnast to accelerate the centre of mass.

Within the simulation model, a spring was used to allow for retraction and protraction of the shoulder. This representation of the shoulder, does not, however, allow for active retraction or protraction of the shoulder. During the Roche performances, when the gymnast was aiming for a high vertical take-off velocity, the gymnast may have actively protracted the shoulder to vertically accelerate the centre of mass.

Cools et al. (2007) tested the strength of the scapular muscles of young elite gymnasts and found that, compared to non-athletic adolescents, the gymnasts had significantly increased protraction strength. This suggests that gymnasts are conditioned to perform active shoulder protraction. Furthermore, the protraction strengths found by Cools et al. (2007) are of an order that would account for a substantial increase in the vertical velocity of the gymnast's centre of mass during the contact phase of a vault. This implies that the lack of active shoulder protraction within the model could, to some degree, explain the inferior match of the Roche vaults.

6.5.5.2 Joint Angles

Evaluation of the torque-driven model showed that the torque generators included in the model were strong enough to match the performance torques for the layout vault, as the joint angles of the gymnast in the simulated vaults matched the joint angles of the performances. For the Roche vault, on the other hand, the agreement was not so good and the simulated joint angles lagged behind the performance joint angles during the second half of the contact phase.

The discrepancies found between the simulated and the performance joint angles of the gymnast during the table contact phase of the Roche vault could be due to differences in the duration of the simulated and recorded contact phases. For the layout vaults the difference in contact time between simulated and recorded performances was minimal, with an average difference of only 4 ms. For the Roche vaults, however, the difference was more substantial, with the simulations spending, on average, 22 ms longer in contact with the vault compared to the recorded performances. The simulations did not vertically accelerate the centre of mass as much as in the recorded performances, and therefore the hands were in contact with the table for longer.

The cost function used to match the simulated and recorded performances (Section 6.5.3), aimed to match both the joint angles during the contact phase (Components C_1 - C_4)

and the joint angles at take-off (Components C_5 - C_8). The difference in length of contact for the Roche vaults led to a compromise between matching the joint angles during the contact phase and matching the joint angles at take-off, which may explain the weak match between the simulated and performance joint angles.

6.5.5.3 Summary

Evaluation of the torque-driven model has demonstrated that the model is capable of realistically simulating handspring entry vaults. While a limitation of the model is that it does not allow for active protraction of the shoulders, the model was still able to replicate key performance features of the vaults, such as the motion of the hands relative to the contact surface, and the motion of the vaulting table. Thus the model is considered to be accurate enough to evaluate and optimise performance of handspring entry vaults. Chapter 7 will describe the application of the simulation model to answer research questions.

6.6 Chapter Summary

In this chapter the method of determining the system parameters using an angle-driven model of the table contact phase was described. The resulting system parameters were evaluated using independent trials and found to be applicable to handspring entry vaults. The method of evaluation of a torque-driven model was also described. The torque-driven simulation model was able to replicate the key performance features of the layout vaults particularly well, with a mean overall difference of 2.5%, and also produced reasonable agreement when simulating Roche vaults with a mean overall difference of 8.6%. The simulation model, which incorporated a novel two-state representation of the contact phase, is thus considered suitable to evaluate and optimise performance of handspring entry vaults.

Chapter 7

Model Application and Performance Analysis

7.1 Chapter Overview

The rationale for the present study was to analyse gymnastics vaulting to gain an understanding of the mechanics of the table contact phase, and then to use this understanding to identify ways to improve performance. Within this chapter the methods used to apply the simulation model of vaulting to answer specific research questions are described.

7.2 Technique Optimisation

In terms of technique optimisation, the question that this study is trying to answer is:

What is the optimum table contact phase technique for handspring somersault vaults?

An optimal performance in vaulting is one in which the gymnast performs a vault with a high difficulty value whilst incurring minimal deductions. Vaults with more rotations about the transverse axis in the post-flight have higher difficulty values. Thus, to perform a high difficulty vault, rotation potential, which is a measure of the number of rotations that could be performed about the transverse axis before landing, must be maximised.

Within the present study a gymnast performed two different handspring entry vaults: handspring forward with salto forward stretched, and handspring forward with double salto forward tucked. Could the gymnast perform a more difficult vault without an increase in strength? Optimisations were carried out to determine the technique that resulted in maximum rotation potential based on the gymnast's strength capabilities.

For a vault of a given difficulty value, the height of the post-flight will have a direct influence on the score, as a specific deduction is made for lack of height in the post-

flight. Increased height in the post-flight is likely, however, to come at the expense of angular momentum. An optimal technique will allow the gymnast to obtain a maximum post-flight height whilst generating the required angular momentum for the vault to be performed. Optimisations were also carried out to determine the technique that resulted in maximised post-flight height, whilst maintaining the rotation potential required to perform a handspring forward with salto forward stretched.

7.2.1 Technique Optimisation Methods

7.2.1.1 Calculation of Kinematic Variables

To determine the optimal performances, it was necessary to determine the duration of post-flight, the rotation potential at take-off from the vaulting table, and the height obtained in post-flight. The procedures for calculating these kinematic variables are explained in the following sections.

Post-flight Time

The post-flight time was defined as the time from the last instant of take-off from the table until the first instant of landing. To determine the time at which the gymnast landed, the height of the gymnast's centre of mass at landing was required. As the gymnast was performing vaults with forward rotation in post-flight, the required landing position was short of vertical, as the angular momentum at landing would cause the gymnast to rotate about the feet during the initial part of the landing phase. It was therefore assumed that the gymnast had a touchdown angle at landing of 30° (Figure 7.1). Assuming that the gymnast landed with flat feet, the resulting height of the mass centre of the gymnast was 0.785 m (based on anthropometric measurements of the segments).

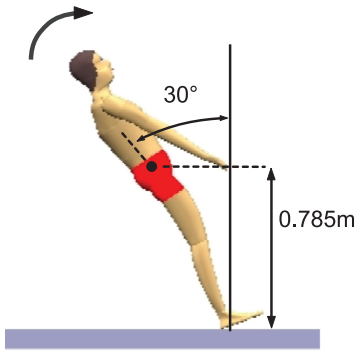

Figure 7.1. Centre of mass height at landing.

Using constant acceleration equations, the post-flight time t_{pf} was then calculated as:

$$t_{pf} = \frac{-V_{z,to} - \sqrt{{V_{z,to}}^2 - 2\,g\,(P_{z,to} - 0.785)}}{g} \tag{7.1}$$

where $V_{z,to}$ is the gymnast's vertical velocity at take-off from the table, $P_{z,to}$ is the vertical position (height) of the gymnast's centre of mass at take-off from the table and g is the constant acceleration of the gymnast due to gravity (-9.81 m s^{-2}).

Rotation Potential

Rotation potential is a measure of the number of rotations in a straight position about the transverse axis that can be performed before landing. The evaluation of rotation potential, took into account the body orientation at take-off from the vaulting table, as well as the angular momentum at take-off and the post-flight time.

The body orientation angle at take-off ϕ_{to} was estimated based on the relative positions of the hands and the centre of mass at take-off. The orientation angle was measured in the direction of rotation, from the vertical to the line from the finger-tips that passes through the centre of mass as shown in Figure 7.2.

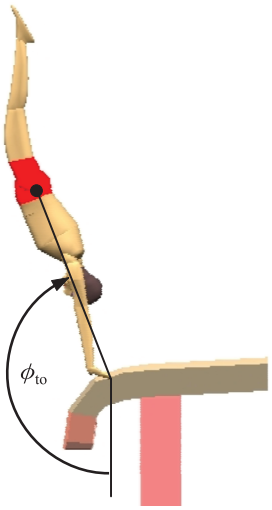

Figure 7.2. Body orientation at take-off from the vaulting table. The orientation angle is measured from the vertical to the line from the finger-tips that passes through the centre of mass.

The angle rotated through during post-flight ϕ_{pf}, was calculated from the angular momentum at take-off H, the post-flight time t_{pf}, and the moment of inertia of the gymnast:

$$\phi_{pf} = \frac{H\,t_{pf}}{I_{cm,s}} \tag{7.2}$$

where $I_{cm,s}$ is the moment of inertia of the gymnast about the centre of mass in a straight position with adducted arms, and was calculated as 10.7 kg m^2 using the inertia model of Yeadon (1990a).

The rotation potential ϕ was the sum of the body orientation angle at take-off ϕ_{to} and the post-flight phase rotation ϕ_{pf}, normalised to the number of straight somersaults:

$$\phi = \frac{\phi_{to} + \phi_{pf}}{2\pi} \tag{7.3}$$

Post-flight Height

The post-flight height h_{pf} was defined as the maximum height that the gymnast's centre of mass reached during the post-flight, and was calculated as the sum of the flight height and the take-off height. The flight height, h_z, is the difference in height between the last instant of take-off and the point of maximum height, and was calculated from constant acceleration equations:

$$h_z = \frac{{V_{z,to}}^2}{-2\,g} \tag{7.4}$$

where $V_{z,to}$ is the gymnast's vertical velocity at take-off from the table and g is the constant acceleration of the gymnast due to gravity (-9.81 m s^{-2}). The post-flight height is the simply the sum of the take-off height $P_{z,to}$, and the flight height h_z:

$$h_{pf} = P_{z,to} + h_z \tag{7.5}$$

7.2.1.2 Optimisation for Maximum Rotation Potential

The technique employed by the gymnast was optimised to determine the technique that resulted in maximum rotation potential. The three layout performances evaluated in Section 6.5 were optimised, as evaluation of the torque-driven model demonstrated that it was capable of realistically simulating the gymnast's technique during these vaults (Section 6.5). The initial conditions of the matched simulations were maintained, and therefore the optimisation involved varying just the 56 muscle activation parameters. A genetic algorithm (Carroll, 2001) varied the muscle activation parameters to maximise an objective function that simply comprised rotation potential.

During optimisation the joint constraint penalties outlined in Section 6.5.3.1 were maintained, to ensure that the simulations did not exceed realistic ranges of motion. A penalty of -1 was incurred for each degree that a joint angle exceeded the gymnast's range of motion. A further constraint was added to ensure the post-flight time was at least 90% of the matched simulation post-flight time. A penalty of -1 was incurred for each 100 ms that the post-flight time was below the required duration. This ensured that the optimised performance would not incur substantial deductions due to lack of height in the post-flight.

7.2.1.3 Optimisation for Maximum Post-flight Height

The technique employed by the gymnast was also optimised to determine the technique that resulted in maximum post-flight height whilst maintaining sufficient rotation potential to perform a handspring forward with salto forward stretched. Optimisations were conducted in the same manner as for optimisation of rotation potential except for differences in the objective function. In the optimisations for maximum post-flight height the objective function comprised post-flight height with a constraint on rotation potential, in that a penalty was incurred if the performance had less rotation potential at table take-off than the matched performance.

7.2.2 Technique Optimisation Results

7.2.2.1 Optimisation for Maximum Rotation Potential

Optimisation of the contact phase technique showed that there was limited capacity for an increase in rotation potential, with increases of 1.1% (L_1), 1.3% (L_2) and 1.2% (L_3) for the three layout vaults respectively. Table 7.1 shows the differences in key variables between the matched and optimised performances for each of the vaults. Penalties were not incurred in any of the optimised performances.

Table 7.1. Differences between matched simulations (M) and simulations optimised for maximum rotation potential (O)

		L_1			L_2			L_3		
		M	O	% Diff.	M	O	% Diff.	M	O	% Diff.
$P_{z,to}$	(m)	2.34	2.29	-2.3%	2.36	2.30	-2.2%	2.34	2.31	-1.3%
$V_{z,to}$	($m\,s^{-1}$)	2.75	2.52	-8.5%	2.93	2.54	-13.2%	2.73	2.45	-10.0%
t_c	(s)	0.18	0.17	-6.4%	0.19	0.18	-3.7%	0.18	0.18	-1.7%
t_{pf}	(s)	0.91	0.87	-4.8%	0.94	0.87	-7.0%	0.91	0.86	-5.0%
H	($kg\,m^2\,s^{-1}$)	101.7	108.7	6.8%	100.9	110.4	9.4%	103.6	110.8	6.9%
ϕ	(SS)	1.84	1.86	1.1%	1.87	1.89	1.3%	1.86	1.89	1.2%
h_{pf}	(m)	2.73	2.61	-4.3%	2.79	2.63	-6.7%	2.72	2.61	-3.8%

Nomenclature: $P_{z,to}$ vertical position of the gymnast's centre of mass at take-off from the table, $V_{z,to}$ vertical velocity of the gymnast's centre of mass at take-off from the table, t_c duration of table contact, t_{pf} post-flight time, H angular momentum at take-off from the table, ϕ rotation potential measured in straight somersaults (SS) and h_{pf} post-flight height.

As shown in Table 7.1 the increases in rotation potential were achieved through higher angular momenta at take-off. The optimised techniques did, however, result in lower

vertical centre of mass velocities at take-off, with associated decreases in post-flight height. The technique changes that facilitated the increases in rotation potential will be considered for vault L_1 as the results for this vault were representative of the results of the three vaults considered.

Joint Angles

The joint angle time histories, for each of the torque-driven joints, are compared for the matched and optimised simulations in Figure 7.3. Overall there was a high level of similarity between the matched and optimised joint angle time histories. The most marked difference can be seen in the wrist angles, where the optimised simulation exhibited greater wrist extension than the matched simulation. Other differences were that in the optimised simulation the shoulders extended more and the knees began to flex later than in the matched simulation.

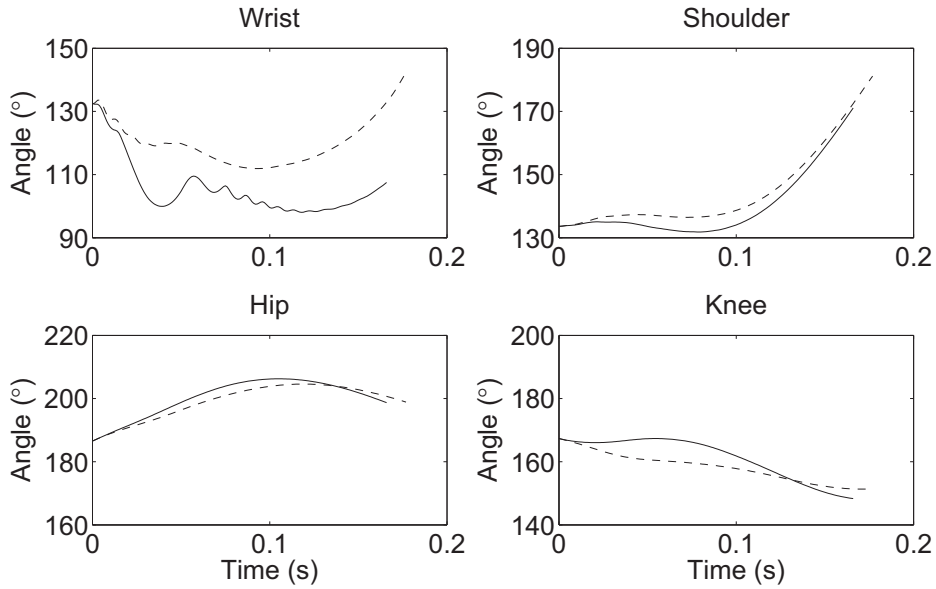

Figure 7.3. Comparison of joint angle time histories for L_1: matched simulation (dashed lines) and simulation optimised for maximum rotation potential (solid lines).

Joint Torque Activation Profiles

The torque generator activation profiles of the matched and optimised simulations are compared in Figure 7.4. Again, the most marked difference was at the wrist. In the optimised simulation the wrist extensors were activated to a higher level than the wrist flexors throughout the table contact phase. This was in contrast to the matched simulation where the wrist flexors were predominantly activated to a substantially higher level than the wrist extensors. In the matched simulation, the wrists were actively flexed to prevent hyper-extension of the wrist. The low level of activation of the wrist flexors dur-

ing the optimised simulation indicates that the technique employed relied on the passive component at the wrists to resist the tendency for the joint angle to decrease during the contact phase.

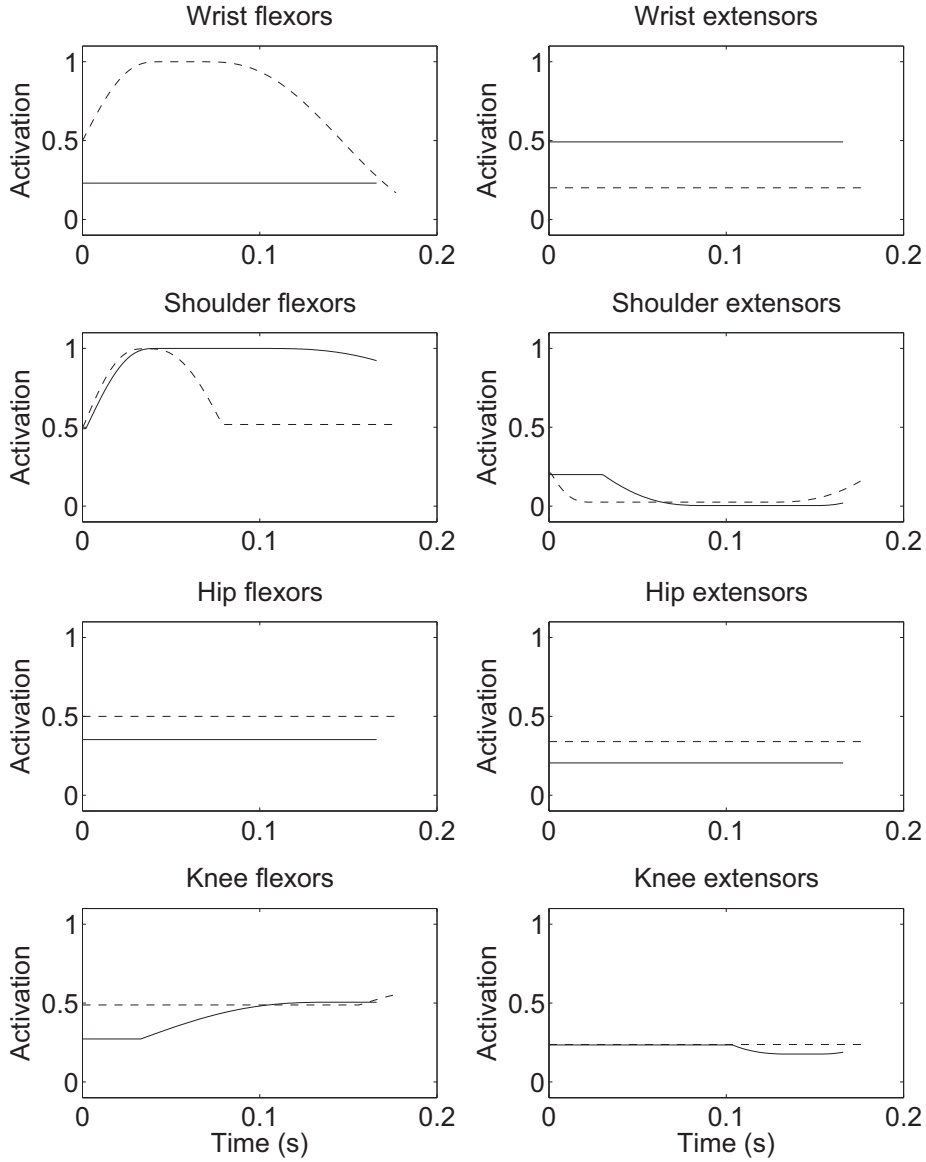

Figure 7.4. Comparison of torque generator activation profiles for L_1: matched simulation (dashed lines) and simulation optimised for maximum rotation potential (solid lines).

Another notable difference was found at the shoulder. The shoulder flexor activation profile of the optimised simulation deviated from that of the matched simulation during the latter part of the contact phase. Conversely, the shoulder extensor activation profile deviated from that of the matched simulation during the initial part of the contact phase. These differences led to the shoulders extending more in the optimised simulation than in the matched simulation as seen in Figure 7.3.

Joint Torques

The joint torque time histories are compared for the matched and optimised simulations in Figure 7.5, where positive torques represent extension and negative torques represent flexion. The joint torques time histories of the shoulder, hip and knee were generally similar for the matched and optimised simulations, with slight differences due to variations in the levels of activation of the torque generators.

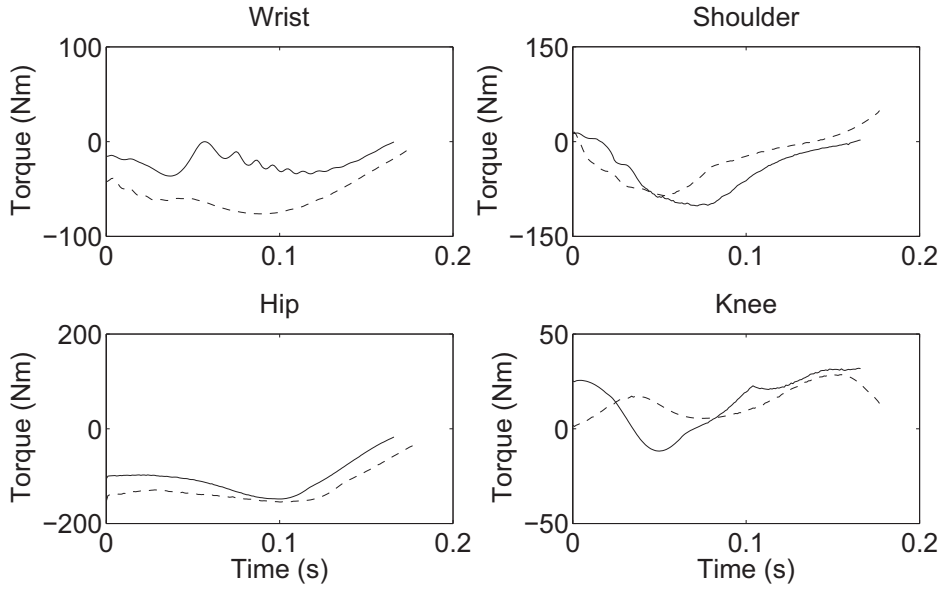

Figure 7.5. Comparison of joint torque time histories for L_1: matched simulation (dashed lines) and simulation optimised for maximum rotation potential (solid lines).

On the other hand the wrist joint torque time history of the optimised simulation was substantially different from that of the matched simulation. While both simulations had torques that acted to flex the wrists, the magnitude of the torque was less in the optimised simulation. Furthermore, the torque acting at the wrist fluctuated in the optimised simulation, whereas there is a more smooth variation in torque in the matched simulation.

The optimised simulation, resulted in relatively similar levels of activation of the wrist extensors and flexors as shown in Figure 7.4. The active torque component was therefore not substantial, and the torque that acted to flex the wrist was, to a large degree, due to the passive component as shown in Figure 7.6 (right). This was not the case for the matched simulation (Figure 7.6 (left)), where the wrist was actively flexed and the passive torque contribution was small in comparison to the active torque contribution.

As discussed in Section 5.3.3, the passive torque acting at the wrist joint was solely a function of the wrist angle, and was independent of the angular velocity of the wrist. The

fluctuations in the level of torque acting at the wrist during the optimised simulation, can be explained as a result of the passive element accelerating and decelerating the wrist.

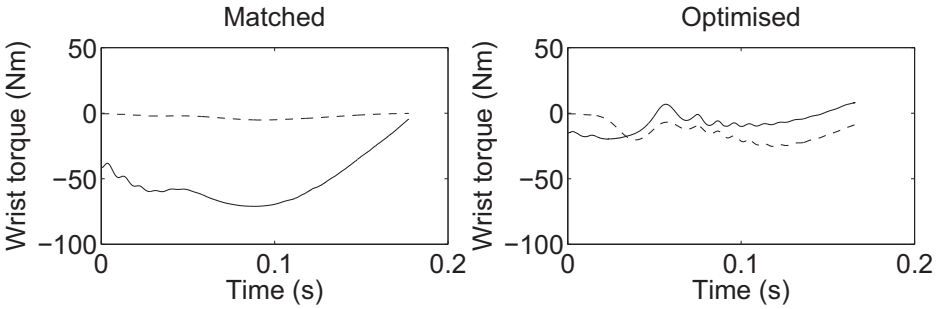

Figure 7.6. Comparison of passive (dashed lines) and active (solid lines) contributions to wrist torque during the matched (left) and optimised (right) simulations of L_1.

7.2.2.2 Optimisation for Maximum Post-flight Height

Optimisation of the contact phase technique for maximum post-flight height showed there was very little potential for improvement, with increases of only 0.01 m (L_1), 0.02 m (L_2) and 0.05 m (L_3). While vault L_3 did have a higher increase in height than the other two vaults, this was partially due to the matched performance of this vault having the lowest post-flight height of the three vaults. Table 7.2 shows the differences in key variables between the matched and optimised performances for each of the vaults. Again, no penalties were incurred in any of the optimised performances.

Table 7.2. Differences between matched simulations (M) and simulations optimised for maximum post-flight height (O)

		L_1			L_2			L_3		
		M	O	% Diff.	M	O	% Diff.	M	O	% Diff.
$P_{z,to}$	(m)	2.34	2.36	0.9%	2.36	2.38	1.1%	2.34	2.35	0.7%
$V_{z,to}$	($m\,s^{-1}$)	2.75	2.73	-0.8%	2.93	2.90	-0.9%	2.73	2.86	4.7%
t_c	(s)	0.18	0.19	4.5%	0.19	0.20	4.5%	0.18	0.18	0.6%
t_{pf}	(s)	0.91	0.91	0.0%	0.94	0.94	0.0%	0.91	0.93	2.4%
H	($kg\,m^2\,s^{-1}$)	101.7	101.1	-0.6%	100.9	101.5	0.6%	103.6	101.1	-2.4%
ϕ	(SS)	1.84	1.84	0.0%	1.87	1.89	0.9%	1.86	1.87	0.5%
h_{pf}	(m)	2.73	2.74	0.6%	2.79	2.81	0.6%	2.72	2.77	2.0%

Nomenclature: $P_{z,to}$ vertical position of the gymnast's centre of mass at take-off from the table, $V_{z,to}$ vertical velocity of the gymnast's centre of mass at take-off from the table, t_c duration of table contact, t_{pf} post-flight time, H angular momentum at take-off from the table, ϕ rotation potential measured in straight somersaults (SS) and h_{pf} post-flight height.

In each case the optimised technique did not differ substantially from the technique employed in the matched simulation. This result suggests there was little potential for the gymnast to increase post-flight height through changes in contact phase technique. As the optimised performances were very similar to the matched performances, further analysis of the results is not presented.

7.2.3 Technique Optimisation Summary

The simulation model was applied to determine:

What is the optimum table contact technique for handspring somersault vaults?

The results of the technique optimisation suggest that the gymnast's table contact phase technique was very close to the optimal technique. There was limited scope to increase rotation potential or post-flight height through changes in contact phase technique. The implications of these findings will be discussed in Section 7.5.

7.3 Performance Optimisation

In terms of performance optimisation the question that this study is trying to answer is:

What is the optimal body configuration at table contact to maximise vaulting performance, for given pre-flight conditions?

The gymnast's pre-flight angular momentum and centre of mass trajectory are determined during the approach and vaulting board contact phases of the vault, and therefore are limited by the speed with which the gymnast approaches the vaulting table and the vaulting board technique. The gymnast's body configuration at table contact is not so limited, as the gymnast can change configuration during the pre-flight phase. Optimisations were carried out to determine the optimal body configuration at table contact to maximise vaulting performance. Maximal performance was again considered in two ways: maximum rotation potential and maximum post-flight height.

7.3.1 Performance Optimisation Methods

Vaulting performance was optimised by varying the gymnast's configuration at table contact and the contact phase technique whilst maintaining the pre-flight conditions of

the matched performance. The orientation of the head + upper trunk segment and the shoulder and hip angles were varied along with 56 muscle activation parameters to search for optimal performances. Performances were optimised for maximum rotation potential and maximum post-flight height. Details of the method used to determine the initial conditions such that the gymnast had the same angular momentum at table contact and was on the same parabolic pre-flight trajectory as the matched performance are given below, along with details of the objective functions.

7.3.1.1 Initial Conditions

The configuration of the gymnast at table contact was defined by three angles: orientation angle θ_{OR}, shoulder angle θ_S and hip angle θ_H, as illustrated in Figure 7.7. These three angles were varied to modify the gymnast's configuration at table contact.

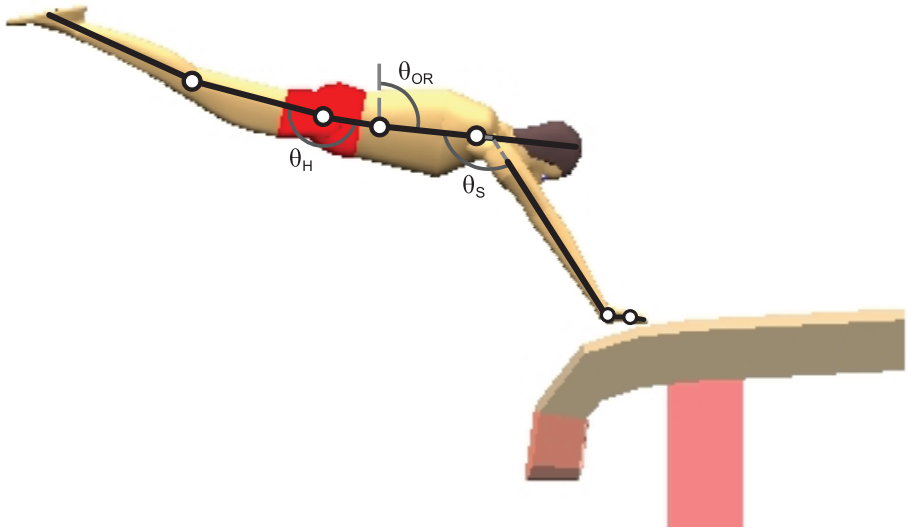

Figure 7.7. Gymnast configuration at table contact: θ_{OR} orientation angle, θ_S shoulder angle and θ_H hip angle.

The lower and upper bounds of the orientation angle were set 40° below and above the mean orientation angle at table contact of the matched performances. The lower and upper bounds of the shoulder and hip angles were set based on anatomical constraints and reasonably expected values. The lower and upper bounds are given in Table 7.3.

Table 7.3. Lower and upper bounds of the contact configuration

Angle		Lower bound	Upper bound
Orientation angle	θ_{OR}	55°	135°
Shoulder angle	θ_S	90°	185°
Hip angle	θ_H	160°	200°

For each simulated configuration the resulting centre of mass position ($P_{y,c}$, $P_{z,c}$) at table contact was determined. Any simulation for which the configuration resulted in a centre of mass position lower than the fingers or a shoulder position horizontally in front of the fingers, was aborted and heavily penalised. These two constraints limited the solution space to that which contained reasonable combinations of angles.

The horizontal and vertical velocities of the gymnast's centre of mass and the angular velocity of the head + upper trunk segment were determined such that the gymnast had the same angular momentum at table contact and was on the same pre-flight trajectory as the matched performance. The horizontal velocity of the gymnast's centre of mass was assumed to be constant during pre-flight and therefore the horizontal velocity of the gymnast's centre of mass just prior to table contact was the same as that in the matched performance.

It was assumed that the only force acting on the gymnast in the vertical direction was gravity and therefore the centre of mass of the gymnast was assumed to be constantly accelerating in the vertical direction. The vertical velocity of the gymnast's centre of mass was determined using a constant acceleration equation, based on the position and velocity of the gymnast's centre of mass at table contact in the matched performance:

$$V_{z,c}{}^2 = V_{z,c_m}{}^2 + 2g\,(P_{z,c} - P_{z,c_m}) \tag{7.6}$$

where $V_{z,c}$ is the vertical velocity of the centre of mass at table contact for a given vertical centre of mass position $P_{z,c}$, P_{z,c_m} and V_{z,c_m} are the vertical position and velocity of the centre of mass at table contact for the matched performance and g is -9.81 m s^{-2}.

Analysis of Equation 7.6 shows that there is a limit on the height of the gymnast's centre of mass at table contact:

$$P_{z_{\text{limit}}} = P_{z,c_m} - \frac{V_{z,c_m}{}^2}{2g} \tag{7.7}$$

where $P_{z_{\text{limit}}}$ is the maximum possible centre of mass height. Any simulation for which the configuration resulted in a centre of mass height higher than $P_{z_{\text{limit}}}$ was aborted and heavily penalised.

The angular momentum of the gymnast H, can be considered to be composed of two parts:

$$H = H_{\text{whole body}} + H_{relative} \tag{7.8}$$

where $H_{\text{whole body}}$ is the angular momentum of the body as a whole and $H_{relative}$ is the

angular momentum due to movements of segments relative to the base segment (Yeadon, 1990b). In this case the head + upper trunk segment was considered the base segment.

During optimisation, the initial velocities of each segment relative to the base segment were maintained at the values obtained in the matched performances. Thus, for a given configuration, $H_{relative}$ was known. $H_{\text{whole body}}$ is given by:

$$H_{\text{whole body}} = I_{\text{whole body}}\,\omega_{OR} \tag{7.9}$$

where $I_{\text{whole body}}$ is the moment of inertia of the gymnast about the mass centre, and ω_{OR} is the angular velocity of the base segment. For a given configuration $I_{\text{whole body}}$ was known. Thus, ω_{OR} was determined such that the total angular momentum of the gymnast about the mass centre was the same as that in the matched performance.

7.3.1.2 Objective Functions

A genetic algorithm (Carroll, 2001) was used to determine the configuration at table contact and the contact phase technique that resulted in, firstly, maximum rotation potential and, secondly, maximum post flight height. Again, two objective functions were used. In the first case the objective function simply maximised rotation potential, while in the second case the objective function maximised post-flight height with a constraint on rotation potential, in that a penalty was incurred if the performance had less rotation potential at table take-off than the matched performance. A number of additional penalties were included in both objective functions:

- Joint angle constraint penalties as described in Section 6.5.3.1, which penalised simulations if the joint angles went outside the acceptable range of motion.

- Post-flight time penalties, which penalised simulations if the length of the post-flight was below 90% of that of the matched simulation (Section 7.2.1.2).

- Contact phase duration penalties, which penalised simulations if the duration of the contact phase was below 90% of the lowest recorded performance value of 150 ms. A penalty of -1 was incurred for each 100 ms that the table contact phase was below 135 ms. This constraint ensured that simulations were not substantially different from the recorded performances.

7.3.2 Performance Optimisation Results

7.3.2.1 Optimisation for Maximum Rotation Potential

Optimisation of vaulting performance showed that rotation potential could be increased through changes in the gymnast's configuration at table touchdown and contact phase technique. Table 7.4 shows the differences in key variables between the matched and optimised performances of vault L_3. This vault was chosen as it was representative of the results obtained for layout vaults. The optimised simulation incurred a penalty of -0.001 as the contact phase was at the lower limit of duration, but did not incur any joint angle constraint penalties.

Table 7.4. Differences between matched simulation of L_3 and simulation optimised for maximum rotation potential when contact configuration was varied

		Matched	Optimised	% Difference
θ_{OR}	(°)	96.0	119.5	24.5%
θ_S	(°)	137.0	173.0	26.2%
θ_H	(°)	178.5	166.2	-6.9%
$P_{z,to}$	(m)	2.34	2.19	-6.3%
$V_{z,to}$	($m\,s^{-1}$)	2.73	3.14	15.1%
t_c	(s)	0.18	0.13	-24.3%
t_{pf}	(s)	0.91	0.94	4.2%
H	($kg\ m^2\ s^{-1}$)	103.6	116.1	12.1%
ϕ	(SS)	1.86	2.05	9.8%
h_{pf}	(m)	2.72	2.69	-0.9%

Nomenclature: θ_{OR} orientation angle, θ_S shoulder angle, θ_H hip angle, $P_{z,to}$ vertical position of the gymnast's centre of mass at take-off from the table, $V_{z,to}$ vertical velocity of the gymnast's centre of mass at take-off from the table, t_c duration of table contact, t_{pf} post-flight time, H angular momentum at take-off from the table, ϕ rotation potential measured in straight somersaults (SS) and h_{pf} post-flight height.

The 9.8% increase in rotation potential, as shown in Table 7.4, was achieved through a higher angular momentum at take-off from the vaulting table, and a longer post-flight time. Although the optimised configuration and technique resulted in a higher vertical centre of mass velocity at take-off, as the height of the gymnast's centre of mass at take-off was lower than that in the matched simulation there was a small decrease of 0.03 m in post-flight height. The configuration and technique changes that facilitated the increase in rotation potential will be considered in the following sections.

Gymnast's Configuration at Table Contact

Visual representations of the table contact phase during the matched simulation and the optimised simulation of L_3 are given in Figure 7.8, and show substantial differences in the configuration of the gymnast at table contact. For instance the optimised configuration had a higher orientation angle and a more open shoulder angle on contact with the vaulting table (also seen in Table 7.4). The configuration at take-off was similar for the two simulations, although in the optimised simulation the shoulder was again more flexed.

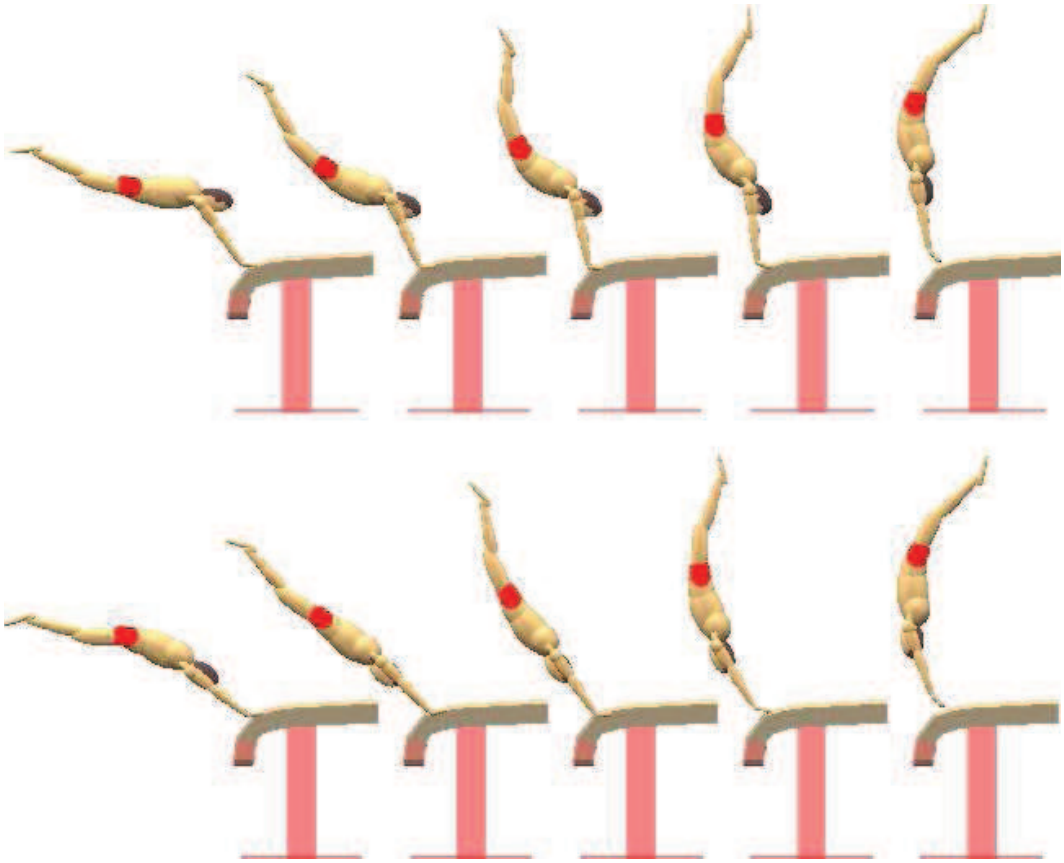

Figure 7.8. Visual comparison of simulations of the table contact phase of L_3 with different contact configurations and table contact phase techniques: matched simulation (upper), simulation optimised for maximum rotation potential (lower).

Joint Angles

The joint angle time histories, for each of the torque-driven joints, are compared for the matched and optimised simulations of L_3 in Figure 7.9. There is a reasonable level of similarity between the matched and optimised joint angle time histories, especially in terms of the shape of the profiles. The most marked difference can be seen in the shoulder angles. In the optimised simulation there was a higher level of shoulder flexion at table contact and the shoulder remained more flexed throughout the contact phase.

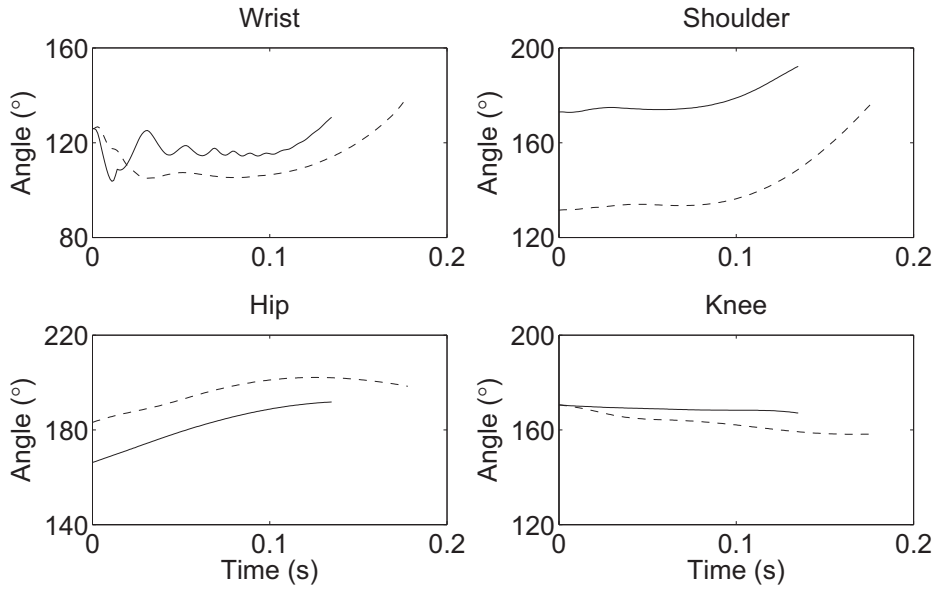

Figure 7.9. Comparison of joint angle time histories for L_3: matched simulation (dashed lines) and simulation optimised for maximum rotation potential with different contact configuration (solid lines).

Another evident difference is at the wrist joint. While the joint angles were similar in magnitude, the joint angle fluctuated in the optimised simulation, whereas there was a more smooth variation in joint angle in the matched simulation. This is an indication that the wrist was less active in the optimised simulation, and that the passive component was acting to prevent hyper-extension of the wrist.

Joint Torque Activation Profiles

The torque generator activation profiles of the matched and optimised simulations of L_3 are compared in Figure 7.10, where differences can be seen at each joint. The most marked difference was at the wrist. The technique employed in the optimised simulation used similar levels of activation of the wrist extensors and flexors whereas in the matched simulation the wrist flexors were predominantly more highly activated than the wrist extensors. Thus the wrist was less active in the optimised simulation, as suggested by the joint angle time history (Figure 7.9).

The other most notable difference was at the shoulder. The flexor profile ramped up during the optimised simulation, whereas during the matched simulation the activation level remained constant. The shoulder flexor profile of the matched simulation was, however, atypical of layout vaults: the typical activation profile of the shoulder flexors ramps up during the initial part of the contact phase, similar to that found for the optimised simulation. This can be seen in Figure 7.4 for the matched simulation of L_1.

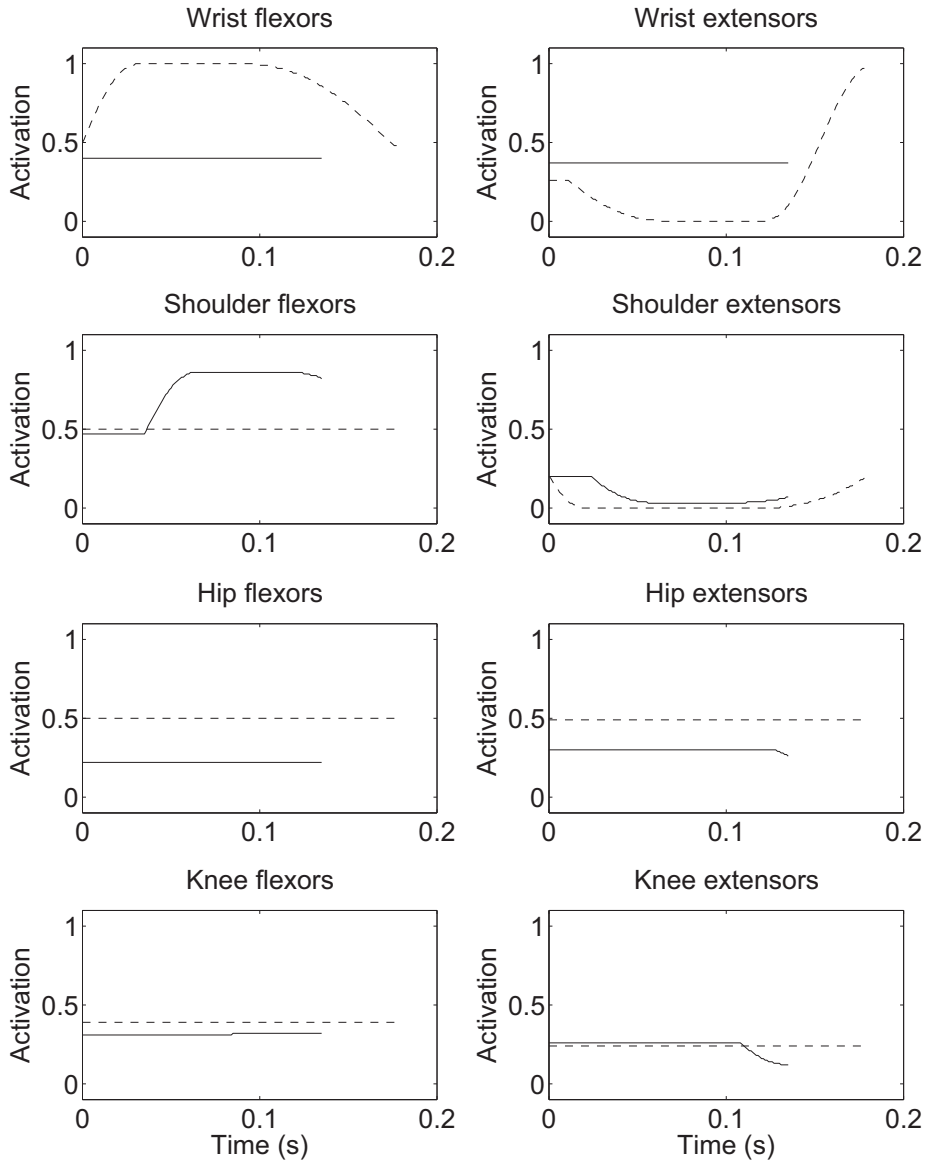

Figure 7.10. Comparison of torque generator activation profiles for L_3: matched simulation (dashed lines) and simulation optimised for maximum rotation potential with different contact configuration (solid lines).

Joint Torques

The joint torque time histories are compared for the matched and optimised simulations of L_3 in Figure 7.11, where positive torques represent extension and negative torques represent flexion. Again, differences were evident at each joint. At the wrist and hip joints, flexor torques acted during both simulations, however, the magnitude of the torques was substantially smaller during the optimised simulation in each case.

Extensor torques were also shown to initially act about the shoulder during the optimised simulation, whereas during the matched simulation flexor torques initially acted about the shoulder. The shoulder angle of the optimised simulation was initially more open

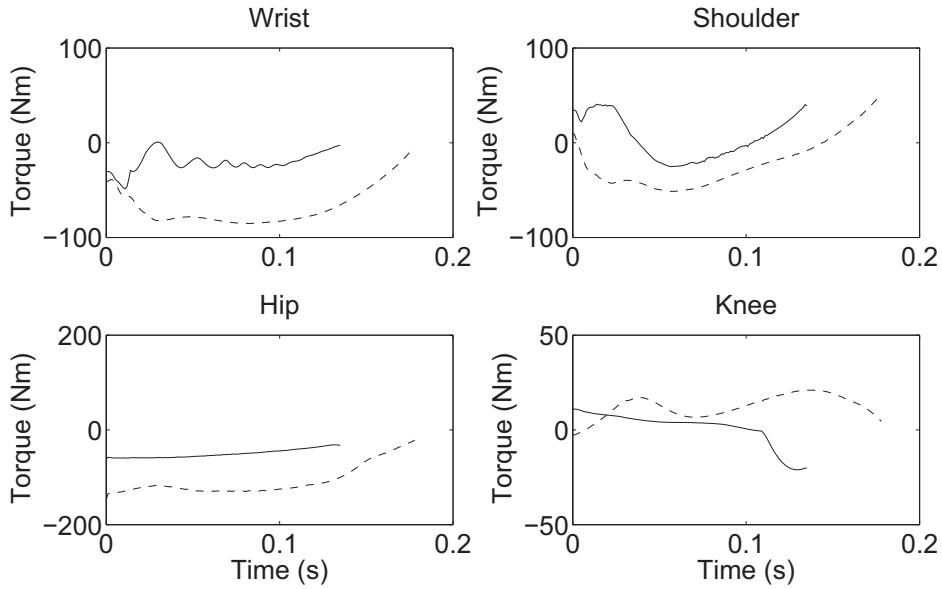

Figure 7.11. Comparison of joint torque time histories for L_3: matched simulation (dashed lines) and simulation optimised for maximum rotation potential with different contact configuration (solid lines).

than in the matched simulation and therefore extensor torques were expected to prevent hyper-flexion of the shoulder. The shape of the shoulder torque profiles were more similar during the latter part of the contact phase, although the matched profile lagged behind the optimised profile. This is not surprising, as the duration of the contact phase was shorter during the optimised simulation than during the matched simulation.

Summary of Rotation Potential Optimisation Results

When the gymnast's configuration at table contact was varied in conjunction with table contact phase technique, rotation potential could be increased by 9.8%. The optimised simulation had a higher orientation angle and also a more open shoulder angle at contact with the vaulting table than the matched simulation. The optimised simulation also required lower activation of the majority of the torque generators. The duration of the contact phase was at the imposed lower limit during the optimised simulation, which suggests that a short contact time is desirable when maximising rotation potential.

7.3.2.2 Optimisation for Maximum Post-flight Height

Optimisation of vaulting performance showed that post-flight height could be increased whilst maintaining the rotation potential required to perform a handspring forward with salto forward stretched, through changes in the gymnast's configuration at table touch-down and contact phase technique. Table 7.5 shows the differences in key variables

between the matched and optimised performances of vault L_3. The optimised solution did not incur any penalties.

Table 7.5. Differences between matched simulation of L_3 and simulation optimised for maximum post-flight height when contact configuration was varied

		Matched	Optimised	% Difference
θ_{OR}	(°)	96.0	117.1	22.0%
θ_S	(°)	137.0	171.1	24.9%
θ_H	(°)	178.5	160.0	-10.4%
$P_{z,to}$	(m)	2.34	2.26	-3.3%
$V_{z,to}$	($\mathrm{m\,s^{-1}}$)	2.73	3.43	25.8%
t_c	(s)	0.18	0.16	-12.1%
t_{pf}	(s)	0.91	1.00	10.5%
H	($\mathrm{kg\ m^2\,s^{-1}}$)	103.6	96.7	-6.6%
ϕ	(SS)	1.86	1.86	0.0%
h_{pf}	(m)	2.72	2.86	5.3%

Nomenclature: θ_{OR} orientation angle, θ_S shoulder angle, θ_H hip angle, $P_{z,to}$ vertical position of the gymnast's centre of mass at take-off from the table, $V_{z,to}$ vertical velocity of the gymnast's centre of mass at take-off from the table, t_c duration of table contact, t_{pf} post-flight time, H angular momentum at take-off from the table, ϕ rotation potential measured in straight somersaults (SS) and h_{pf} post-flight height.

The 0.14 m increase in post-flight height was achieved through a substantially higher vertical centre of mass velocity at take-off from the vaulting table, which resulted in an increase in the duration of post-flight. While the angular momentum at take-off from the table was 6.6% lower than the matched simulation, the rotation potential was the same due to the increased duration of post-flight. The configuration and technique changes that facilitated the increase in post-flight height will be considered in the following sections.

Gymnast's Configuration at Table Contact

Visual representations of the table contact phase during the matched simulation and the optimised simulation are given in Figure 7.12, and show substantial differences in the configuration of the gymnast at table contact. The optimised configuration at table contact was similar to that found when optimising for rotation potential, in that the gymnast had a higher orientation angle at contact and a more open shoulder angle.

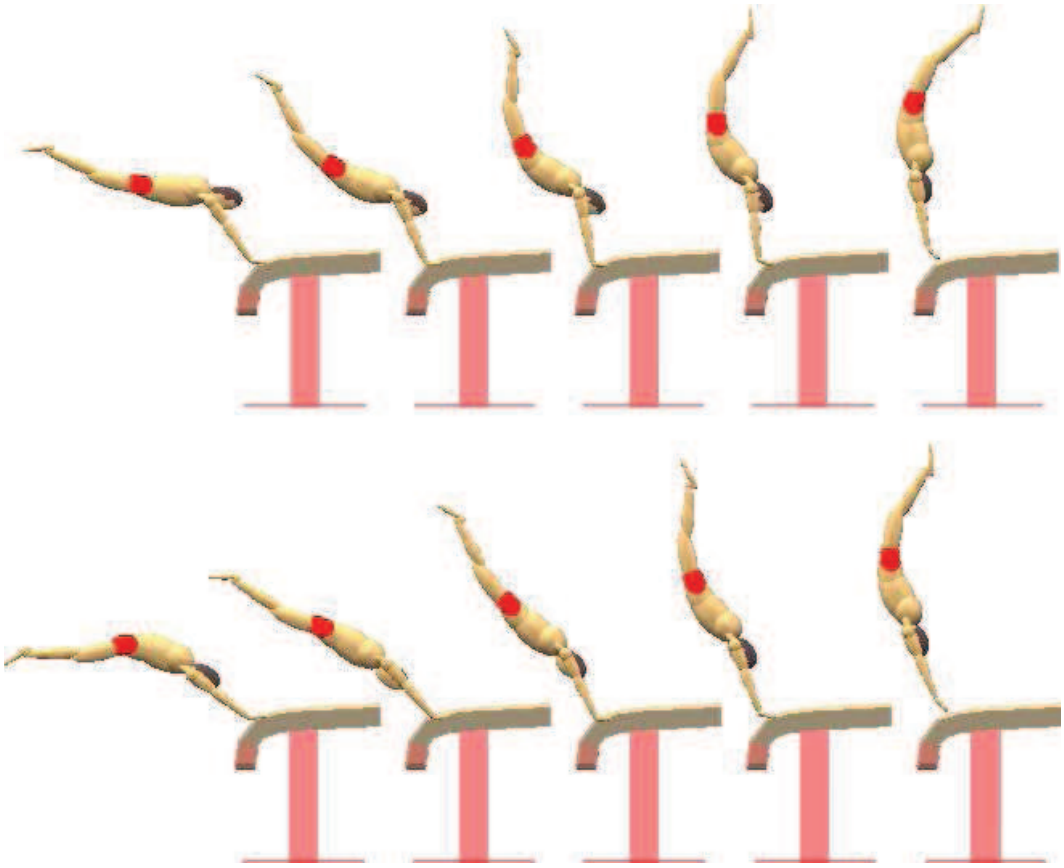

Figure 7.12. Visual comparison of simulations of the table contact phase of L_3 with different contact configurations and table contact phase techniques: matched simulation (upper), simulation optimised for maximum post-flight height (lower).

Joint Angles

The joint angle time histories, for each of the torque-driven joints, are compared for the matched and optimised simulations in Figure 7.13. The most evident differences were at the time of contact, where the shoulder and hip joint angles differed substantially between the two simulations. These shoulder and hip joint angles did, however, tend towards similar angles at the end of the contact phase.

Another notable difference was at the wrist, where the joint angle was more variable in the optimised simulation than in the matched simulation. This was also the case when performance was optimised to maximise rotation potential. The wrist angle time histories did, however, become more similar towards the end of the table contact phase, with very similar wrist angles at take-off.

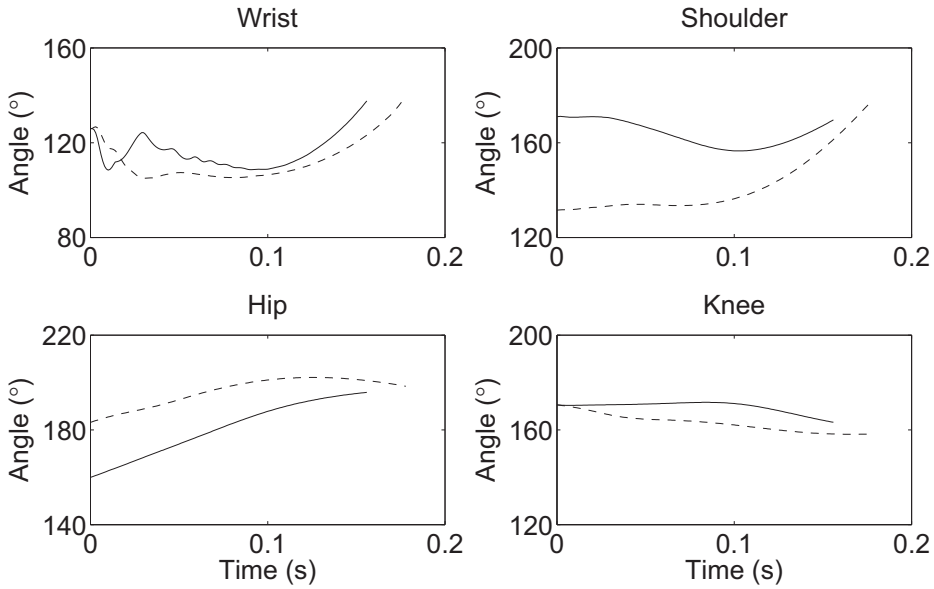

Figure 7.13. Comparison of joint angle time histories for L_3: matched simulation (dashed lines) and simulation optimised for maximum post-flight height with different contact configuration (solid lines).

Joint Torque Activation Profiles

The torque generator activation profiles of the matched and optimised simulations are compared in Figure 7.14, where the most marked differences can be seen at the wrist. The technique employed in the simulation optimised for height used similar levels of activation of the wrist extensors and flexors, which is similar to the technique that was employed in the simulation optimised for rotation potential (Figure 7.10). In the matched simulation, on the other hand, the wrist flexors were predominantly activated to a higher level than the wrist extensors.

The activation profiles of the shoulder, hip and knee torque generators were reasonably similar in the matched and optimised simulations. At each of these joints the extensor and flexor torque generators were co-contracted at similar activation levels.

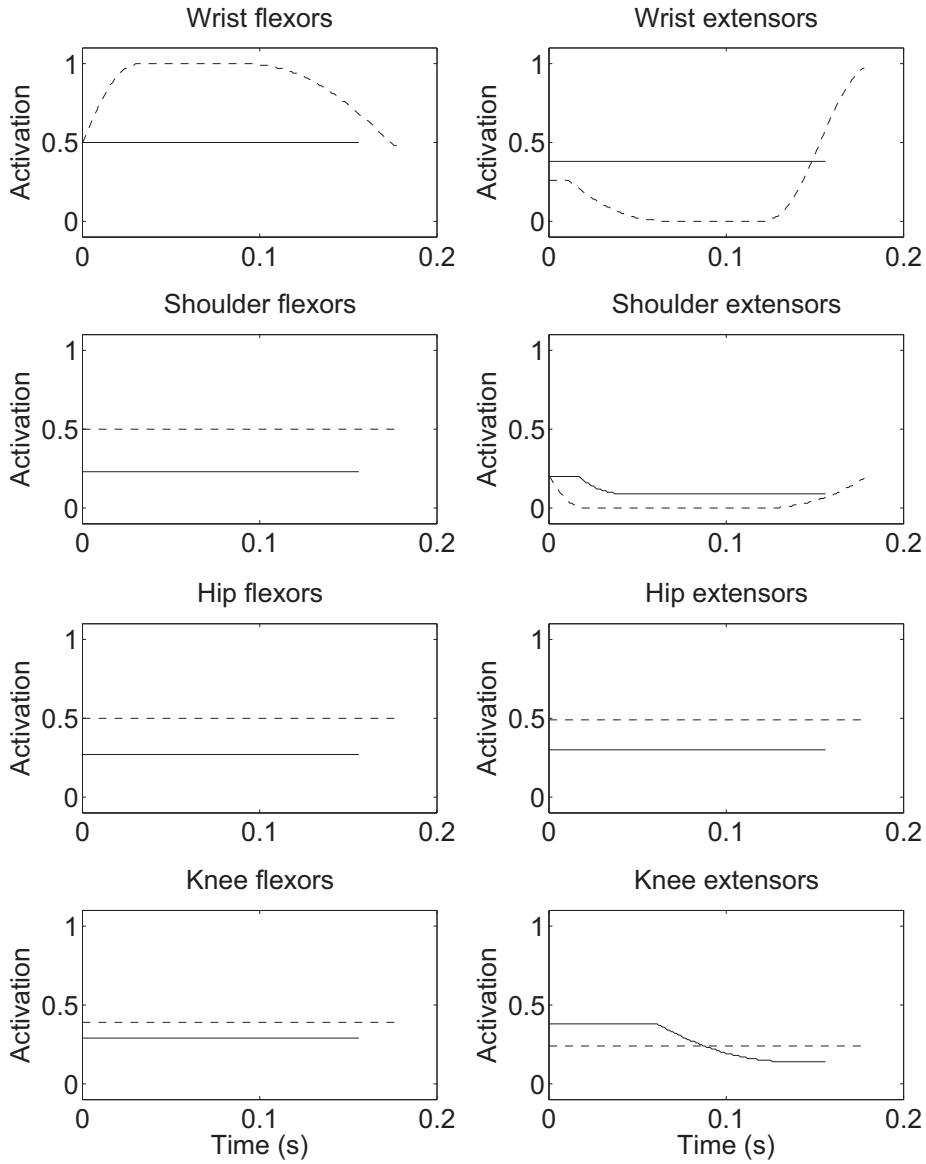

Figure 7.14. Comparison of torque generator activation profiles for L_3: matched simulation (dashed lines) and simulation optimised for maximum post-flight height with different contact configuration (solid lines).

Joint Torques

The joint torque time histories are compared for the matched and optimised simulations in Figure 7.15, where positive torques represent extension and negative torques represent flexion. The most notable difference was at the shoulder, where extensor torques initially acted during the optimised simulation, while during the matched simulation flexor torques initially acted about the shoulder. This result is similar to that found when the performance was optimised for maximum rotation potential and prevents hyper-flexion of the shoulder. The magnitude of the torques about the wrist and hip were generally lower throughout the contact phase in the optimised simulation. The torque about the knee was variable in each simulation, but of a low magnitude.

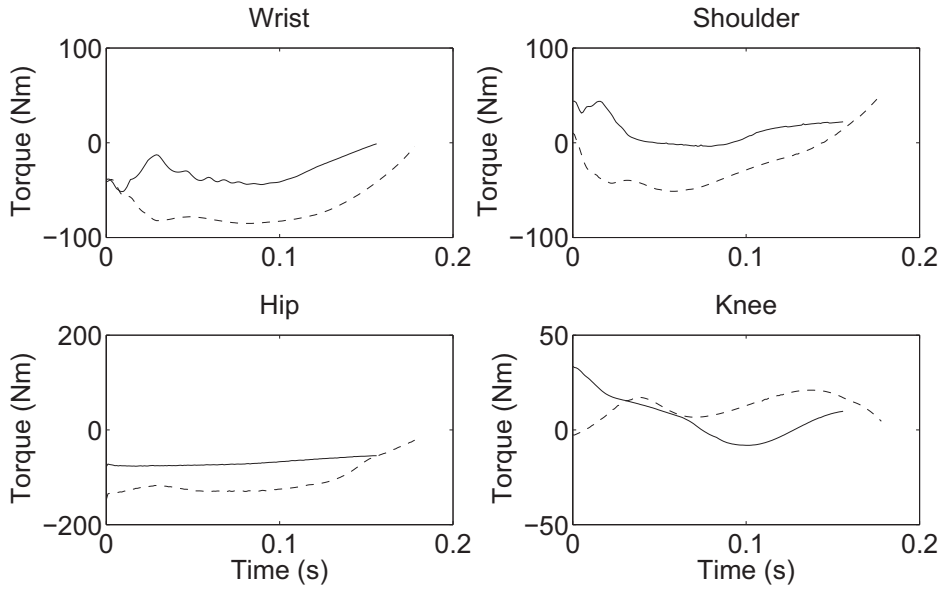

Figure 7.15. Comparison of joint torque time histories for L_3: matched simulation (dashed lines) and simulation optimised for maximum post-flight height with different contact configuration (solid lines).

Summary of Post-flight Height Optimisation Results

When the gymnast's configuration at table contact was varied in conjunction with table contact phase technique, post-flight height could be increased by 0.14 m whilst maintaining the rotation potential required to perform a handspring forward with salto forward stretched. The optimised simulation had a higher orientation angle and a more open shoulder angle on contact with the vaulting table than the matched simulation, and also required lower activation of the majority of the torque generators.

7.3.3 Performance Optimisation Summary

The simulation model was applied to determine:

What is the optimal body configuration at table contact to maximise vaulting performance, for given pre-flight conditions?

The results of the performance optimisation suggest that the optimal configuration at table contact is one in which the body is relatively straight, with a large shoulder angle. This configuration at table contact led to a decreased duration of the table contact phase and higher vertical velocity of the gymnast's centre of mass at take-off compared to the matched simulations. The implications of this result will be discussed in Section 7.5.

7.4 Performance Analysis

7.4.1 Relative Importance of Technique and Initial Conditions

There are two research questions that this study is trying to answer in terms of performance analysis. The first is:

How much does performance depend upon technique during the table contact phase and how much does performance depend on initial conditions?

The mechanics of the table contact phase is dependent on both the technique during the table contact phase and the initial table contact conditions. The relative importance of these factors is, however, not clear. Is it within a gymnast's capability to radically alter the performance of a vault during the table contact phase through technique modifications or is the performance of the vault largely pre-determined by the performance in preceding phases? Simulations were carried out, in which the contact phase technique was varied, to determine the importance of contact phase technique on vaulting performance.

7.4.1.1 Method

The gymnast's technique during the table contact phase was characterised by the activations of the torque generators acting at the wrist, shoulder, hip and knee joints, where activation of the torque generators represents activation of the muscles surrounding the joints. The technique employed in the matched simulation was considered to be the standard technique. Two simulations were subsequently run, in which the activation profiles were constrained, to determine the importance of contact phase technique on vaulting performance.

A 'constant activation' simulation was run in which the pre-contact activation levels of the matched simulation were maintained throughout the contact phase. In effect, the gymnast was co-contracting the extensors and flexors at each joint throughout the contact phase, with a constant level of activation. A 'zero activation' simulation was also run in which the activations were set to zero throughout the contact phase. In effect the gymnast was not exerting any active torques at the joints. The two performances were compared with the matched performance in terms of the conditions at take-off, the rotation potential and post-flight height achieved, and the gymnast's configuration throughout the contact phase.

7.4.1.2 Results

The differences in table take-off conditions and post-flight performance resulting from technique constraints are presented in Table 7.6 for vault L_2 as the results for this vault are representative of the results of the three vaults considered. Percentage differences are comparisons to the matched performance.

Table 7.6. Differences in performance with different table contact phase techniques.

		Matched	Constant activation		Zero activation	
				% Diff.		% Diff.
$P_{z,to}$	(m)	2.36	2.39	1.5%	2.34	-0.9%
$V_{z,to}$	($m\,s^{-1}$)	2.93	2.27	-22.5%	2.07	-29.2%
t_c	(s)	0.19	0.22	15.7%	0.21	12.5%
t_{pf}	(s)	0.94	0.85	-9.6%	0.81	-13.5%
H	($kg\ m^2\,s^{-1}$)	100.9	91.7	-9.2%	104.0	3.0%
ϕ	(SS)	1.87	1.65	-11.8%	1.75	-6.5%
h_{pf}	(m)	2.79	2.65	-5.0%	2.55	-8.6%

Nomenclature: $P_{z,to}$ vertical position of the gymnast's centre of mass at take-off from the table, $V_{z,to}$ vertical velocity of the gymnast's centre of mass at take-off from the table, t_c duration of table contact, t_{pf} post-flight time, H angular momentum at take-off from the table, ϕ rotation potential measured in straight somersaults (SS) and h_{pf} post-flight height.

Substantial variations in contact phase technique resulted in considerable differences in the conditions at take-off, but only moderate differences in post-flight performance. When the technique was constrained such that the activation was held constant at the pre-contact activation levels, the rotation potential was reduced by 11.8% and the post-flight height was reduced by 0.14 m. When the technique was constrained such that there were no active torques, the rotation potential was reduced by 6.5% and the post-flight height was reduced by 0.24 m. In effect, the technique constraints would not prevent the gymnast from performing a vault, although the performance would be not be as good.

Visual representations of the table contact phase during the matched simulation, the constant activation simulation and the zero activation simulation are given for vault L_2 in Figure 7.16. There was reasonably close agreement between the matched performance and the constant activation simulation, but there were evident differences between the matched simulation and the zero activation simulation.

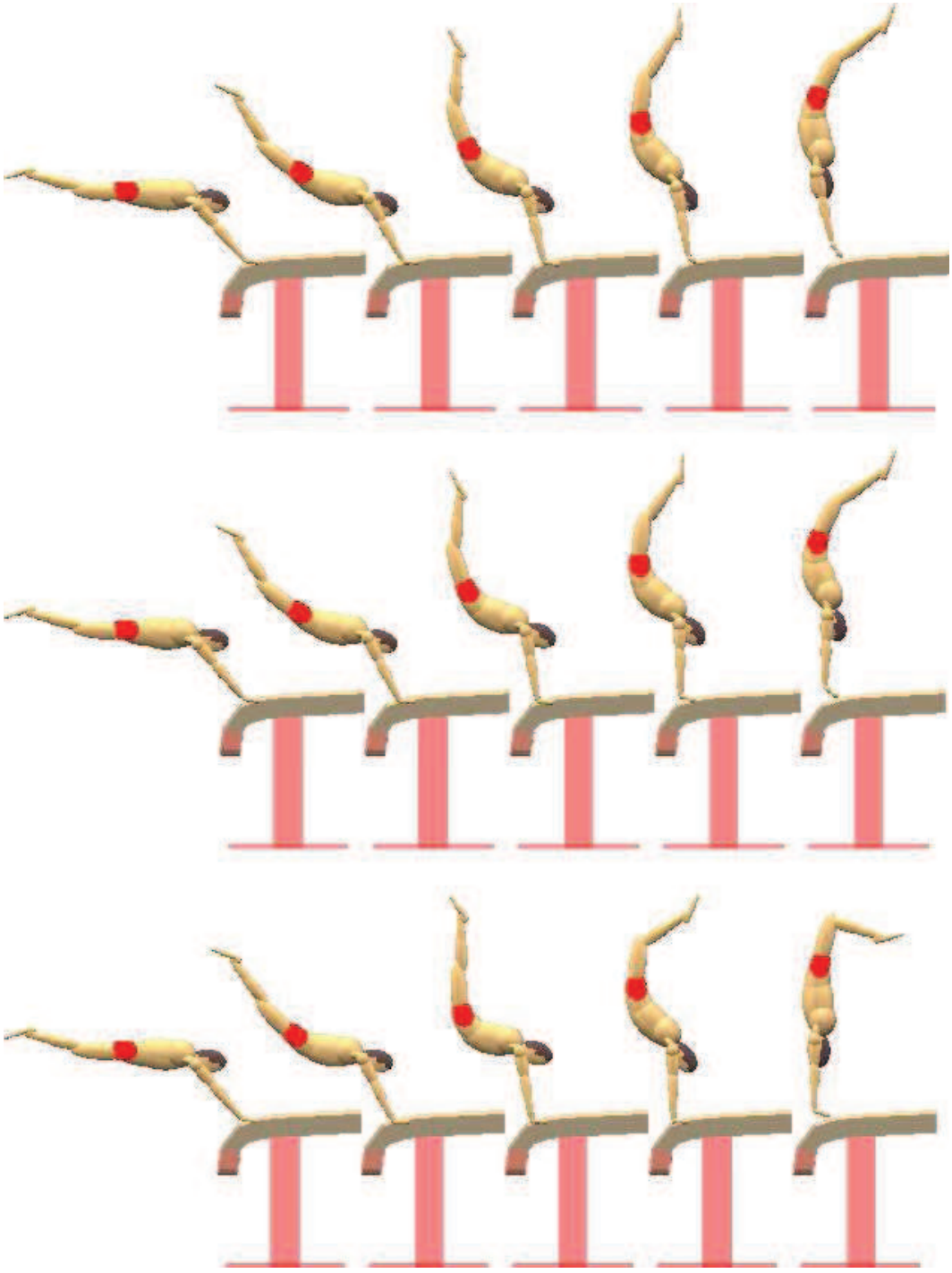

Figure 7.16. Visual comparison of simulations of the table contact phase of L_2 with different table contact phase techniques: matched simulation (upper), constant activation simulation (middle) and zero activation simulation (lower).

Differences in the gymnast's configuration throughout the contact phase are illustrated in Figure 7.17. Of note is that when the technique was constrained such that the activation was held constant at the pre-contact activation levels, the joints did not exceed the gymnast's range of motion (Figure 7.17 (left)). However, when the technique was constrained such that there were no active torques, the hip, wrist and knee joints all exceeded the gymnast's range of motion (Figure 7.17 (right)). Furthermore during the first 100 ms of post-flight, which is not shown in the figure, the shoulder also exceeded the gymnast's range of motion in the zero activation simulation, but not in the matched or constant activation simulations.

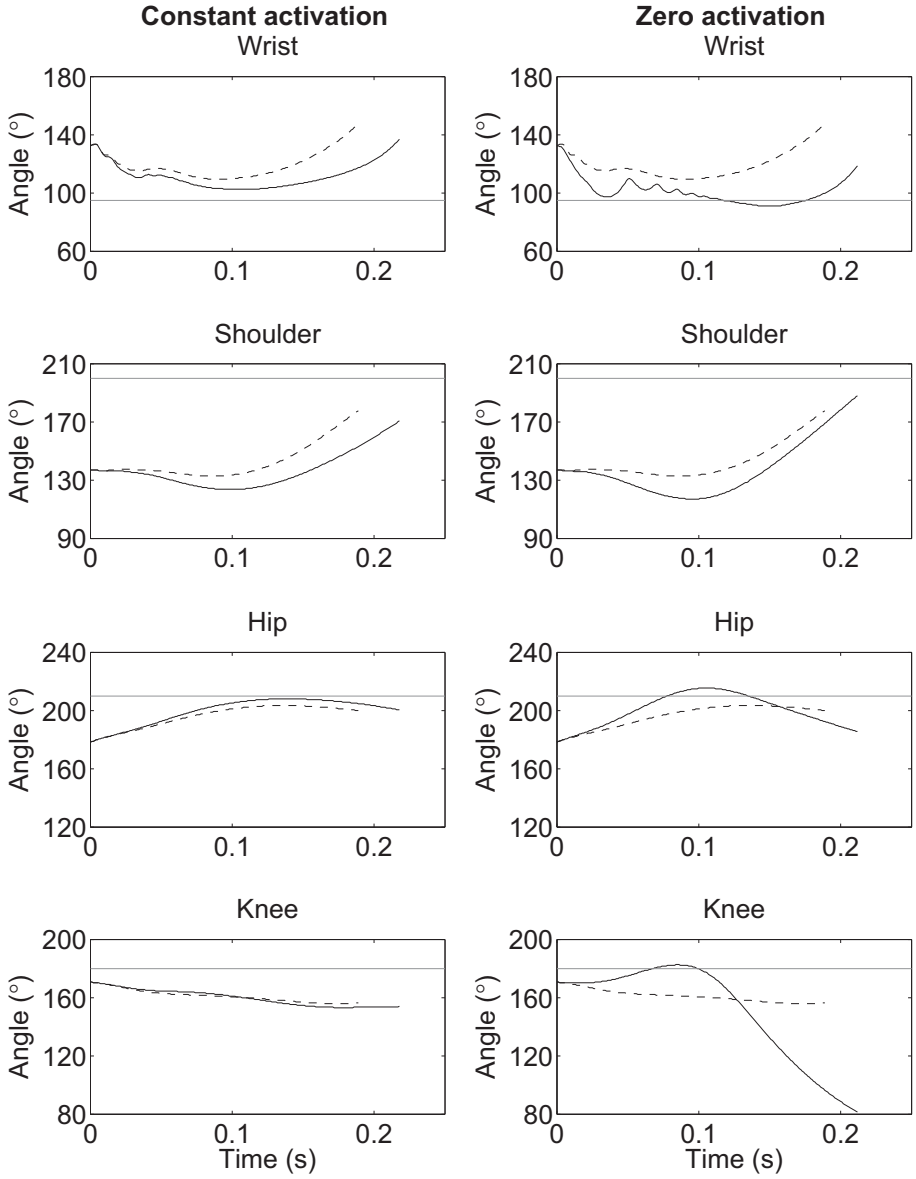

Figure 7.17. Comparison of joint angle time histories during the table contact phase of L_2 with different table contact phase techniques: Left - matched simulation (dashed lines) and constant activation simulation (solid lines), Right - matched simulation (dashed lines) and zero activation simulation (solid lines). In both cases the horizontal lines represent the limits of the gymnast's range of motion.

In the zero activation simulation, there was also substantial knee flexion during the latter part of the contact phase. This would decrease the moment of inertia of the gymnast about the mass centre, and increase the whole body angular velocity at take-off. Resisting this knee flexion using knee extensor torques, as in the matched simulation, will result in a greater decrease in the whole body angular momentum due to the reaction force at the hands. This accounts for the zero activation simulation having a slightly higher angular momentum at table take-off compared to the matched simulation (see Table 7.6). However, flexion of the knees during the table contact phase is not desirable as it would cause the gymnast to incur deductions for poor form.

The results suggest that performance of the vault is largely pre-determined by the performance in the phases preceding table contact, as considerable variations in technique during the table contact phase resulted in only moderate changes to post-flight performance. However, some degree of active torque is required not only to prevent joint angles from exceeding their anatomical limits, but also to allow the gymnast to maintain good form throughout the table contact phase. This result will be discussed in more detail in Section 7.5.

7.4.2 Angular Momentum of the Gymnast

The second research question that this study addresses in terms of performance analysis is:

For an optimal performance, how does the angular momentum about the gymnast's centre of mass change?

The gymnast will have angular momentum about the centre of mass on contact with the vaulting table. During the table contact phase of the vault, the gymnast interacts with the vaulting table and, therefore, the angular momentum about the centre of mass will change. It is generally accepted that angular momentum decreases during the table contact phase of a vault (Prassas et al., 2006). However, in contrast, Koh et al. (2003b) found that for a simulated optimal performance of a Yurchenko vault the angular momentum could be increased during the table contact phase. The simulation model was used to analyse the changes in angular momentum that occur during the table contact phase of handspring entry vaults.

7.4.2.1 Method

The simulation model of vaulting allowed the angular momentum about the gymnast's mass centre to be determined throughout the table contact phase. Within this study simulations that matched performance, and simulations that optimised performance were completed. The changes in angular momentum that occurred during the table contact phase of these simulations were compared.

7.4.2.2 Results

The angular momentum throughout the table contact phase is compared for different simulations of vault L_3 in Figure 7.18. In each graph the matched performance is represented with dashed lines and the optimised performance is represented with solid lines. The upper graphs show simulations in which only the contact phase technique was varied while the lower graphs show simulations in which the configuration at contact was varied in conjunction with contact phase technique. The left column shows simulations that were optimised for maximum rotation potential while the right column shows simulations that were optimised for maximum post-flight height.

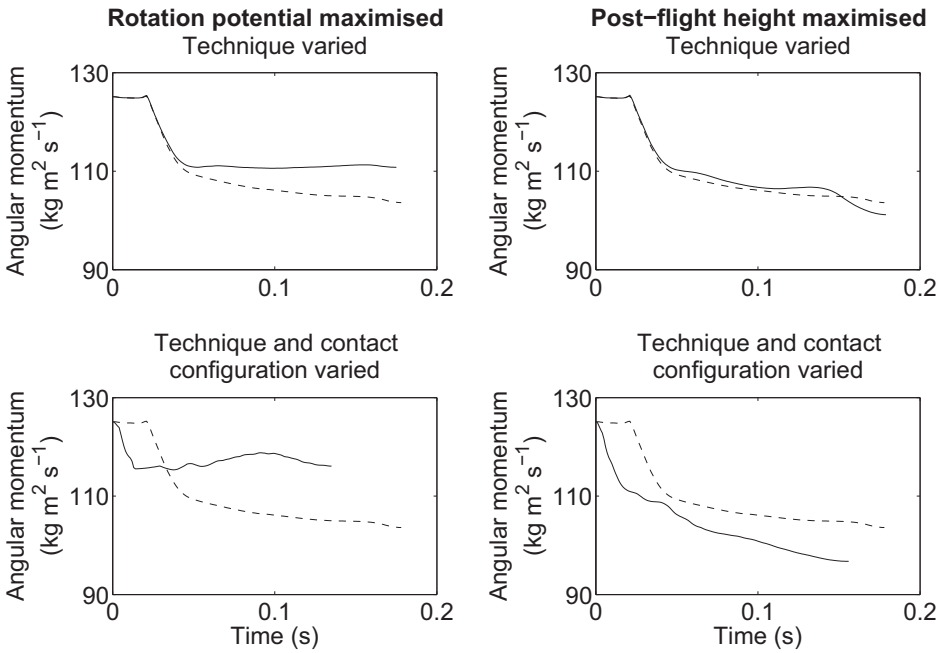

Figure 7.18. Comparison of angular momentum during the table contact phase of different simulations of vault L_3: Left - matched simulation (dashed lines) and simulations optimised for maximum rotation potential (solid lines). Right - matched simulation (dashed lines) and simulations optimised for maximum post-flight height (solid lines).

In all simulations, the angular momentum decreased during the table contact phase of the vault. The changes in angular momentum are summarised in Table 7.7.

Table 7.7. Changes in angular momentum (ΔH) during the table contact phase of simulations of L_3

Simulation	ΔH
Matched	-17.2%
Optimised for rotation potential, technique varied	-11.4%
Optimised for post-flight height, technique varied	-19.2%
Optimised for rotation potential, technique + configuration varied	-7.2%
Optimised for post-flight height, technique + configuration varied	-22.7%

A shown in Table 7.7, in the simulations that were optimised for maximum rotation potential, the decreases in angular momentum during the table contact phase were not as large as those in the matched performance. Conversely in the simulations that were optimised for maximum post-flight height, the decreases in angular momentum during the table contact phase were slightly larger than those in the matched performance.

The biggest reductions in angular momentum occurred during the initial part of the table contact phase, and even when optimising for maximum rotation potential the large initial decreases could not be avoided. In all of the simulations the gymnast's orientation at table contact was just above the horizontal and thus, the resultant force acted posteriorly to the gymnast's centre of mass, producing a torque that decreased the angular momentum. As the contact phase progressed and the gymnast rotated towards the vertical, the reductions in angular momentum flattened out due to the perpendicular distance between the line of action of the resultant force and the gymnast's centre of mass decreasing.

The results suggest that when performing a handspring entry vault, the gymnast's angular momentum about the mass centre will decrease due to the interaction with the table. For a performance in which post-flight rotation is maximised, the angular momentum will still decrease during the table contact phase but the reduction in angular momentum will be less than for a standard performance. However, for a performance in which post-flight height is maximised, the reduction in angular momentum about the mass centre may be slightly more than for a standard performance. This result will be discussed in more detail in the following section.

7.5 Discussion

Application of the simulation model of the contact phase of vaulting showed that vaulting performance is largely pre-determined by the performance in the phases preceding table contact. While adjustment of the configuration at table contact had the potential to improve performance, there was limited scope for the gymnast to alter the performance through technique modifications during the table contact phase. This finding supports the statement of Prassas and Giankellis (2002); "the gymnast can do little to affect the rotational and translational requirements of most vaults during the contact phase".

Optimisation of table contact phase technique led to limited increases in performance: the maximum increase in rotation potential was 1.3% while the maximum increase in post-flight height was 0.05 m. This suggests that the gymnast's technique was close to the optimal technique for the given initial conditions. Furthermore, substantial variation of the gymnast's technique was shown to have only a moderate effect on performance: when the table contact phase technique required no active contribution from the gymnast the rotation potential decreased by 6.5% and the post-flight height decreased by 0.24 m. However, during this simulation, the anatomical limits of the wrist, shoulder, hip and knee joints were all slightly exceeded. Thus, while the gymnast has limited capability to improve the performance of the vault during the table contact phase, active contributions about the joints are required to prevent joint angles from exceeding their anatomical limits.

Optimisation of the gymnast's configuration at table contact in conjunction with contact phase technique led to moderate increases in performance: for a given vault the rotation potential could be increased by 9.8% or the post-flight height could be increased by 0.14 m. In both cases the configuration at table contact was different from that in the recorded performance. The body was slightly dished rather than arched, the orientation angle was higher and the shoulder angle was substantially larger. In this configuration, the gymnast acted more like a single rigid segment resulting in a decreased duration of the table contact phase and a higher vertical velocity at take-off from the vaulting table.

The configuration at table contact was, however, restricted in that the gymnast's pre-flight angular momentum and centre of mass trajectory were the same as those of the recorded performance. The height of the gymnast's centre of mass was limited in that it had to be on the pre-determined parabolic pre-flight trajectory, while the angular

velocity of the head + upper trunk segment was constrained by the gymnast's moment of inertia. Constraining the simulations in this way, resulted in performances that the gymnast could reasonably be expected to achieve. For different pre-flight conditions a different configuration might be optimal, but there would be uncertainty as to whether or not the performance was within the gymnast's capabilities.

In all simulations, the gymnast's angular momentum about the centre of mass decreased during the table contact phase. This is in line with the statement of Prassas and Giankellis (2002) that "analysis of the table contact phase reveals that gymnasts generally lose angular momentum in this phase but better performers tend to lose less". It is not clear though what is meant by "better". In the present study, simulations that were optimised for maximum rotation potential had lower decreases in angular momentum about the mass centre than matched simulations, while on the other hand simulations that were optimised for maximum post-flight height had slightly larger decreases in angular momentum about the mass centre than matched simulations.

7.6 Chapter Summary

In this chapter the methods used to apply the simulation model of vaulting to answer specific research questions were described. Optimisation showed that there was limited potential for the gymnast to improve performance through technique changes during the table contact phase. However, more substantial improvements could be made with additional changes in configuration at table contact. Future applications of the model will be discussed in Chapter 8.

Chapter 8

Summary and Conclusions

8.1 Chapter Overview

The purpose of the present study was to analyse gymnastics vaulting to gain an understanding of the mechanics of the table contact phase, and then to use this understanding to identify ways to improve performance. Within this chapter, the extent to which this aim has been achieved through the development, evaluation and application of a simulation model of the table contact phase of vaulting, is considered. The methods used within the study are also summarised and limitations and potential improvements are identified. The research questions posed in Chapter 1 are addressed and future applications of the simulation model are also outlined.

8.2 Thesis Summary

8.2.1 Simulation Model

A torque-driven simulation model of gymnastics vaulting was developed using Autolev^{TM} (Chapter 4). The two-dimensional model simulated the interaction between a seven-segment gymnast and the vaulting table during the table contact phase. A damped linear spring was used to represent shoulder retraction and protraction, displacement of the glenohumeral joint centre was modelled as a function of the shoulder angle, a damped torsional spring was used to represent flexion/extension of the fingers and a damped torsional spring allowed the table to rotate about its centre of rotation. Extensor and flexor torque generators acted at the wrist, shoulder, hip and knee joints, and passive torque elements acted at the wrist, shoulder and hip joints.

A novel two-state contact phase representation was utilised to simulate the interaction between the gymnast's hands and the vaulting table. This allowed the gymnast's hands to not only compress the vaulting table in the direction normal to the table surface, but to also slide and/or remain stationary relative to the table in the direction tangential to

the table surface. This contact model was shown to replicate the motion of the hands relative to the table surface (Section 6.3).

Within the simulation model the gymnast's trunk was represented by two segments, the head + upper trunk segment and the lower trunk segment, and the angle between the two segments was constrained to be the same as the hip angle, as suggested by analysis of kinematic data. This is not a true representation of the spine, which can curve along its length and move independently of the thighs. The results of the model evaluation did, however, show that the simulation model was able to replicate the key performance features of handspring entry vaults (Section 6.4) and therefore the model is an acceptable compromise between accuracy and simplicity. If greater accuracy were required, a more complex representation of the spine could be used, although for use in a torque-driven model knowledge of the torque generating capacity of the spine would also be required, which could prove difficult to determine.

One limitation of the simulation model is that the body was considered to be composed of rigid segments. This is not the case in reality, where there is motion of soft tissue relative to the rigid skeletal elements. The damped spring at the shoulder could, to a degree, account for soft tissue motion in the direction of the arms but could not account for soft tissue motion in other directions. In order to more accurately represent soft tissue motion wobbling masses could be incorporated into the model, especially in the trunk segments. However, as the model was able to match recorded performances reasonably well, omissions from the model were not likely to have had a substantial effect on the results.

8.2.2 Data Collection

Performance, strength and flexibility data were collected from an elite level gymnast as outlined below.

8.2.2.1 Performance Data

Performance data were collected from an elite level gymnast performing two different handspring entry vaults (Section 3.2): a handspring forward with salto forward stretched (layout) and a handspring forward with double salto forward tucked (Roche). A Vicon optoelectronic motion capture system, sampling at 480 Hz, was used to track the motion

of markers attached to the gymnast and the vaulting table during vaulting performances.

A chain model was used to process the kinematic data and determine the motion of both the gymnast and the vaulting table during each vaulting trial (Section 3.3). The position and velocity of the gymnast's centre of mass were determined, as were flexion / extension joint angles, and the orientation angles of the gymnast and the table.

The assumptions of the chain model (degrees of freedom and constraints) were such that the definition of the gymnast was the same as that in the simulation model. This similarity between the chain model and the simulation model ensured that the kinematics were consistently defined. A limitation of the gymnast definition was that it did not allow for movement out of the sagittal plane. During vaulting performances the gymnast's hands were sometimes adducted, which the models did not allow for. Adduction of the hands is not, however, expected to significantly affect the kinematics of the table contact phase.

8.2.2.2 Torque Data

Gymnast-specific strength parameters for the knee, hip, shoulder and wrist joints were determined from maximum voluntary joint torque measurements obtained on an isovelocity dynamometer (Section 5.2). Dynamometer data of torque, crank angle and crank angular velocity were collected, while a Vicon optoelectronic motion capture system was used to track the motion of markers attached to the gymnast during the trials. The Vicon data were used to determine the joint angle and angular velocity throughout the trials as the joint kinematics can deviate substantially from the crank values necessitating independent measurement (Herzog, 1988; Deslandes et al., 2008).

A limitation of the method was that the gymnast was unfamiliar with use of the dynamometer. To ensure that the gymnast is able and willing to produce maximal efforts a familiarisation protocol, that involves a number of repetitions of the test procedure, should be completed before the measurement trials take place. This would, however, greatly increase the duration of the gymnasts involvement in the project.

During the torque data collection bilateral symmetry was assumed and therefore measurements were taken from only one side of the body. The majority of movements in artistic gymnastics involve both sides of the body and therefore it is unlikely that the

gymnast would exhibit substantial asymmetry in strength. If greater accuracy were required the protocol could be modified to incorporate measurements from both sides of the body. This would, however, again increase the duration of the data collection.

8.2.2.3 Flexibility Data

Gymnast-specific flexibility parameters for the hip, shoulder and wrist joints were determined from passive joint torque measurements obtained on an isovelocity dynamometer (Section 5.3). Again, an optoelectronic motion capture system was used to determine the joint angle. Exponential functions were fitted to the data to express the passive torque generated at the joints as a function of joint angle.

A limitation of the method was that the passive torque was modelled solely as a function of joint angle. Modelling the passive torque in this way meant that the passive torque acted like a spring and was prone to vibration. This could be overcome in future by adding a term that was dependent on velocity to the exponential function.

8.2.2.4 Anthropometric Data

Gymnast-specific segmental inertia parameters were determined using the inertia model of Yeadon (1990a) (Section 5.4). Body segmental parameters calculated using this model have been used in various rigid segment simulation models and have been shown to realistically reproduce human movement (King and Yeadon, 2005; Wilson et al., 2006; Hiley et al., 2009).

8.2.3 Determination of Model Parameters

An angle-driven model was used in conjunction with a genetic algorithm to determine the viscoelastic parameters of the shoulder, knuckle, contact and table springs and also the coefficient of friction between the hands and the contact surface (Section 6.3). The simulated table contact phases of four vaults, two layout and two Roche, were matched concurrently to their respective performances to determine a common parameter set. The resulting system parameters were evaluated using two independent trials, one layout and one Roche, and found to be applicable to handspring entry vaults (Section 6.4).

8.2.4 Evaluation of the Torque-driven Model

The torque-driven model was matched to performance data by varying the torque generator activation parameters using a genetic algorithm (Section 6.5). The horizontal and vertical velocities of the gymnast's centre of mass and the angular velocity of the head + upper trunk segment were also allowed a small amount of variation in order to compensate for errors in the kinematic data.

The simulations matched the layout performances particularly well, with a mean overall difference of 2.5%, and also showed a close match to the Roche performances, with a mean overall difference of 8.6%. The torque-driven simulation model was able to replicate key performance features of the vaults well and was therefore considered suitable to evaluate and optimise performance of handspring entry vaults.

A limitation of the simulation model was that it did not allow for active protraction of the shoulders. This could have accounted for the slightly inferior match of the Roche vaults. An element that allows for active protraction of the shoulders should be developed and included in future models.

In addition, the structure of the genetic algorithm, that was used to match simulations to performance data, is such that it lends itself to parallel processing (van Soest and Casius, 2003). While parallel processing was not employed in the present study, it should be considered in future work as it could reduce the total processing time.

8.3 Research Questions

The research questions posed in Chapter 1 were addressed in detail in Chapter 7. The torque-driven simulation model was used in conjunction with a genetic algorithm to optimise vaulting performance, and was also applied to further understanding of the mechanics of the table contact phase. The research questions are restated below and the results summarised.

1. What is the optimum table contact phase technique for handspring somersault vaults?

An optimal vaulting performance was considered to be one in which post-flight rotation and height were maximised. Optimisation of table contact phase technique showed that there was limited potential for the gymnast to improve performance through technique

changes during the table contact phase, with a maximum increase in rotation potential of 1.3% and a maximum increase in post-flight height of 0.05 m. This suggests that the gymnast's table contact phase technique, in which the wrists and shoulders were actively flexed, was very close to the optimal technique.

2. What is the optimal body configuration at table contact to maximise vaulting performance, for given pre-flight conditions?

Further optimisations were conducted in which additional changes in configuration at table contact were made while maintaining the gymnast's pre-flight centre of mass trajectory and angular momentum. These optimisations resulted in more substantial improvements: the rotation potential was increased by 9.8% and the post-flight height was increased by 0.14 m. The optimal configuration at table contact had an open shoulder angle, a dished body, and a higher orientation angle than the recorded performance.

3. How much does performance depend upon technique during the table contact phase and how much does performance depend on initial conditions?

Substantial variation of the gymnast's technique was shown to result in only moderate changes to post-flight performance. When the table contact phase technique required no active contribution from the gymnast the rotation potential decreased by 6.5% and the post-flight height decreased by 0.24 m. These result indicates that performance of the vault is largely pre-determined by the table contact phase initial conditions, as the gymnast's technique during the table contact phase had only limited potential to affect performance. However, technique during the table contact phase is not insignificant, as active contributions about the joints were found to be required to prevent joint angles from exceeding their anatomical limits.

4. For an optimal performance, how does the angular momentum about the gymnast's centre of mass change?

The gymnast's angular momentum about the centre of mass was found to decrease during the table contact phase, even for optimised performances. Less substantial reductions were found for optimisations in which post-flight rotation was maximised: for a matched simulation the angular momentum decreased by 17.2%, whereas when contact phase technique and table contact configuration were varied to maximise rotation potential the angular momentum decreased by only 7.2%.

Application of the simulation model showed that large decreases during the initial part of the contact phase could not be avoided. For handspring entry vaults, the orientation of the gymnast at table contact is such that the resultant force due to the interaction with the vaulting table acts posteriorly to the gymnast's centre of mass, at least during the initial part of the table contact phase, resulting in a torque that reduces the gymnast's angular momentum about their mass centre.

8.4 Future Applications

As the simulation model of the table contact phase of vaulting was successfully evaluated it can be used with confidence to further investigate the mechanics of the table contact phase. Additional research questions that could be addressed include:

- What is the optimal table contact phase technique for round-off entry (Yurchenko) vaults?
- How sensitive is vaulting performance to the positioning of the hands on the vaulting table?
- What is the effect of a change in strength on vaulting performance?
- How sensitive is vaulting performance to variations in muscle activation timings?

8.5 Conclusions

The aim of the present study was to analyse gymnastics vaulting to gain an understanding of the mechanics of the table contact phase, and then to use this understanding to identify ways to improve performance. To achieve this, a torque-driven simulation model of the table contact phase of vaulting was developed, incorporating a novel two-state contact phase representation to simulate the interaction between the gymnast and the vaulting table during the contact phase. The torque-driven model was successfully evaluated and shown to produce realistic movements. The model was then applied to further understanding of the mechanics of the table contact phase of gymnastics vaulting. Optimisation showed that there was limited potential for the gymnast to improve performance through technique changes during the table contact phase, but with additional changes in configuration at table contact more substantial improvements to vaulting performance could be made.

References

Anderson, D. E., Madigan, M. L., and Nussbaum, M. A. (2007). Maximum voluntary joint torque as a function of joint angle and angular velocity: model development and application to the lower limb. *Journal Of Biomechanics*, 40(14):3105–13.

Audu, M. L. and Davy, D. (1985). The influence of muscle model complexity in musculoskeletal motion modeling. *Journal Of Biomechanical Engineering*, 107(2):147–57.

Bajin, B. (1978). Three Tsukahara vaults. *International gymnast*, 20(6):58–59.

Bassett, R. W., Browne, A. O., Morrey, B. F., and An, K. N. (1990). Glenohumeral muscle force and moment mechanics in a position of shoulder instability. *Journal Of Biomechanics*, 23(5):405–15.

Bauchau, O. and Ju, C. (2006). Modeling friction phenomena in flexible multibody dynamics. *Computer Methods in Applied Mechanics and Engineering*, 195(50):6909–6924.

Begon, M., Wieber, P., and Yeadon, M. (2008). Kinematics estimation of straddled movements on high bar from a limited number of skin markers using a chain model. *Journal of Biomechanics*, 41(3):581–586.

Boone, W. T. (1976). *Illustrated handbook of gymnastics, tumbling and trampolining.* Parker Publishing Company, Inc.

Camomilla, V., Cereatti, A., Vannozzi, G., and Cappozzo, A. (2006). An optimized protocol for hip joint centre determination using the functional method. *Journal Of Biomechanics*, 39(6):1096–106.

Carroll, D. L. (2001). FORTRAN genetic algorithm driver. Downloaded from: http://cuaerospace.com/carroll/ga.html.

Chandler, R., Clauser, C., McConville, J., Reynolds, H., and Young, J. (1975). Investigation of inertial properties of the human body. Technical report, Aerospace Medical Research Laboratories, Wright-Patterson Air Force Base, Ohio.

Cools, A. M., Geerooms, E., Van den Berghe, D. F. M., Cambier, D. C., and Witvrouw, E. E. (2007). Isokinetic scapular muscle performance in young elite gymnasts. *Journal of Athletic Training*, 42(4):458–463.

Corana, A., Marchesi, M., Martini, C., and Ridella, S. (1987). Minimizing multimodal functions of continuous variables with the simulated annealing algorithm. *ACM Transactions on Mathematical Software*, 13(3):262–80.

Cormie, P., Sands, W., and Smith, S. (2004). A comparative case study of Roche vaults performed by elite male gymnasts. *Technique*, 24(8):6–9.

Dainis, A. (1979). Cinematographic analysis of the handspring vault. *Research Quarterly*, 50(3):341–349.

Dainis, A. (1980a). A model and analysis of vaulting. Part 1. *International Gymnast*, 22:1–6. Technical Supplement.

Dainis, A. (1980b). A model and analysis of vaulting. Part 2. *International Gymnast*, 22:7–12. Technical Supplement.

Dainis, A. (1981). A model for gymnastics vaulting. *Medicine and Science in Sports and Exercise*, 13(1):34–43.

Davis, L. (1991). *Handbook of Genetic Algorithms*. Van Nostrand Reinhold, New York.

Deslandes, S., Mariot, J.-P., and Serveto, S. (2008). Offset of rotation centers creates a bias in isokinetics: a virtual model including stiffness or friction. *Journal Of Biomechanics*, 41(10):2112–20.

Duda, G. N., Brand, D., Freitag, S., Lierse, W., and Schneider, E. (1996). Variability of femoral muscle attachments. *Journal Of Biomechanics*, 29(9):1185–90.

Dudley, G. A., Harris, R. T., Duvoisin, M. R., Hather, B. M., and Buchanan, P. (1990). Effect of voluntary vs. artificial activation on the relationship of muscle torque to speed. *Journal of Applied Physiology*, 69:2215–2221.

Ehrig, R., Taylor, W., Duda, G., and Heller, M. (2006). A survey of formal methods for determining the centre of rotation of ball joints. *Journal of Biomechanics*, 39(15):2798–2809.

Esteki, A. and Mansour, J. M. (1996). An experimentally based nonlinear viscoelastic model of joint passive moment. *Journal Of Biomechanics*, 29(4):443–50.

FIG (2009a). *Apparatus Norms*. Fédération Internationale de Gymnastique.

FIG (2009b). *Code of Points - Men's Technical Committee*. Fédération Internationale de Gymnastique.

Finni, T. and Komi, P. V. (2002). Two methods for estimating tendinous tissue elongation during human movement. *Journal of Applied Biomechanics*, 18:180–188.

Floyd, R. (2007). *Manual of structural kinesiology*. McGraw-Hill, 16 edition.

Forrester, S. E., Yeadon, M. R., King, M. A., and Pain, M. T. G. (2010). Comparing different approaches for determining joint torque parameters from isovelocity dynamometer measurements. *Submitted to Journal Of Biomechanics*.

Freund, H. J. and Budingen, H. J. (1978). The relationship between speed and amplitude of the fastest voluntary contractions of human arm muscles. *Experimental Brain Research*, 31(1):1–12.

George, G. S. (1980). *Biomechanics of Women's Gymnastics*. Prentice-Hall, Inc.

Gervais, P. (1994). A prediction of an optimal performance of the handspring 1 1/2 front salto longhorse vault. *Journal of Biomechanics*, 27(1):67–75.

GYMmedia.com (2005). Pegases - the new vaulting table of Janssen and Fritsen. Retrieved July 24, 2009 from http://www.gymmedia.com/janssen-fritsen/index.htm.

Harik, G., Cantau-Paz, E., Goldberg, D. E., and Miller, B. L. (1999). The gambler's ruin problem, genetic algorithms, and the sizing of populations. *Evolutionary Computation*, 7(3):231–253.

Hatze, H. (1997). A three-dimensional multivariate model of passive human joint torques and articular boundaries. *Clinical Biomechanics*, 12(2):128–135.

Hay, J. G. (1993). *The biomechanics of sports techniques. 4th Ed.* Prentice-Hall.

Herzog, W. (1988). The relation between the resultant moments at a joint and the moments measured by an isokinetic dynamometer. *Journal of Biomechanics*, 21(1):5–12.

Hiley, M., Wangler, R., and Predescu, G. (2009). Optimization of the felge on parallel bars. *Sports Biomechanics*, 8(1):39–51.

Hill, A. V. (1938). The heat of shortening and the dynamic constants of muscle. In *Proceedings of the Royal Society Series B*, volume 126, pages 136–195.

Hunn, D. (1978). *The complete book of gymnastics*. Ward Lock.

Huxley, A. F. (1957). Muscle structure and theories of contraction. *Progress in Biophysics and Biophysical Chemistry*, 7:255–318.

Irwin, G., Bown, R., and Thomas, E. (2004). Kinematic comparison of the handspring front somersault on the vaulting horse and new table. (abstract). *Journal of Sports Sciences*, 22:240.

Irwin, G. and Kerwin, D. (2009). The influence of the vaulting table on the handspring front somersault. *Sports Biomechanics*, 8(2):114–128.

Jacobs, R., Bobbert, M. F., and van Ingen Schenau, G. J. (1996). Mechanical output from individual muscles during explosive leg extensions: the role of biarticular muscles. *Journal Of Biomechanics*, 29(4):513–23.

King, M. A. and Yeadon, M. R. (2002). Determining subject-specific torque parameters for use in a torque-driven simulation model of dynamic jumping. *Journal of Applied Biomechanics*, 18(3):207–217.

King, M. A. and Yeadon, M. R. (2005). Factors influencing performance in the Hecht vault and implications for modelling. *Journal of Biomechanics*, 38(1):145–151.

King, M. A., Yeadon, M. R., and Kerwin, D. G. (1999). A two-segment simulation model of long horse vaulting. *Journal of Sports Sciences*, 17(4):313–324.

Knoll, K. and Krug, J. (2002). The vaulting table. Retrieved August 12, 2007 from http://coachesinfo.com/category/gymnastics/61/.

Koh, M. and Jennings, L. (2003). Dynamic optimization: inverse analysis for the Yurchenko layout vault in women's artistic gymnastics. *Journal of Biomechanics*, 36(8):1177–1183.

Koh, M. and Jennings, L. (2007). Strategies in preflight for an optimal Yurchenko layout vault. *Journal of Biomechanics*, 40(6):1256–1261.

Koh, M., Jennings, L., and Elliott, B. (2003a). Role of joint torques generated in an optimised Yurchenko layout vault. *Sports Biomechanics*, 2:177–190.

Koh, M., Jennings, L., Elliott, B., and Lloyd, D. (2003b). A predicted optimal performance of the Yurchenko layout vault in women's artistic gymnastics. *Journal of Applied Biomechanics*, 19(3):187–204.

Kwon, Y., Fortney, V., and Shin, I. (1990). 3-D analysis of Yurchenko vaults performed by female gymnasts during the 1988 Seoul Olympic games. *International Journal of Sport Biomechanics*, 6:157–176.

Langenderfer, J., Jerabek, S. A., Thangamani, V. B., Kuhn, J. E., and Hughes, R. E. (2004). Musculoskeletal parameters of muscles crossing the shoulder and elbow and the effect of sarcomere length sample size on estimation of optimal muscle length. *Clinical Biomechanics*, 19(7):664–670.

Lieber, R. L., Fazeli, B. M., and Botte, M. J. (1990). Architecture of selected wrist flexor and extensor muscles. *The Journal Of Hand Surgery*, 15(2):244–50.

Loren, G. J., Shoemaker, S. D., Burkholder, T. J., Jacobson, M., Friden, J., and Lieber, R. (1996). Human wrist motors: biomechanical design and application to tendon transfers. *Journal Of Biomechanics*, 29(3):331–42.

Lu, T.-W. and O'Connor, J. (1999). Bone position estimation from skin marker coordinates using global optimisation with joint constraints. *Journal of Biomechanics*, 32(2):129–134.

McLean, S. G., Su, A., and van den Bogert, A. J. (2003). Development and validation of a 3-D model to predict knee joint loading during dynamic movement. *Journal of Biomechanical Engineering*, 125(6):864–874.

Monnet, T., Desailly, E., Begon, M., Vallée, C., and Lacouture, P. (2007). Comparison of the SCoRE and HA methods for locating in vivo the glenohumeral joint centre. *Journal of Biomechanics*, 40(15):3487–3492.

Murray, M. (1979). *Women's Gymnastics: Coach, participant, spectator*. Allyn and Bacon, Inc.

Neptune, R., Wright, I., and van den Bogert, A. (2000). A method for numerical simulation of single limb ground contact events: application to heel-toe running. *Journal of Computer Methods in Biomechanics and Biomedical Engineering*, 3:321–334.

Pierrynowski, M. R. (1995). *Three-Dimensional Analysis of Human Movement*, chapter Analytic Representation of Muscle Line of Action and Geometry, pages 215–256. Champaign: Human Kinetics.

Prassas, S. and Giankellis, K., editors (2002). *Vaulting Mechanics, Applied Proceedings of the XX International Symposium on Biomechanics in Sports*.

Prassas, S., Kwon, Y.-H., and Sands, W. A. (2006). Biomechanical research in artistic gymnastics: A review. *Sports Biomechanics*, 5(2):261–291.

Riener, R. and Edrich, T. (1999). Identification of passive elastic joint moments in the lower extremities. *Journal Of Biomechanics*, 32(5):539–44.

Robbinssports.com (2009). Vaulting. Retrieved July24, 2009 from http://www.robbinssports.com/sporting-goods-store/gymnastics-c-137.html.

Roux, E., Bouilland, S., Godillion-Maquinghen, A.-P., and Bouttens, D. (2002). Evaluation of the global optimisation method within the upper limb kinematics analysis. *Journal Of Biomechanics*, 35(9):1279–83.

Sands, W., Caine, D., and Borms, J. (2003). *Scientific aspects of women's gymnastics*. Karger.

Sands, W. and McNeal, J. (2002). Some guidelines on the transition from the old horse to the new table. *Technique*, 22(1):22.

Scovil, C. Y. and Ronsky, J. L. (2006). Sensitivity of a Hill-based muscle model to perturbations in model parameters. *Journal Of Biomechanics*, 39(11):2055–63.

Seger, J. Y. and Thorstensson, A. (1994). Muscle strength and myoelectric activity in prepubertal and adult males and females. *European Journal Of Applied Physiology And Occupational Physiology*, 69(1):81–7.

Smith, T. (1982). *Gymnastics: A Mechanical Understanding*. Hodder and Stoughton.

Sprigings, E. J. and Yeadon, M. R. (1997). An insight into the reversal of rotation in the Hecht vault. *Human Movement Science*, 16(4):517–532.

Still, C. (1990). *BAGA Women's Gymnastics Manual*. Springfield Books Limited.

Takei, Y. (1990). Techniques used by elite women gymnasts performing the handspring vault at the 1987 Pan American Games. *International Journal of Sport Biomechanics*, 6:29–55.

Takei, Y. (1991). A comparison of techniques used in performing the men's compulsory gymnastic vault at the 1988 Olympics. *International Journal of Sport Biomechanics*, 7:54–75.

Takei, Y., Blucker, E., Dunn, J., Myers, S., and Fortney, V. (1996). A three dimensional analysis of the men's compulsory vault performed at the 1992 Olympic Games. *Journal of Applied Biomechanics*, 12:237–257.

Takei, Y., Blucker, E. P., Nohara, H., and Yamashita, N. (2000). The Hecht vault performed at the 1995 World Gymnastics Championships: deterministic model and judges' scores. *Journal of Sports Sciences*, 18(11):849–863.

Takei, Y. and Kim, E. (1990). Techniques used in performing the handspring and salto forward tucked vault at the 1988 Olympic Games. *International Journal of Sport Biomechanics*, 6:111–138.

van Soest, A. J. and Casius, L. J. R. (2003). The merits of a parallel genetic algorithm in solving hard optimization problems. *Journal of Biomechanical Engineering*, 125(1):141–146.

Westing, S. H., Cresswell, A. G., and Thorstensson, A. (1991). Muscle activation during maximal voluntary eccentric and concentric knee extension. *European Journal of Applied Physiology and Occupational Physiology*, 62(2):104–108.

Wieber, P.-B., Billet, F., Boissieux, L., and Pissard-Gibollet, R. (2006). The HuMAnS toolbox, a homogeneous framework for motion capture, analysis and simulation. In *9th International Symposium on 3D analysis of human movement*.

Wilson, C., King, M., and Yeadon, M. (2006). Determination of subject-specific model parameters for visco-elastic elements. *Journal of Biomechanics*, 39(10):1883–1890.

Winter, D. A. (1990). *Biomechanics and Motor Control of Human Movement*. Wiley.

Wojtyra, M. (2003). Multibody simulation model of human walking. *Mechanics Based Design of Structures and Machines*, 31(3):357–379.

Wood, G. A. and Jennings, L. S. (1979). On the use of spline functions for data smoothing. *Journal of Biomechanics*, 12(6):477–479.

Yamaguchi, G. T. (2006). *Dynamic Modeling of Musculoskeletal Motion - A vectorized approach for biomechanical analysis in three dimensions*. Springer Science+Business Media Inc.

Yeadon, M. R. (1990a). The simulation of aerial movement–II. A mathematical inertia model of the human body. *Journal of Biomechanics*, 23(1):67–74.

Yeadon, M. R. (1990b). The simulation of aerial movement–III. The determination of the angular momentum of the human body. *Journal of Biomechanics*, 23(1):75–83.

Yeadon, M. R. and Hiley, M. J. (2000). The mechanics of the backward giant circle on the high bar. *Human Movement Science*, 19(2):153–173.

Yeadon, M. R., King, M., Forrester, S., Caldwell, G., and Pain, M. (2010). The need for muscle co-contraction prior to a landing. *Journal of Biomechanics*, 43(2):364–369.

Yeadon, M. R. and King, M. A. (2002). Evaluation of a torque-driven simulation model of tumbling. *Journal of Applied Biomechanics*, 18(3):195–206.

Yeadon, M. R., King, M. A., and Sprigings, E. J. (1998). Pre-flight characteristics of Hecht vaults. *Journal of Sports Sciences*, 16(4):349–356.

Yeadon, M. R., King, M. A., and Wilson, C. (2006). Modelling the maximum voluntary joint torque/angular velocity relationship in human movement. *Journal Of Biomechanics*, 39(3):476–82.

Yoon, Y. S. and Mansour, J. M. (1982). The passive elastic moment at the hip. *Journal Of Biomechanics*, 15(12):905–10.

Appendix A

Informed Consent Form

DATA ACQUISITION FOR THE ANALYSIS OF HUMAN MOVEMENTS

LAY SUMMARY

The study comprises a biomechanical analysis of human movement. This analysis requires kinematic data for vaulting. Subject specific inertia and strength parameters are also required.

The data of actual human movements are required to give detailed information about the current techniques used. The data collected will then be used to understand and explain techniques currently used, demonstrate the contributions of different techniques to performance and injury, as well as to optimise performance.

The kinematic data will be obtained in a number of different ways:

- Video and cinematographic recordings.
- Automatic displacement acquisition system. This is similar to being videoed but reflective markers or LEDs will be taped to you and only their image recorded.

The subject specific parameters will be obtained from:

- Anthropometric measurements. Measuring certain lengths, widths and circumferences of your body with a tape measure.
- Muscular torque measurements. This involves measuring your strength at different joints through a range of angles and speeds.

Data will be acquired in the National Gymnastics Performance and Research Centre at Loughborough University and in the biomechanics research laboratory. Any data collection session will last no longer than two hours, with the subject actively involved for only a fraction of the total time:

- Actual performance of movements: 10 minutes
- Anthropometric measurements: 30 minutes
- Strength measurements: 45 minutes

DATA ACQUISITION FOR THE ANALYSIS OF HUMAN MOVEMENTS
INFORMATION FOR PARTICIPANT

The study in which you have been invited to participate will involve a biomechanical analysis of your vaulting technique. The study will be divided into three parts; firstly, you will be videoed, using a number of different cameras, as you perform vaults. The second part of the study will involve measurements to determine the lengths, widths and circumferences of your body segments (e.g. your arms, legs, trunk and head). Thirdly strength tests will be carried out on an isovelocity dynamometer to estimate your strength characteristics during various activities (e.g. extending and flexing your knee or hip). The measurement procedures will be described and demonstrated in advance. It may be necessary to shave certain areas of your body to attach monitoring equipment using adhesive tape. The data collected will be used to help increase our understanding of the mechanics of human movements.

You will perform the data collection in a suitable environment. The risk of injury during the data collection will be minimal since we will only ask you to perform movements with which you are familiar and comfortable. It is considered that no increased risks, discomforts or distresses are likely to result from the data collection of vaulting above those associated with the normal performance of those movements. You will undergo a familiarisation protocol for the isovelocity dynamometer prior to capturing data to minimise any potential for injury.

The information obtained from the study will be collected and stored in adherence with the Data Protection Act and furthermore any information/data that may reveal your identity (such as photographs) will not be used in any publications without your prior consent. If you agree to take part in the study, you are free to withdraw from the study at any stage, without having to give any reasons. A contact name and phone number will be provided to you for use if you have any queries about any part of your participation in the study.

INFORMED CONSENT FORM (SUBJECTS)

PURPOSE: To obtain kinematic and kinetic data during human movements.

PROCEDURES: The kinematic data of human movements will be obtained using:

- Video and cinematographic recordings.
- Automatic displacement acquisition system.
- Body inertia parameters will be ascertained from various body measurements.
- Muscular torque data will be gathered using an isovelocity dynamometer.

ACTIVITIES: You will be asked to perform the following activities:

- Handspring entry vaults.
- Strength and flexibility tests on an isovelocity dynamometer.

A number of trials will be requested with suitable breaks to minimise fatigue and boredom. During the measurements a number of researchers will be present, at least one of whom will be the same sex as you.

QUESTIONS: The researchers will be pleased to answer any questions you may have at any time.

WITHDRAWL: You are free to withdraw from the study at any stage, without having to give any reasons.

CONFIDENTIALITY: Any information/data that may reveal your identity (such as photographs) will not be used in any publications without your prior consent.

I have read the outline of the procedures which are involved in this study, and I understand what will be required of me. I have had the opportunity to ask for further information and for clarification of the demands of each of the procedures and understand what is entailed. I am aware that I have the right to withdraw from the study at any time with no obligation to give reasons for my decision. As far as I am aware I do not have any injury or infirmity which would affect the procedures outlined.

Name.....

Signed.....(subject) Date.....

In the presence of:

Name.....

Appendix B

Chain Model Code

Gymnast Model

```
# Chain Model of Vaulting (Gymnast)

# Author(s): Monique Jackson

# Kinematics of the model
# X: Flexion-Extension; Y: Abduction/Adduction; Z: Medio-lateral Rotation
# Sequence of angles: XYZ


#------------------------------------------------------------------------#
# System Characteristics

NSOL := 13:   # Number of solids
NDDL := 10:   # Number of degrees of freedom
NTAG := 59:   # Number of tags

#------------------------------------------------------------------------#

# Initialisation of vectors
q    := vector(NDDL):
qdot := vector(NDDL):
Mass := vector(NSOL):              # Mass vector
Gravity := vector([0, -9.81, 0]):  # Gravity vector


# Segments
# 1  Thorax
# 2  Pelvis
# 3  Left thigh
# 4  Right thigh
# 5  Left shank
# 6  Right shank
# 7  Scapula girdle
# 8  Left arm
# 9  Right arm
# 10 Left palm
# 11 Right palm
# 12 Left fingers
# 13 Right fingers


# Joints
# 1         Thorax orientation X
# 2, 3, 4   Thorax position X, Y, Z
```

```
# 5         Trunk /Hip flexion X
# 6         Knee flexion
# f(q7)     Shoulder translation Z
# 7         Shoulder flexion X (arm wrt thorax)
# 8         Arm lengthening/shortening Z
# 9         Wrist flexion X (palm wrt arm)
# 10        Hand flexion X (fingers wrt palm)


# Mass
m_1  := 26.15 : # Thorax/chest/head
m_2  := 10.26 :
m_3  :=  8.34 :
m_4  :=  8.34 :
m_5  :=  4.19 :
m_6  :=  4.19 :
m_7  :=  0.00 :
m_8  :=  3.72 :
m_9  :=  3.72 :
m_10 :=  0.30 :
m_11 :=  0.30 :
m_12 :=  0.20 :
m_13 :=  0.20 :


# Centre of Mass Location
G_1  := [0,0,-0.066]:
G_2  := [0,0,-0.111]:
G_3  := [0,0,-0.171]:
G_4  := [0,0,-0.171]:
G_5  := [0,0,-0.229]:
G_6  := [0,0,-0.229]:
G_7  := [0,0,0]:
G_8  := [0,0,-0.197]:
G_9  := [0,0,-0.197]:
G_10 := [0,0,-0.044]:
G_11 := [0,0,-0.044]:
G_12 := [0,0,-0.044]:
G_13 := [0,0,-0.044]:


##################################
# Skeleton dimensions
##################################
z_1    := 0.312: # Thorax length (length to joint centre)
z_2    := 0.210: # Pelvis
x_3    := 0.102: # Hip width (L)
x_4    := 0.091: # Hip width (R)
z_34   := 0.404: # Thigh length
z_56   := 0.602: # Shank length
x_8    := 0.192: # Shoulder width
x_9    := 0.194: # Shoulder width
z_89   := 0.505: # Arm length (Layout)
z_1011 := 0.087: # Palm length
z_1213 := 0.103: # Finger length

f_1:= -0.01207*q[8]**3 + 0.05446*q[8]**2 - 0.01139*q[8] - 0.04963:
```

```
####################################
# System of Coordinates
####################################
#-------------------------------------------------------------------------#
ref_1 := 0  : psi_1 := -q[1]    : theta_1 := 0 : phi_1 := 0
            : Tx_1 := q[2]      : Ty_1 := q[4] : Tz_1 := -q[3]   : # Thorax
ref_2 := 1  : psi_2 := Pi-q[5]  : theta_2 := 0 : phi_2 := 0
            : Tx_2 := 0         : Ty_2 := 0    : Tz_2 := -z_1    : # Pelvis
ref_3 := 2  : psi_3 := Pi-q[5]  : theta_3 := 0 : phi_3 := 0
            : Tx_3 := -x_3      : Ty_3 := 0    : Tz_3 := -z_2    : # L thigh
ref_4 := 2  : psi_4 := Pi-q[5]  : theta_4 := 0 : phi_4 := 0
            : Tx_4 := x_4       : Ty_4 := 0    : Tz_4 := -z_2    : # R thigh
ref_5 := 3  : psi_5 := Pi+q[6]  : theta_5 := 0 : phi_5 := 0
            : Tx_5 := 0         : Ty_5 := 0    : Tz_5 := -z_34   : # L shank
ref_6 := 4  : psi_6 := Pi+q[6]  : theta_6 := 0 : phi_6 := 0
            : Tx_6 := 0         : Ty_6 := 0    : Tz_6 := -z_34   : # R shank
ref_7 := 1  : psi_7 := q[7]     : theta_7 := 0 : phi_7 := 0
            : Tx_7 := 0         : Ty_7 := 0    : Tz_7 := f_1     : # Scapula
ref_8 := 7  : psi_8 := 0        : theta_8 := 0 : phi_8 := 0
            : Tx_8 := -x_8      : Ty_8 := 0    : Tz_8 := q[8]    : # L arm
ref_9 := 7  : psi_9 := 0        : theta_9 := 0 : phi_9 := 0 :
            : Tx_9 := x_9       : Ty_9 := 0    : Tz_9 := q[8]    : # R arm
ref_10:= 8  : psi_10:= Pi-q[9]  : theta_10:= 0 : phi_10:= 0
            : Tx_10:= 0         : Ty_10:= 0    : Tz_10:= -z_89   : # L palm
ref_11:= 9  : psi_11:= Pi-q[9]  : theta_11:= 0 : phi_11:= 0
            : Tx_11:= 0         : Ty_11:= 0    : Tz_11:= -z_89   : # R palm
ref_12:= 10 : psi_12:= Pi-q[10] : theta_12:= 0 : phi_12:= 0
            : Tx_12:= 0         : Ty_12:= 0    : Tz_12:= -z_1011 : # L finger
ref_13:= 11 : psi_13:= Pi-q[10] : theta_13:= 0 : phi_13:= 0
            : Tx_13:= 0         : Ty_13:= 0    : Tz_13:= -z_1011 : # R finger
#-------------------------------------------------------------------------#


####################################
# Tags
####################################
reftag_1 := 1 : tag_1 := vector([ 0.002,  0.089,  0.0  ]) : # STR
reftag_2 := 1 : tag_2 := vector([ 0.004,  0.141, -0.148]) : # XYP
reftag_3 := 1 : tag_3 := vector([-0.057,  0.153, -0.267]) : # LRib
reftag_4 := 1 : tag_4 := vector([ 0.095,  0.153, -0.268]) : # RRib
reftag_5 := 1 : tag_5 := vector([-0.002, -0.089,  0.0  ]) : # C7
reftag_6 := 1 : tag_6 := vector([ 0.001, -0.098, -0.183]) : # T10

reftag_7 := 2 : tag_7 := vector([-0.014, -0.049, -0.095]) : # LPSIS
reftag_8 := 2 : tag_8 := vector([ 0.020, -0.048, -0.094]) : # RPSIS
reftag_9 := 2 : tag_9 := vector([-0.060,  0.167, -0.120]) : # LAHip
reftag_10:= 2 : tag_10:= vector([ 0.074,  0.174, -0.118]) : # RAHip
reftag_11:= 2 : tag_11:= vector([-0.129,  0.130, -0.094]) : # LASIS
reftag_12:= 2 : tag_12:= vector([ 0.152,  0.132, -0.094]) : # RASIS

reftag_13:= 3 : tag_13:= vector([-0.090,  0.009, -0.024]) : # LHip
reftag_14:= 3 : tag_14:= vector([-0.009,  0.108, -0.167]) : # LUAThigh
reftag_15:= 3 : tag_15:= vector([-0.057,  0.066, -0.291]) : # LLAThigh
reftag_16:= 3 : tag_16:= vector([ 0.012, -0.088, -0.250]) : # LPThigh

reftag_17:= 4 : tag_17:= vector([ 0.084, -0.005, -0.034]) : # RHip
reftag_18:= 4 : tag_18:= vector([-0.038,  0.090, -0.168]) : # RUAThigh
reftag_19:= 4 : tag_19:= vector([ 0.045,  0.056, -0.268]) : # RLAThigh
reftag_20:= 4 : tag_20:= vector([-0.034, -0.099, -0.232]) : # RPThigh
```

```
reftag_21:= 5 : tag_21:= vector([-0.065, -0.001,  0.007]) : # LLKN
reftag_22:= 5 : tag_22:= vector([ 0.064, -0.001,  0.007]) : # LMKN
reftag_23:= 5 : tag_23:= vector([ 0.009, -0.007, -0.406]) : # LANK

reftag_24:= 6 : tag_24:= vector([ 0.063,  0.001, -0.007]) : # RLKN
reftag_25:= 6 : tag_25:= vector([-0.064,  0.001, -0.007]) : # RMKN
reftag_26:= 6 : tag_26:= vector([ 0.0  , -0.006, -0.388]) : # RANK

reftag_27:= 8 : tag_27:= vector([ 0.046, -0.064, -0.249]) : # LMEL
reftag_28:= 8 : tag_28:= vector([-0.033,  0.020, -0.248]) : # LLEL
reftag_29:= 8 : tag_29:= vector([-0.038,  0.022, -0.117]) : # LAArm
reftag_30:= 8 : tag_30:= vector([-0.038, -0.086, -0.126]) : # LPArm

reftag_31:= 9 : tag_31:= vector([-0.063, -0.051, -0.257]) : # RMEL
reftag_32:= 9 : tag_32:= vector([ 0.044,  0.004, -0.252]) : # RLEL
reftag_33:= 9 : tag_33:= vector([ 0.026,  0.031, -0.145]) : # RAArm
reftag_34:= 9 : tag_34:= vector([ 0.026, -0.082, -0.137]) : # RPArm

reftag_35:= 10 : tag_35:= vector([ 0.048, -0.004, -0.001]) : # LLWR
reftag_36:= 10 : tag_36:= vector([-0.047, -0.004, -0.001]) : # LMWR
reftag_37:= 10 : tag_37:= vector([-0.008,  0.022, -0.101]) : # LHand

reftag_38:= 11 : tag_38:= vector([-0.045,  0.004,  0.002]) : # RLW
reftag_39:= 11 : tag_39:= vector([ 0.048,  0.004,  0.001]) : # RMW
reftag_40:= 11 : tag_40:= vector([ 0.016,  0.031, -0.088]) : # RHand

reftag_41:= 12 : tag_41:= vector([ 0.0  ,  0.020, -0.105]) : # LFIN

reftag_42:= 13 : tag_42:= vector([ 0.0  ,  0.020, -0.099]) : # RFIN


reftag_43:= 1 : tag_43:= vector([ 0.0  ,  0.0  ,  0.0  ])  : # TCU
reftag_44:= 2 : tag_44:= vector([ 0.0  ,  0.0  ,  0.0  ])  : # TCL

reftag_45:= 3 : tag_45:= vector([ 0.0  ,  0.0  ,  0.0  ])  : # HCL
reftag_46:= 4 : tag_46:= vector([ 0.0  ,  0.0  ,  0.0  ])  : # HCR

reftag_47:= 5 : tag_47:= vector([ 0.0  ,  0.0  ,  0.0  ])  : # KCL
reftag_48:= 6 : tag_48:= vector([ 0.0  ,  0.0  ,  0.0  ])  : # KCR

reftag_49:= 5 : tag_49:= vector([ 0.0  ,  0.0  , -z_56 ])  : # ACL
reftag_50:= 6 : tag_50:= vector([ 0.0  ,  0.0  , -z_56 ])  : # ACR

reftag_51:= 8 : tag_51:= vector([ 0.0  ,  0.0  ,  0.0  ])  : # SCL
reftag_52:= 9 : tag_52:= vector([ 0.0  ,  0.0  ,  0.0  ])  : # SCR

reftag_53:= 10 : tag_53:= vector([ 0.0  ,  0.0  ,  0.0  ]) : # WCL
reftag_54:= 11 : tag_54:= vector([ 0.0  ,  0.0  ,  0.0  ]) : # WCR

reftag_55:= 12 : tag_55:= vector([ 0.0  ,  0.0  ,  0.0  ]) : # KnL
reftag_56:= 13 : tag_56:= vector([ 0.0  ,  0.0  ,  0.0  ]) : # KnR

reftag_57:= 12 : tag_57:= vector([ 0.0  ,  0.0  ,-z_1213]) : # FinL
reftag_58:= 13 : tag_58:= vector([ 0.0  ,  0.0  ,-z_1213]) : # FinR

reftag_59:= 7  : tag_59:= vector([ 0.0  ,  0.0  ,  0.0  ]) : # ScapJC
#------------------------------------------------------------------------#
```

Table Model

```
# Chain Model of Vaulting (Table)

# Author(s): Monique Jackson

# Kinematics of the model
# X: Flexion-Extension; Y: Abduction/Adduction; Z: Medio-lateral Rotation
# Sequence of angles: XYZ


#------------------------------------------------------------------------#
# System Characteristics

NSOL := 2:  # Number of solids
NDDL := 5:  # Number of degrees of freedom
NTAG := 32: # Number of tags

#------------------------------------------------------------------------#

# Initialisation of vectors
q    := vector(NDDL):
qdot := vector(NDDL):
Mass := vector(NSOL):                 # Mass vector
Gravity := vector([0, -9.81, 0]):     # Gravity vector


# Segments
# 1  Ground
# 2  Table


# Joints
# 1        Ground orientation X
# 2, 3, 4  Ground position X, Y, Z
# 5        Table rotation X


###################################
# Skeleton dimensions
###################################
y_1    := 0.416 : # Distance to CoR
z_1    := 0.252 :
z_2    := 1.350 : # Height (as a reference)


###################################
# System of Coordinates
###################################
#------------------------------------------------------------------------#
ref_1 := 0 : psi_1 := -q[1] : theta_1 := 0 : phi_1 := 0
           : Tx_1 := q[2]   : Ty_1 := q[4] : Tz_1 := -q[3] : # Ground #
ref_2 := 1 : psi_2 := q[5]  : theta_2 := 0 : phi_2 := 0
           : Tx_2 := 0      : Ty_2 := y_1  : Tz_2 := z_1   : # Table  #

#------------------------------------------------------------------------#
```

```
###################################
# Tags
###################################
# wrt Table:    T1 - T26
# wrt Ground: G1  G2  G3

#-------------------------------------------------------------------------#

reftag_1 := 2 : tag_1 := vector([-0.495,  0.681,  1.047]) : # T1
reftag_2 := 2 : tag_2 := vector([-0.496,  0.669,  0.909]) : # T2
reftag_3 := 2 : tag_3 := vector([-0.492,  0.479,  1.043]) : # T3
reftag_4 := 2 : tag_4 := vector([-0.491,  0.485,  0.894]) : # T4
reftag_5 := 2 : tag_5 := vector([-0.486,  0.264,  1.033]) : # T5
reftag_6 := 2 : tag_6 := vector([-0.487,  0.264,  0.889]) : # T6
reftag_7 := 2 : tag_7 := vector([-0.482,  0.012,  1.020]) : # T7
reftag_8 := 2 : tag_8 := vector([-0.481,  0.022,  0.883]) : # T8
reftag_9 := 2 : tag_9 := vector([-0.477, -0.237,  0.975]) : # T9
reftag_10:= 2 : tag_10:= vector([-0.476, -0.229,  0.834]) : # T10
reftag_11:= 2 : tag_11:= vector([-0.474, -0.404,  0.823]) : # T11
reftag_12:= 2 : tag_12:= vector([-0.473, -0.291,  0.630]) : # T12
reftag_13:= 2 : tag_13:= vector([-0.470, -0.427,  0.625]) : # T13
reftag_14:= 2 : tag_14:= vector([ 0.482,  0.702,  1.038]) : # T14
reftag_15:= 2 : tag_15:= vector([ 0.480,  0.700,  0.897]) : # T15
reftag_16:= 2 : tag_16:= vector([ 0.486,  0.506,  1.042]) : # T16
reftag_17:= 2 : tag_17:= vector([ 0.485,  0.506,  0.890]) : # T17
reftag_18:= 2 : tag_18:= vector([ 0.491,  0.264,  1.033]) : # T18
reftag_19:= 2 : tag_19:= vector([ 0.492,  0.255,  0.883]) : # T19
reftag_20:= 2 : tag_20:= vector([ 0.499,  0.050,  1.017]) : # T20
reftag_21:= 2 : tag_21:= vector([ 0.497,  0.045,  0.870]) : # T21
reftag_22:= 2 : tag_22:= vector([ 0.506, -0.230,  0.955]) : # T22
reftag_23:= 2 : tag_23:= vector([ 0.502, -0.209,  0.822]) : # T23
reftag_24:= 2 : tag_24:= vector([ 0.511, -0.371,  0.842]) : # T24
reftag_25:= 2 : tag_25:= vector([ 0.504, -0.267,  0.630]) : # T25
reftag_26:= 2 : tag_26:= vector([ 0.508, -0.407,  0.632]) : # T26

reftag_27:= 1 : tag_27:= vector([ 0.009,  0.037,  0.005]) : # G1
reftag_28:= 1 : tag_28:= vector([-0.138,  0.992, -0.004]) : # G2
reftag_29:= 1 : tag_29:= vector([ 0.155,  0.993, -0.001]) : # G3

reftag_30:= 1 : tag_30:= vector([ 0.0  ,  0.0  ,  0.0  ]) : # GndOri
reftag_31:= 2 : tag_31:= vector([ 0.0  ,  0.0  ,  0.0  ]) : # TCoR
reftag_32:= 2 : tag_32:= vector([ 0.0  ,  0.0  ,  z_2  ]) : # Post


#-------------------------------------------------------------------------#
```

Appendix C

Autolev Code

Torque-driven model - flight and sliding

```
% Vaulting_TD_SL.al
% Torque driven simulation model of gymnastics vaulting.
% Multi-segment gymnast interacts with the vaulting table.
% Sprung shoulder to allow arm lengthening/shortening.
% Shoulder joint centre position moves as a function of shoulder angle.
% Trunk angle varies as a function of hip angle.
% Hands contact a surface segment that has a variable position
% and orientation.
% Reaction at the hands due to surface friction and table surface
% deformation.


% Flight/Sliding part of the model

%--------------------------------------------------

% PHYSICAL DECLARATIONS

Newtonian n
Bodies FIN, HAN, ARM, TRU, PEL, THI, SHA, TBL
Frames Sur, Sho, Scp % Table surface, shoulder and scapula frame
Points O
Points TC, BF, TF, TS
Points FI, HA, WR, SH, HE, SC, ST, RC, HI, KN, TO
Points cmG, cmT
Points P1, P2, P3     % Known table points (points of force
                      % application)

autoz on

%--------------------------------------------------

% MATHEMATICAL DECLARATIONS

% Degrees of freedom
Variables q10'
Variables u10'

% Length of segments, length to mass centre
Constants lTCy, lTCz, lTC2y, lTC2z
Constants lTBL, lTBLo
Constants lFIN, lFINo
Constants lHAN, lHANo
Constants lARM, lARMo
```

```
Constants lTRU, lTRUo
Constants lPEL, lPELo
Constants lTHI, lTHIo
Constants lSHA, lSHAo
Constants lTho          % Length of thorax

% Mass of segments
Constants mTBL, mFIN, mHAN, mARM, mTRU, mPEL, mTHI, mSHA
Mass TBL = mTBL
Mass FIN = mFIN
Mass HAN = mHAN
Mass ARM = mARM
Mass TRU = mTRU
Mass PEL = mPEL
Mass THI = mTHI
Mass SHA = mSHA

% Inertia of segments
Constants iTBL, iFIN, iHAN, iARM, iTRU, iPEL, iTHI, iSHA
Inertia TBL,0,0,iTBL,0,0,0
Inertia FIN,0,0,iFIN,0,0,0
Inertia HAN,0,0,iHAN,0,0,0
Inertia ARM,0,0,iARM,0,0,0
Inertia TRU,0,0,iTRU,0,0,0
Inertia PEL,0,0,iPEL,0,0,0
Inertia THI,0,0,iTHI,0,0,0
Inertia SHA,0,0,iSHA,0,0,0

% System constants
Constants g              % Gravity
Constants D1, D2, D3     % Position of known table points

% System parameters
Constants SSp                    % Static arm-spring length
Constants SF1, SF2, SF3, SF4     % Scapula function
Constants S1, S2, S3             % Position and orientation of surface

Constants KSSp, DSSp             % Shoulder spring stiffness and damping
Constants KKSp, DKSp             % Knuckle spring stiffness and damping
Constants KTSp, KTSp2, DTSp      % Table spring stiffness and damping
Constants KCSp, DCSp             % Contact spring stiffness and damping
Constants mu                     % Friction co-efficient

%--------------------------------------------------

% SPECIFIED JOINT TORQUES

Specified TQWR, TQSH, TQHI, TQKN

% Values to be overwritten in Fortran
TQWR = T^3
TQSH = T^3
TQHI = T^3
TQKN = T^3

%--------------------------------------------------
```

```
% KINEMATIC DIFFERENTIAL EQUATIONS

q1' = u1
q2' = u2
q3' = u3
q4' = u4
q5' = u5
q6' = u6
q7' = u7
q8' = u8
q9' = u9
q10'= u10

%-----------------------------------------------

% GEOMETRY RELATING UNIT VECTORS

simprot (n,   TRU, 3, q3)
simprot (TRU, PEL, 3, q9)
simprot (PEL, THI, 3, q9)
simprot (THI, SHA, 3, q10)
simprot (TRU, Scp, 3, 0)
simprot (Scp, Sho, 3, q8)
simprot (Sho, ARM, 3, 0)
simprot (ARM, HAN, 3, q7)
simprot (HAN, FIN, 3, q5)

simprot (n,   TBL, 3, q6)
simprot (TBL, Sur, 3, S3)


%-----------------------------------------------

% POSITION VECTORS

p_o_TC>    = LTCy*n1>+LTCz*n2>
p_TC_BF>   = LTC2y*TBL1>-LTC2z*TBL2>
p_BF_TBLo> = lTBLo*TBL2>
p_BF_TF>   = lTBL*TBL2>
p_TF_TS>   = S1*TBL1>+S2*TBL2>

p_TS_P1> = -D1*Sur2>
p_TS_P2> = D2*Sur1>
p_TS_P3> = -D3*Sur1>

p_TS_FI>   = q1*Sur1>+q2*Sur2>
p_FI_HA>   = -lFIN*FIN1>
p_HA_FINo> = lFINo*FIN1>
p_HA_WR>   = -lHAN*HAN1>
p_WR_HANo> = lHANo*HAN1>
p_WR_SH>   = -lARM*ARM1>
p_SH_ARMo> = lARMo*ARM1>
p_SH_SC>   = -(SSp+q4)*Sho1>
p_SC_ST>   = -(SF1*(Pi+q8)^3+SF2*(Pi+Q8)^2+SF3*(Pi+q8)+SF4)*Scp1>
p_ST_RC>   = -lTho*TRU1>
p_RC_HE>   = lTRU*TRU1>
p_RC_TRUo> = lTRUo*TRU1>
p_RC_HI>   = -lPEL*PEL1>
p_HI_PELo> = lPELo*PEL1>
```

```
p_HI_THIo> = -lTHIo*THI1>
p_HI_KN>   = -lTHI*THI1>
p_KN_SHAo> = -lSHAo*SHA1>
p_KN_TO>   = -lSHA*SHA1>

p_O_BF>   = p_O_TC>+p_TC_BF>
p_O_TBLo> = p_o_BF>+p_BF_TBLo>
p_O_TF>   = p_O_BF>+p_BF_TF>
p_O_TS>   = p_O_TF>+p_TF_TS>

p_O_P1> = p_O_TS>+p_TS_P1>
p_O_P2> = p_O_TS>+p_TS_P2>
p_O_P3> = p_O_TS>+p_TS_P3>

p_O_FI>   = p_O_TS>+p_TS_FI>
p_O_HA>   = p_O_FI>+p_FI_HA>
p_O_FINo> = p_O_HA>+p_HA_FINo>
p_O_WR>   = p_O_HA>+p_HA_WR>
p_O_HANo> = p_O_WR>+p_WR_HANo>
p_O_SH>   = p_O_WR>+p_WR_SH>
p_O_ARMo> = p_O_SH>+p_SH_ARMo>
p_O_SC>   = p_O_SH>+p_SH_SC>
p_O_ST>   = p_O_SC>+p_SC_ST>
p_O_RC>   = p_O_ST>+p_ST_RC>
p_O_HE>   = p_O_RC>+p_RC_HE>
p_O_TRUo> = p_O_RC>+p_RC_TRUo>
p_O_HI>   = p_O_RC>+p_RC_HI>
p_O_PELo> = p_O_HI>+p_HI_PELo>
p_O_THIo> = p_O_HI>+p_HI_THIo>
p_O_KN>   = p_O_HI>+p_HI_KN>
p_O_SHAo> = p_O_KN>+p_KN_SHAo>
p_O_TO>   = p_O_KN>+p_KN_TO>

p_P1_FI> = p_O_FI>-p_O_P1>
p_P2_FI> = p_O_FI>-p_O_P2>
p_P3_FI> = p_O_FI>-p_O_P3>

p_TS_HA> = p_O_HA>-p_O_TS>
p_P1_HA> = p_O_HA>-p_O_P1>
p_P2_HA> = p_O_HA>-p_O_P2>
p_P3_HA> = p_O_HA>-p_O_P3>

p_TS_WR> = p_O_WR>-p_O_TS>
p_P1_WR> = p_O_WR>-p_O_P1>
p_P2_WR> = p_O_WR>-p_O_P2>
p_P3_WR> = p_O_WR>-p_O_P3>

p_O_cmG> = cm(O,FIN,HAN,ARM,TRU,PEL,THI,SHA)
p_O_cmT> = cm(O,TBL)

%-------------------------------------------------

% POSITIONS IN Y-Z CO-ORDINATES

poTCy = dot(p_O_TC>,n1>)
poTCz = dot(p_O_TC>,n2>)
poBFy = dot(p_O_BF>,n1>)
poBFz = dot(p_O_BF>,n2>)
poTFy = dot(p_O_TF>,n1>)
```

```
poTFz = dot(p_O_TF>,n2>)
poTSy = dot(p_O_TS>,n1>)
poTSz = dot(p_O_TS>,n2>)

poFIy = dot(p_O_FI>,n1>)
poFIz = dot(p_O_FI>,n2>)
poHAy = dot(p_O_HA>,n1>)
poHAz = dot(p_O_HA>,n2>)
poWRy = dot(p_O_WR>,n1>)
poWRz = dot(p_O_WR>,n2>)
poSHy = dot(p_O_SH>,n1>)
poSHz = dot(p_O_SH>,n2>)
poSCy = dot(p_O_SC>,n1>)
poSCz = dot(p_O_SC>,n2>)
poSTy = dot(p_O_ST>,n1>)
poSTz = dot(p_O_ST>,n2>)
poRCy = dot(p_O_RC>,n1>)
poRCz = dot(p_O_RC>,n2>)
poHEy = dot(p_O_HE>,n1>)
poHEz = dot(p_O_HE>,n2>)
poHIy = dot(p_O_HI>,n1>)
poHIz = dot(p_O_HI>,n2>)
poKNy = dot(p_O_KN>,n1>)
poKNz = dot(p_O_KN>,n2>)
poTOy = dot(p_O_TO>,n1>)
poTOz = dot(p_O_TO>,n2>)

pocmGy = dot(p_O_cmG>,n1>)
pocmGz = dot(p_O_cmG>,n2>)
pocmTy = dot(p_O_cmT>,n1>)
pocmTz = dot(p_O_cmT>,n2>)

%-------------------------------------------------

% POSITIONS RELATIVE TO SUR-FRAME

poTSFIt = dot(p_TS_FI>,Sur1>)
poTSFIn = dot(p_TS_FI>,Sur2>)
poP1FIt = dot(p_P1_FI>,Sur1>)
poP1FIn = dot(p_P1_FI>,Sur2>)
poP2FIt = dot(p_P2_FI>,Sur1>)
poP2FIn = dot(p_P2_FI>,Sur2>)
poP3FIt = dot(p_P3_FI>,Sur1>)
poP3FIn = dot(p_P3_FI>,Sur2>)

poTSHAt = dot(p_TS_HA>,Sur1>)
poTSHAn = dot(p_TS_HA>,Sur2>)
poP1HAt = dot(p_P1_HA>,Sur1>)
poP1HAn = dot(p_P1_HA>,Sur2>)
poP2HAt = dot(p_P2_HA>,Sur1>)
poP2HAn = dot(p_P2_HA>,Sur2>)
poP3HAt = dot(p_P3_HA>,Sur1>)
poP3HAn = dot(p_P3_HA>,Sur2>)

poTSWRt = dot(p_TS_WR>,Sur1>)
poTSWRn = dot(p_TS_WR>,Sur2>)
poP1WRt = dot(p_P1_WR>,Sur1>)
poP1WRn = dot(p_P1_WR>,Sur2>)
poP2WRt = dot(p_P2_WR>,Sur1>)
```

```
poP2WRn = dot(p_P2_WR>,Sur2>)
poP3WRt = dot(p_P3_WR>,Sur1>)
poP3WRn = dot(p_P3_WR>,Sur2>)

%-------------------------------------------------

% ANGULAR AND LINEAR VELOCITIES

w_TRU_n>   = u3*TRU3>
w_PEL_TRU> = u9*PEL3>
w_THI_PEL> = u9*THI3>
w_SHA_THI> = u10*SHA3>
w_Scp_TRU> = 0>
w_Sho_Scp> = u8*Sho3>
w_ARM_Sho> = 0>
w_HAN_ARM> = u7*HAN3>
w_FIN_HAN> = u5*FIN3>
w_TBL_n>   = u6*TBL3>
w_Sur_TBL> = 0>

v_O_n> = 0>

v_TC_n> = dt(p_O_TC>,n)
v2pts(n,TBL,TC,BF)
v2pts(n,TBL,BF,TBLo)
v2pts(n,TBL,BF,TF)
v2pts(n,TBL,BF,TS)

v2pts(n,TBL,BF,P1)
v2pts(n,TBL,BF,P2)
v2pts(n,TBL,BF,P3)

v_FI_n> = dt(p_O_FI>,n)
v2pts(n,FIN,FI,HA)
v2pts(n,FIN,HA,FINo)
v2pts(n,HAN,HA,WR)
v2pts(n,HAN,WR,HANo)
v2pts(n,ARM,WR,SH)
v2pts(n,ARM,SH,ARMo)
v_SC_n> = v_SH_n>+dt(p_SH_SC>,n)
v_ST_n> = v_SC_n>+dt(p_SC_ST>,n)
v2pts(n,TRU,ST,RC)
v2pts(n,TRU,RC,HE)
v2pts(n,TRU,RC,TRUo)
v2pts(n,PEL,RC,HI)
v2pts(n,PEL,HI,PELo)
v2pts(n,THI,HI,THIo)
v2pts(n,THI,HI,KN)
v2pts(n,SHA,KN,SHAo)
v2pts(n,SHA,KN,TO)

v_cmG_n>=dt(p_O_cmG>,n)
v_cmT_n>=dt(p_O_cmT>,n)

%-------------------------------------------------

% VELOCITIES IN Y-Z CO-ORDINATES

vocmGy = dt(pocmGy)
```

```
vocmGz = dt(pocmGz)
vocmTy = dt(pocmTy)
vocmTz = dt(pocmTz)


% VELOCITIES RELATIVE TO SUR-FRAME

voTSFIt = dt(poTSFIt)
voTSFIn = dt(poTSFIn)
voTSHAt = dt(poTSHAt)
voTSHAn = dt(poTSHAn)
voTSWRt = dt(poTSWRt)
voTSWRn = dt(poTSWRn)

%-------------------------------------------------

% ANGULAR AND LINEAR ACCELERATIONS

alf_TRU_n>   = dt(w_TRU_n>,n)
alf_PEL_TRU> = dt(w_PEL_TRU>,n)
alf_THI_PEL> = dt(w_THI_PEL>,n)
alf_SHA_THI> = dt(w_SHA_THI>,n)
alf_Scp_TRU> = dt(w_Scp_TRU>,n)
alf_Sho_Scp> = dt(w_Sho_Scp>,n)
alf_ARM_Sho> = dt(w_ARM_Sho>,n)
alf_HAN_ARM> = dt(w_HAN_ARM>,n)
alf_FIN_HAN> = dt(w_FIN_HAN>,n)
alf_TBL_n>   = dt(w_TBL_n>,n)
alf_Sur_TBL> = dt(w_Sur_TBL>,n)


a_O_n> = 0>

a_TC_n>   = dt(v_TC_n>,n)
a_BF_n>   = dt(v_BF_n>,n)
a_TBLo_n> = dt(v_TBLo_n>,n)
a_TF_n>   = dt(v_TF_n>,n)
a_TS_n>   = dt(v_TS_n>,n)

a_FI_n>   = dt(v_FI_n>,n)
a_FINo_n> = dt(v_FINo_n>,n)
a_HA_n>   = dt(v_HA_n>,n)
a_HANo_n> = dt(v_HANo_n>,n)
a_WR_n>   = dt(v_WR_n>,n)
a_ARMo_n> = dt(v_ARMo_n>,n)
a_SH_n>   = dt(v_SH_n>,n)
a_SC_n>   = dt(v_SC_n>,n)
a_ST_n>   = dt(v_ST_n>,n)
a_TRUo_n> = dt(v_TRUo_n>,n)
a_HE_n>   = dt(v_HE_n>,n)
a_RC_n>   = dt(v_RC_n>,n)
a_PELo_n> = dt(v_PELo_n>,n)
a_HI_n>   = dt(v_HI_n>,n)
a_THIo_n> = dt(v_THIo_n>,n)
a_KN_n>   = dt(v_KN_n>,n)
a_SHAo_n> = dt(v_SHAo_n>,n)
a_TO_n>   = dt(v_TO_n>,n)

a_cmG_n> = dt(v_cmG_n>,n)
```

```
a_cmT_n> = dt(v_cmT_n>,n)

%--------------------------------------------------

% FORCES AND TORQUES

% Forces

% Gravity
gravity(g*n2>)

% Shoulder spring
FSSp = -KSSp*q4-DSSp*u4
Force(SC/SH,FSSp*Sho1>)

% Contact forces on hands - Values to be overwritten in
% Fortran with IF loop for contact / non-contact
FnFI = -KCSp*poTSFIn-DCSp*voTSFIn*ABS(poTSFIn)
FtFI = mu*FnFI

FnHA = -KCSp*poTSHAn-DCSp*voTSHAn*ABS(poTSHAn)
FtHA = mu*FnHA

FnWR = -KCSp*poTSWRn-DCSp*voTSWRn*ABS(poTSWRn)
FtWR = mu*FnWR

force(FI,FtFI*Sur1>+FnFI*Sur2>)
force(HA,FtHA*Sur1>+FnHA*Sur2>)
force(WR,FtWR*Sur1>+FnWR*Sur2>)


% Contact forces on table - Values to be overwritten in
% Fortran with IF loop for contact / non-contact
Ft0 = 0
Ft1 = 0
Fn2 = 0
Fn3 = 0

force(TS,-Ft0*Sur1>)
force(P1,-Ft1*Sur1>)
force(P2,-Fn2*Sur2>)
force(P3,-Fn3*Sur2>)

% Torques

% Knuckle spring
TKSp = -KKSp*q5-DKSp*u5
Torque(HAN/FIN,TKSp*HAN3>)

% Table
% To be overwritten in Fortran with IF loop for second
% stiffness term
TTSp = -KTSp*q6-KTSp2*q6^2-DTSp*u6*ABS(q6)
       -(mTBL*g*(LTC2Y*COS(Q6)-(LTBLO-LTC2Z)*SIN(Q6)))
Torque(TBL,TTSp*TBL3>)

% Joint Torques

Torque(ARM/HAN,TQWR*ARM3>)
```

```
Torque(Sho/Scp,TQSH*Scp3>)
Torque(THI/PEL,TQHI*PEL3>)
Torque(THI/SHA,TQKN*SHA3>)

%-------------------------------------------------

% EQUATIONS OF MOTION

zero=fr()+frstar()
kane()

%-------------------------------------------------

% ENERGY AND MOMENTUM

% Calculate kinetic and potential energy

ke   = ke()
peg  = (mFIN+mHAN+mARM+mTRU+mPEL+mTHI+mSHA)*(-g)*pocmGz
       + mTBL*(-g)*pocmTz
peas = 0.5*KSSp*q4^2
peks = 0.5*KKSp*q5^2
pets = 0.5*KTSp*q6^2+(1/3)*KTSp2*(ABS(Q6))^3
pecs = 0.5*KCSp*poTSFIn^2+0.5*KCSp*poTSHAn^2+0.5*KCSp*poTSWRn^2
te   = ke + peg + peas + peks + pets + pecs

% Calculate angular momentum about gymnast mass centre

amom> = momentum(angular,cmG,FIN,HAN,ARM,TRU,PEL,THI,SHA)
amom  = dot(amom>,N3>)

% Calculate linear momentum

lmom> = momentum(linear) - momentum(linear,TBL)
hormom = dot(lmom>,N1>)
vermom = dot(lmom>,N2>)

%-------------------------------------------------

% INPUTS

% Inputs overwritten in relevant .in files for each vault

input tinitial=0.0, tfinal=0.5
input integstp=0.0001, printint=10
input abserr=1.0e-8, relerr=1.0e-07

input q1=0, q2=0, q3=0, q4=0, q5=0, q6=0, q7=0, q8=0, q9=0, q10=0
input u1=0, u2=0, u3=0, u4=0, u5=0, u6=0, u7=0, u8=0, u9=0, u10=0

input lFIN=0, lFINo=0, lHAN=0, lHANo=0, lARM=0, lARMo=0, lTRU=0, lTRUo=0
input lPEL=0, lPELo=0, lTHI=0, lTHIo=0, lSHA=0, lSHAo=0, lTho=0
input lTCy=0, lTCz=0, lTC2y=0, lTC2z=0, lTBL=0, lTBLo=0

input mTBL=0, mFIN=0, mHAN=0, mARM=0, mTRU=0, mPEL=0, mTHI=0, mSHA=0
input iTBL=0, iFIN=0, iHAN=0, iARM=0, iTRU=0, iPEL=0, iTHI=0, iSHA=0

input g=0
input S1=0, S2=0, S3=0
```

```
input D1=0, D2=0, D3=0

input SSp=0, SF1=0, SF2=0, SF3=0, SF4=0
input KSSp=0, DSSp=0
input KKSp=0, DKSp=0
input KCSp=0, DCSp=0
input mu=0
input KTSp=0, KTSp2=0, DTSp=0

%-------------------------------------------------

% OUTPUTS

output t,q1,q2,q3,q4,q5,q6,q7,q8,q9,q10,u1,u2,u3,u4,u5,u6,u7,u8,u9,u10
output t,poBFy,poBFz,poTFy,poTFz,poTSy,poTSz,poFIy,poFIz,poHAy,poHAz,
       poWRy,poWRz,poSHy,poSHz,poSCy,poSCz,poHEy,poHEz,poSTy,poSTz,
       poRCy,poRCz,poHIy,poHIz,poKNy,poKNz,poTOy,poTOz,pocmGy,pocmGz
output t,pocmGy,pocmGz,vocmGy,vocmGz,pocmTy,pocmTz,vocmTy,vocmTz
output t,amom,hormom,vermom,te,ke,peg,peas,peks,pets,pecs
output t,FSSp,TKSp,TTSp,FnFI,FtFI,FnHA,FtHA,FnWR,FtWR,Ft0,Ft1,Fn2,Fn3
output t,poTSFIt,poTSFIn,poP1FIt,poP1FIn,poP2FIt,poP2FIn,poP3FIt,poP3FIn,
       poTSHAt,poTSHAn,poP1HAt,poP1HAn,poP2HAt,poP2HAn,poP3HAt,poP3HAn,
       poTSWRt,poTSWRn,poP1WRt,poP1WRn,poP2WRt,poP2WRn,poP3WRt,poP3WRn
output t,voTSFIt,voTSFIn,voTSHAt,voTSHAn,voTSWRt,voTSWRn

%-------------------------------------------------

% UNITS

units [t] = s
units [q1, q2, q4] = m,   [q3, q5, q6, q7, q8, q9, q10] = rads
units [u1, u2, u4] = m/s, [u3, u5, u6, u7, u8, u9, u10] = rads/s


units [lFIN, lFINo, lHAN, lHANo, lARM, lARMo, lTRU, lTRUo] = m
units [lPEL, lPELo, lTHI, lTHIo, lSHA, lSHAo, lTho] = m
units [lTCy, lTCz, lTC2y, lTC2z, lTBL, lTBLo] = m

units [mTBL, mFIN, mHAN, mARM, mTRU, mPEL, mTHI, mSHA] = kg
units [iTBL, iFIN, iHAN, iARM, iTRU, iPEL, iTHI, iSHA] = kg.m^2

units [g] = m/s^2
units [S1, S2] = m, [S3] = rad
units [D1, D2, D3] = m

units [SSp] = m
units [SF1] = m/rad^3, [SF2] = m/rad^2, [SF3] = m/rad, [SF4] = m
units [KSSp] = N/m, [DSSp] = N.s/m
units [KKSp] = N.m/rad, [DKSp] = N.m.s/rad
units [KCSp] = N/m, [DCSp] = N.s/m
units [KTSp] = N.m/rad, [KTSp2] = N.m/rad^2, [DTSp] = N.m.s/rad
units [mu] = unitless

units [poBFy,poBFz,poTFy,poTFz,poTSy,poTSz] = m
units [poFIy,poFIz,poHAy,poHAz,poWRy,poWRz,poSHy,poSHz,poSCy,poSCz] = m
units [poHEy,poHEz,poSTy,poSTz,poRCy,poRCz,poHIy,poHIz,poKNy,poKNz] = m
units [poTOy,poTOz] = m
units [pocmGy,pocmGz,pocmTy,pocmTz] = m
units [vocmGy,vocmGz,vocmTy,vocmTz] = m/s
```

```
units [amom] = kg.m^2.rad/s, [hormom, vermom] = kg.m/s^2
units [ke,peg,peas,peks,pets,pecs,te] = kg.m^2/s^2
units [FSSp,FnFI,FtFI,FnHA,FtHA,FnWR,FtWR,Ft0,Ft1,Fn2,Fn3] = N,
units [TKSp] = N.m, [TTSp] = N.m
units [poTSFIt,poTSFIn,poP1FIt,poP1FIn,poP2FIt,poP2FIn] = m
units [poP3FIt,poP3FIn,poTSHAt,poTSHAn,poP1HAt,poP1HAn] = m
units [poP2HAt,poP2HAn,poP3HAt,poP3HAn,poTSWRt,poTSWRn] = m
units [poP1WRt,poP1WRn,poP2WRt,poP2WRn,poP3WRt,poP3WRn] = m
units [voTSFIt,voTSFIn,voTSHAt,voTSHAn,voTSWRt,voTSWRn] = m/s

%-----------------------------------------------

% GENERATE FORTRAN CODE

save Vaulting_TD_SL.all

code dynamics() Vaulting_TD_SL.f, subs
```

Torque-driven model - stiction

```
% Vaulting_TD_ST.al

% Torque driven simulation model of gymnastics vaulting.
% Multi-segment gymnast interacts with the vaulting table.
% Sprung shoulder to allow arm lengthening/shortening.
% Shoulder joint centre position moves as a function of shoulder angle.
% Trunk angle varies as a function of hip angle.
% Hands contact a surface segment that has a variable position
% and orientation.
% Reaction at the hands due to surface friction and table surface
% deformation.


% Stiction part of the model - auxiliary force in tangential direction

%--------------------------------------------------

% PHYSICAL DECLARATIONS

Newtonian n
Bodies FIN, HAN, ARM, TRU, PEL, THI, SHA, TBL
Frames Sur, Sho, Scp % Table surface, shoulder and scapula frame
Points O
Points TC, BF, TF, TS
Points FI, HA, WR, SH, HE, SC, ST, RC, HI, KN, TO
Points cmG, cmT
Points P1, P2, P3     % Known table points (points of force
                      % application)
Points PC             % Point of auxiliary force application

autoz on

%--------------------------------------------------

% MATHEMATICAL DECLARATIONS

% Degrees of freedom
Variables q10'
Variables u10'

Variables Fax
zee_not = [Fax]

% Length of segments, length to mass centre
Constants lTCy, lTCz, lTC2y, lTC2z
Constants lTBL, lTBLo
Constants lFIN, lFINo
Constants lHAN, lHANo
Constants lARM, lARMo
Constants lTRU, lTRUo
Constants lPEL, lPELo
Constants lTHI, lTHIo
Constants lSHA, lSHAo
Constants lTho          % Length of thorax
```

```
% Mass of segments
Constants mTBL, mFIN, mHAN, mARM, mTRU, mPEL, mTHI, mSHA
Mass TBL = mTBL
Mass FIN = mFIN
Mass HAN = mHAN
Mass ARM = mARM
Mass TRU = mTRU
Mass PEL = mPEL
Mass THI = mTHI
Mass SHA = mSHA

% Inertia of segments
Constants iTBL, iFIN, iHAN, iARM, iTRU, iPEL, iTHI, iSHA
Inertia TBL,0,0,iTBL,0,0,0
Inertia FIN,0,0,iFIN,0,0,0
Inertia HAN,0,0,iHAN,0,0,0
Inertia ARM,0,0,iARM,0,0,0
Inertia TRU,0,0,iTRU,0,0,0
Inertia PEL,0,0,iPEL,0,0,0
Inertia THI,0,0,iTHI,0,0,0
Inertia SHA,0,0,iSHA,0,0,0

% System constants
Constants g             % Gravity
Constants D1, D2, D3    % Position of known table points

% System parameters
Constants SSp                   % Static arm-spring length
Constants SF1, SF2, SF3, SF4    % Scapula function
Constants S1, S2, S3            % Position and orientation of surface

Constants KSSp, DSSp            % Shoulder spring stiffness and damping
Constants KKSp, DKSp            % Knuckle spring stiffness and damping
Constants KTSp, KTSp2, DTSp     % Table spring stiffness and damping
Constants KCSp, DCSp            % Contact spring stiffness and damping
Constants mu                    % Friction co-efficient

Constants C1                    % Tangential position of hands relative
                                % to surface at the start of stiction

%-------------------------------------------------

% SPECIFIED JOINT TORQUES

Specified TQWR, TQSH, TQHI, TQKN

% Values to be overwritten in Fortran
TQWR = T^3
TQSH = T^3
TQHI = T^3
TQKN = T^3

%-------------------------------------------------

% KINEMATIC DIFFERENTIAL EQUATIONS

q1' = u1
q2' = u2
q3' = u3
```

```
q4' = u4
q5' = u5
q6' = u6
q7' = u7
q8' = u8
q9' = u9
q10'= u10

%-------------------------------------------------

% GEOMETRY RELATING UNIT VECTORS

simprot (n,   TRU, 3, q3)
simprot (TRU, PEL, 3, q9)
simprot (PEL, THI, 3, q9)
simprot (THI, SHA, 3, q10)
simprot (TRU, Scp, 3, 0)
simprot (Scp, Sho, 3, q8)
simprot (Sho, ARM, 3, 0)
simprot (ARM, HAN, 3, q7)
simprot (HAN, FIN, 3, q5)

simprot (n,   TBL, 3, q6)
simprot (TBL, Sur, 3, S3)

%-------------------------------------------------

% POSITION VECTORS

p_o_TC>    = LTCy*n1>+LTCz*n2>
p_TC_BF>   = LTC2y*TBL1>-LTC2z*TBL2>
p_BF_TBLo> = lTBLo*TBL2>
p_BF_TF>   = lTBL*TBL2>
p_TF_TS>   = S1*TBL1>+S2*TBL2>

p_TS_P1> = -D1*Sur2>
p_TS_P2> = D2*Sur1>
p_TS_P3> = -D3*Sur1>

p_TS_FI>   = C1*Sur1>+q2*Sur2>
p_FI_HA>   = -lFIN*FIN1>
p_HA_FINo> = lFINo*FIN1>
p_HA_WR>   = -lHAN*HAN1>
p_WR_HANo> = lHANo*HAN1>
p_WR_SH>   = -lARM*ARM1>
p_SH_ARMo> = lARMo*ARM1>
p_SH_SC>   = -(SSp+q4)*Sho1>
p_SC_ST>   = -(SF1*(Pi+q8)^3+SF2*(Pi+Q8)^2+SF3*(Pi+q8)+SF4)*Scp1>
p_ST_RC>   = -lTho*TRU1>
p_RC_HE>   = lTRU*TRU1>
p_RC_TRUo> = lTRUo*TRU1>
p_RC_HI>   = -lPEL*PEL1>
p_HI_PELo> = lPELo*PEL1>
p_HI_THIo> = -lTHIo*THI1>
p_HI_KN>   = -lTHI*THI1>
p_KN_SHAo> = -lSHAo*SHA1>
p_KN_TO>   = -lSHA*SHA1>

p_O_BF>   = p_O_TC>+p_TC_BF>
```

```
p_O_TBLo> = p_o_BF>+p_BF_TBLo>
p_O_TF>   = p_O_BF>+p_BF_TF>
p_O_TS>   = p_O_TF>+p_TF_TS>

p_O_P1> = p_O_TS>+p_TS_P1>
p_O_P2> = p_O_TS>+p_TS_P2>
p_O_P3> = p_O_TS>+p_TS_P3>

p_O_FI>   = p_O_TS>+p_TS_FI>
p_O_HA>   = p_O_FI>+p_FI_HA>
p_O_FINo> = p_O_HA>+p_HA_FINo>
p_O_WR>   = p_O_HA>+p_HA_WR>
p_O_HANo> = p_O_WR>+p_WR_HANo>
p_O_SH>   = p_O_WR>+p_WR_SH>
p_O_ARMo> = p_O_SH>+p_SH_ARMo>
p_O_SC>   = p_O_SH>+p_SH_SC>
p_O_ST>   = p_O_SC>+p_SC_ST>
p_O_RC>   = p_O_ST>+p_ST_RC>
p_O_HE>   = p_O_RC>+p_RC_HE>
p_O_TRUo> = p_O_RC>+p_RC_TRUo>
p_O_HI>   = p_O_RC>+p_RC_HI>
p_O_PELo> = p_O_HI>+p_HI_PELo>
p_O_THIo> = p_O_HI>+p_HI_THIo>
p_O_KN>   = p_O_HI>+p_HI_KN>
p_O_SHAo> = p_O_KN>+p_KN_SHAo>
p_O_TO>   = p_O_KN>+p_KN_TO>

p_P1_FI> = p_O_FI>-p_O_P1>
p_P2_FI> = p_O_FI>-p_O_P2>
p_P3_FI> = p_O_FI>-p_O_P3>

p_TS_HA> = p_O_HA>-p_O_TS>
p_P1_HA> = p_O_HA>-p_O_P1>
p_P2_HA> = p_O_HA>-p_O_P2>
p_P3_HA> = p_O_HA>-p_O_P3>

p_TS_WR> = p_O_WR>-p_O_TS>
p_P1_WR> = p_O_WR>-p_O_P1>
p_P2_WR> = p_O_WR>-p_O_P2>
p_P3_WR> = p_O_WR>-p_O_P3>

p_O_cmG> = cm(O,FIN,HAN,ARM,TRU,PEL,THI,SHA)
p_O_cmT> = cm(O,TBL)

%--------------------------------------------------

% POSITIONS IN Y-Z CO-ORDINATES

poTCy = dot(p_O_TC>,n1>)
poTCz = dot(p_O_TC>,n2>)
poBFy = dot(p_O_BF>,n1>)
poBFz = dot(p_O_BF>,n2>)
poTFy = dot(p_O_TF>,n1>)
poTFz = dot(p_O_TF>,n2>)
poTSy = dot(p_O_TS>,n1>)
poTSz = dot(p_O_TS>,n2>)

poFIy = dot(p_O_FI>,n1>)
poFIz = dot(p_O_FI>,n2>)
```

```
poHAy = dot(p_O_HA>,n1>)
poHAz = dot(p_O_HA>,n2>)
poWRy = dot(p_O_WR>,n1>)
poWRz = dot(p_O_WR>,n2>)
poSHy = dot(p_O_SH>,n1>)
poSHz = dot(p_O_SH>,n2>)
poSCy = dot(p_O_SC>,n1>)
poSCz = dot(p_O_SC>,n2>)
poSTy = dot(p_O_ST>,n1>)
poSTz = dot(p_O_ST>,n2>)
poRCy = dot(p_O_RC>,n1>)
poRCz = dot(p_O_RC>,n2>)
poHEy = dot(p_O_HE>,n1>)
poHEz = dot(p_O_HE>,n2>)
poHIy = dot(p_O_HI>,n1>)
poHIz = dot(p_O_HI>,n2>)
poKNy = dot(p_O_KN>,n1>)
poKNz = dot(p_O_KN>,n2>)
poTOy = dot(p_O_TO>,n1>)
poTOz = dot(p_O_TO>,n2>)

pocmGy = dot(p_O_cmG>,n1>)
pocmGz = dot(p_O_cmG>,n2>)
pocmTy = dot(p_O_cmT>,n1>)
pocmTz = dot(p_O_cmT>,n2>)

%-------------------------------------------------

% POSITIONS RELATIVE TO SUR-FRAME

poTSFIt = dot(p_TS_FI>,Sur1>)
poTSFIn = dot(p_TS_FI>,Sur2>)
poP1FIt = dot(p_P1_FI>,Sur1>)
poP1FIn = dot(p_P1_FI>,Sur2>)
poP2FIt = dot(p_P2_FI>,Sur1>)
poP2FIn = dot(p_P2_FI>,Sur2>)
poP3FIt = dot(p_P3_FI>,Sur1>)
poP3FIn = dot(p_P3_FI>,Sur2>)

poTSHAt = dot(p_TS_HA>,Sur1>)
poTSHAn = dot(p_TS_HA>,Sur2>)
poP1HAt = dot(p_P1_HA>,Sur1>)
poP1HAn = dot(p_P1_HA>,Sur2>)
poP2HAt = dot(p_P2_HA>,Sur1>)
poP2HAn = dot(p_P2_HA>,Sur2>)
poP3HAt = dot(p_P3_HA>,Sur1>)
poP3HAn = dot(p_P3_HA>,Sur2>)

poTSWRt = dot(p_TS_WR>,Sur1>)
poTSWRn = dot(p_TS_WR>,Sur2>)
poP1WRt = dot(p_P1_WR>,Sur1>)
poP1WRn = dot(p_P1_WR>,Sur2>)
poP2WRt = dot(p_P2_WR>,Sur1>)
poP2WRn = dot(p_P2_WR>,Sur2>)
poP3WRt = dot(p_P3_WR>,Sur1>)
poP3WRn = dot(p_P3_WR>,Sur2>)

%-------------------------------------------------
```

```
% ANGULAR AND LINEAR VELOCITIES

w_TRU_n>   = u3*TRU3>
w_PEL_TRU> = u9*PEL3>
w_THI_PEL> = u9*THI3>
w_SHA_THI> = u10*SHA3>
w_Scp_TRU> = 0>
w_Sho_Scp> = u8*Sho3>
w_ARM_Sho> = 0>
w_HAN_ARM> = u7*HAN3>
w_FIN_HAN> = u5*FIN3>
w_TBL_n>   = u6*TBL3>
w_Sur_TBL> = 0>

v_O_n> = 0>

v_TC_n> = dt(p_O_TC>,n)
v2pts(n,TBL,TC,BF)
v2pts(n,TBL,BF,TBLo)
v2pts(n,TBL,BF,TF)
v2pts(n,TBL,BF,TS)

v2pts(n,TBL,BF,P1)
v2pts(n,TBL,BF,P2)
v2pts(n,TBL,BF,P3)

v_PC_n> = u1*Sur1>
v_FI_n> = dt(p_O_FI>,n)+v_PC_n>
v2pts(n,FIN,FI,HA)
v2pts(n,FIN,HA,FINo)
v2pts(n,HAN,HA,WR)
v2pts(n,HAN,WR,HANo)
v2pts(n,ARM,WR,SH)
v2pts(n,ARM,SH,ARMo)
v_SC_n> = v_SH_n>+dt(p_SH_SC>,n)
v_ST_n> = v_SC_n>+dt(p_SC_ST>,n)
v2pts(n,TRU,ST,RC)
v2pts(n,TRU,RC,HE)
v2pts(n,TRU,RC,TRUo)
v2pts(n,PEL,RC,HI)
v2pts(n,PEL,HI,PELo)
v2pts(n,THI,HI,THIo)
v2pts(n,THI,HI,KN)
v2pts(n,SHA,KN,SHAo)
v2pts(n,SHA,KN,TO)

v_cmG_n>=dt(p_O_cmG>,n)
v_cmT_n>=dt(p_O_cmT>,n)

%-------------------------------------------------

% VELOCITIES IN Y-Z CO-ORDINATES

vocmGy = dt(pocmGy)
vocmGz = dt(pocmGz)
vocmTy = dt(pocmTy)
vocmTz = dt(pocmTz)
```

```
% VELOCITIES RELATIVE TO SUR-FRAME

voTSFIt = dt(poTSFIt)
voTSFIn = dt(poTSFIn)
voTSHAt = dt(poTSHAt)
voTSHAn = dt(poTSHAn)
voTSWRt = dt(poTSWRt)
voTSWRn = dt(poTSWRn)

%--------------------------------------------------

% IMPOSE MOTION CONSTRAINTS

Auxiliary[1] = u1
constrain(Auxiliary[u1])

%--------------------------------------------------

% ANGULAR AND LINEAR ACCELERATIONS

alf_TRU_n>   = dt(w_TRU_n>,n)
alf_PEL_TRU> = dt(w_PEL_TRU>,n)
alf_THI_PEL> = dt(w_THI_PEL>,n)
alf_SHA_THI> = dt(w_SHA_THI>,n)
alf_Scp_TRU> = dt(w_Scp_TRU>,n)
alf_Sho_Scp> = dt(w_Sho_Scp>,n)
alf_ARM_Sho> = dt(w_ARM_Sho>,n)
alf_HAN_ARM> = dt(w_HAN_ARM>,n)
alf_FIN_HAN> = dt(w_FIN_HAN>,n)
alf_TBL_n>   = dt(w_TBL_n>,n)
alf_Sur_TBL> = dt(w_Sur_TBL>,n)


a_O_n> = 0>

a_TC_n>   = dt(v_TC_n>,n)
a_BF_n>   = dt(v_BF_n>,n)
a_TBLo_n> = dt(v_TBLo_n>,n)
a_TF_n>   = dt(v_TF_n>,n)
a_TS_n>   = dt(v_TS_n>,n)

a_FI_n>   = dt(v_FI_n>,n)
a_FINo_n> = dt(v_FINo_n>,n)
a_HA_n>   = dt(v_HA_n>,n)
a_HANo_n> = dt(v_HANo_n>,n)
a_WR_n>   = dt(v_WR_n>,n)
a_ARMo_n> = dt(v_ARMo_n>,n)
a_SH_n>   = dt(v_SH_n>,n)
a_SC_n>   = dt(v_SC_n>,n)
a_ST_n>   = dt(v_ST_n>,n)
a_TRUo_n> = dt(v_TRUo_n>,n)
a_HE_n>   = dt(v_HE_n>,n)
a_RC_n>   = dt(v_RC_n>,n)
a_PELo_n> = dt(v_PELo_n>,n)
a_HI_n>   = dt(v_HI_n>,n)
a_THIo_n> = dt(v_THIo_n>,n)
a_KN_n>   = dt(v_KN_n>,n)
a_SHAo_n> = dt(v_SHAo_n>,n)
a_TO_n>   = dt(v_TO_n>,n)
```

```
a_cmG_n> = dt(v_cmG_n>,n)
a_cmT_n> = dt(v_cmT_n>,n)

%--------------------------------------------------

% FORCES AND TORQUES

% Forces

% Gravity
gravity(g*n2>)

% Shoulder spring
FSSp = -KSSp*q4-DSSp*u4
Force(SC/SH,FSSp*Sho1>)

% Contact forces on hands - Values to be overwritten in
% Fortran with IF loop for contact / non-contact
FnFI = -KCSp*poTSFIn-DCSp*voTSFIn
FnHA = -KCSp*poTSHAn-DCSp*voTSHAn
FnWR = -KCSp*poTSWRn-DCSp*voTSWRn

force(FI,FnFI*Sur2>)
force(HA,FnHA*Sur2>)
force(WR,FnWR*Sur2>)

% Contact forces on table - Values to be overwritten in
% Fortran with IF loop for contact / non-contact
Fn2 = 0
Fn3 = 0

force(P2,-Fn2*Sur2>)
force(P3,-Fn3*Sur2>)

force(PC,Fax*Sur1>)


% Torques

% Knuckle spring
TKSp = -KKSp*q5-DKSp*u5
Torque(HAN/FIN,TKSp*HAN3>)

% Table
% To be overwritten in Fortran with IF loop for second
% stiffness term
TTSp = -KTSp*q6-KTSp2*q6^2-DTSp*u6*ABS(q6)
       -(mTBL*g*(LTC2Y*COS(Q6)-(LTBLO-LTC2Z)*SIN(Q6)))
Torque(TBL,TTSp*TBL3>)

% Joint Torques

Torque(ARM/HAN,TQWR*ARM3>)
Torque(Sho/Scp,TQSH*Scp3>)
Torque(THI/PEL,TQHI*PEL3>)
Torque(THI/SHA,TQKN*SHA3>)

%--------------------------------------------------
```

```
% EQUATIONS OF MOTION

zero=fr()+frstar()
kane(Fax)

%-------------------------------------------------

% ENERGY AND MOMENTUM

% Calculate kinetic and potential energy

ke   = ke()
peg  = (mFIN+mHAN+mARM+mTRU+mPEL+mTHI+mSHA)*(-g)*pocmGz
       + mTBL*(-g)*pocmTz
peas = 0.5*KSSp*q4^2
peks = 0.5*KKSp*q5^2
pets = 0.5*KTSp*q6^2+(1/3)*KTSp2*(ABS(Q6))^3
pecs = 0.5*KCSp*poTSFIn^2+0.5*KCSp*poTSHAn^2+0.5*KCSp*poTSWRn^2
te   = ke + peg + peas + peks + pets + pecs

% Calculate angular momentum about gymnast mass centre

amom> = momentum(angular,cmG,FIN,HAN,ARM,TRU,PEL,THI,SHA)
amom  = dot(amom>,N3>)

% Calculate linear momentum

lmom> = momentum(linear) - momentum(linear,TBL)
hormom = dot(lmom>,N1>)
vermom = dot(lmom>,N2>)

%-------------------------------------------------

% INPUTS

% Inputs overwritten in relevant .in files for each vault

input tinitial=0.0, tfinal=0.5
input integstp=0.0001, printint=10
input abserr=1.0e-8, relerr=1.0e-07

input q2=0, q3=0, q4=0, q5=0, q6=0, q7=0, q8=0, q9=0, q10=0
input u2=0, u3=0, u4=0, u5=0, u6=0, u7=0, u8=0, u9=0, u10=0

input lFIN=0, lFINo=0, lHAN=0, lHANo=0, lARM=0, lARMo=0, lTRU=0, lTRUo=0
input lPEL=0, lPELo=0, lTHI=0, lTHIo=0, lSHA=0, lSHAo=0, lTho=0
input lTCy=0, lTCz=0, lTC2y=0, lTC2z=0, lTBL=0, lTBLo=0

input mTBL=0, mFIN=0, mHAN=0, mARM=0, mTRU=0, mPEL=0, mTHI=0, mSHA=0
input iTBL=0, iFIN=0, iHAN=0, iARM=0, iTRU=0, iPEL=0, iTHI=0, iSHA=0

input g=0
input S1=0, S2=0, S3=0
input D1=0, D2=0, D3=0

input SSp=0, SF1=0, SF2=0, SF3=0, SF4=0
input KSSp=0, DSSp=0
input KKSp=0, DKSp=0
```

```
input KCSp=0, DCSp=0
input mu=0
input KTSp=0, KTSp2=0, DTSp=0
input C1 = 0

%-----------------------------------------------

% OUTPUTS

output t,q1,q2,q3,q4,q5,q6,q7,q8,q9,q10,u1,u2,u3,u4,u5,u6,u7,u8,u9,u10
output t,poBFy,poBFz,poTFy,poTFz,poTSy,poTSz,poFIy,poFIz,poHAy,poHAz,
       poWRy,poWRz,poSHy,poSHz,poSCy,poSCz,poHEy,poHEz,poSTy,poSTz,
       poRCy,poRCz,poHIy,poHIz,poKNy,poKNz,poTOy,poTOz,pocmGy,pocmGz
output t,pocmGy,pocmGz,vocmGy,vocmGz,pocmTy,pocmTz,vocmTy,vocmTz
output t,amom,hormom,vermom,te,ke,peg,peas,peks,pets,pecs
output t,FSSp,TKSp,TTSp,FnFI,FnHA,FnWR,Fn2,Fn3,Fax
output t,poTSFIt,poTSFIn,poP1FIt,poP1FIn,poP2FIt,poP2FIn,poP3FIt,poP3FIn,
       poTSHAt,poTSHAn,poP1HAt,poP1HAn,poP2HAt,poP2HAn,poP3HAt,poP3HAn,
       poTSWRt,poTSWRn,poP1WRt,poP1WRn,poP2WRt,poP2WRn,poP3WRt,poP3WRn
output t,voTSFIt,voTSFIn,voTSHAt,voTSHAn,voTSWRt,voTSWRn

%-----------------------------------------------

% UNITS

units [t] = s
units [q1, q2, q4] = m,   [q3, q5, q6, q7, q8, q9, q10] = rads
units [u1, u2, u4] = m/s, [u3, u5, u6, u7, u8, u9, u10] = rads/s

units [lFIN, lFINo, lHAN, lHANo, lARM, lARMo, lTRU, lTRUo] = m
units [lPEL, lPELo, lTHI, lTHIo, lSHA, lSHAo, lTho] = m
units [lTCy, lTCz, lTC2y, lTC2z, lTBL, lTBLo] = m

units [mTBL, mFIN, mHAN, mARM, mTRU, mPEL, mTHI, mSHA] = kg
units [iTBL, iFIN, iHAN, iARM, iTRU, iPEL, iTHI, iSHA] = kg.m^2

units [g] = m/s^2
units [S1, S2] = m, [S3] = rad
units [D1, D2, D3] = m

units [SSp] = m
units [SF1] = m/rad^3, [SF2] = m/rad^2, [SF3] = m/rad, [SF4] = m
units [KSSp] = N/m, [DSSp] = N.s/m
units [KKSp] = N.m/rad, [DKSp] = N.m.s/rad
units [KCSp] = N/m, [DCSp] = N.s/m
units [mu] = unitless
units [KTSp] = N.m/rad, [KTSp2] = N.m/rad^2, [DTSp] = N.m.s/rad
units [C1] = m

units [poBFy,poBFz,poTFy,poTFz,poTSy,poTSz] = m
units [poFIy,poFIz,poHAy,poHAz,poWRy,poWRz,poSHy,poSHz,poSCy,poSCz] = m
units [poHEy,poHEz,poSTy,poSTz,poRCy,poRCz,poHIy,poHIz,poKNy,poKNz] = m
units [poTOy,poTOz] = m
units [pocmGy,pocmGz,pocmTy,pocmTz] = m
units [vocmGy,vocmGz,vocmTy,vocmTz] = m/s
units [amom] = kg.m^2.rad/s, [hormom, vermom] = kg.m/s^2
units [ke,peg,peas,peks,pets,pecs,te] = kg.m^2/s^2
units [FSSp,FnFI,FnHA,FnWR,Fn2,Fn3,Fax] = N, [TKSp] = N.m, [TTSp] = N.m
units [poTSFIt,poTSFIn,poP1FIt,poP1FIn,poP2FIt,poP2FIn] = m
```

```
units [poP3FIt,poP3FIn,poTSHAt,poTSHAn,poP1HAt,poP1HAn] = m
units [poP2HAt,poP2HAn,poP3HAt,poP3HAn,poTSWRt,poTSWRn] = m
units [poP1WRt,poP1WRn,poP2WRt,poP2WRn,poP3WRt,poP3WRn] = m
units [voTSFIt,voTSFIn,voTSHAt,voTSHAn,voTSWRt,voTSWRn] = m/s

%-------------------------------------------------

% GENERATE FORTRAN CODE

save Vaulting_TD_ST.all

code dynamics() Vaulting_TD_ST.f, subs
```

Appendix D

Calculation of Series Elastic Component Stiffness

Table D.1. Determination of series elastic component length

Joint action	Muscle	α (deg)	L_b (mm)	L_f (mm)	L_t (mm)	L_{SEC} (mm)
Knee extension	Rectus femoris	10	302	88	186	391
	Vastus lateralis	11	273	110	138	295
	Vastus medialis	10	360	112	49	291
	Vastus intermedius	6	320	106	87	293
Knee flexion	Biceps femoris	15	152	146	96	104
	Hamstrings	11	291	99	141	326
	Gastrocnemius	13	241	74	213	371
Hip extension	Gluteus maximus	1	172	163	233	236
	Hamstrings	11	291	99	141	326
Hip flexion	Psoas major	5	238	190	54	100
	Rectus femoris	10	302	88	186	391
Shoulder extension	Teres major	16	140	124	26	49
	Latissimus dorsi	21	279	205	87	183
	Posterior deltoid	18	153	120	40	83
Shoulder flexion	Pectoralis major (cl.)	17	154	137	23	48
	Pectoralis major (st.)	25	171	143	47	93
	Anterior deltoid	22	126	99	26	64
Wrist extension	Extensor carpi ulnaris	12	228	48	174	356
	Ext. carpi radialis brevis	9	127	50	146	223
	Ext. carpi radialis longus	1	94	77	162	179
Wrist flexion	Flexor carpi radialis	3	164	51	198	310
	Flexor carpi ulnaris	12	228	42	206	393

Table D.2. Determination of series elastic component stiffness

Joint action	Muscle	d (mm)	PCSA (mm^2)	K ($Nm\,rad^{-1}$)	K_{SEC} ($Nm\,rad^{-1}$)
Knee extension	Rectus femoris	40	3357	104	805
	Vastus lateralis	40	6880	283	
	Vastus medialis	40	4674	195	
	Vastus intermedius	40	5368	222	
Knee flexion	Biceps femoris	25	1024	42	173
	Hamstrings	25	7807	101	
	Gastrocnemius	16	6167	30	
Hip extension	Gluteus maximus	60	4171	325	1004
	Hamstrings	74	7807	679	
Hip flexion	Psoas major	14	1383	68	306
	Rectus femoris	34	3357	238	
Shoulder extension	Teres major	59	293	453	1988
	Latissimus dorsi	117	730	1191	
	Posterior deltoid	53	469	345	
Shoulder flexion	Pectoralis major (cl.)	62	307	611	1574
	Pectoralis major (st.)	62	568	587	
	Anterior deltoid	42	546	376	
Wrist extension	Extensor carpi ulnaris	9	260	2	25
	Ext. carpi radialis brevis	19	273	16	
	Ext. carpi radialis longus	16	146	7	
Wrist flexion	Flexor carpi radialis	17	199	16	37
	Flexor carpi ulnaris	17	342	21	

Appendix E

Anthropometric Measurements

All measurements are in millimetres

Torso

Level	hip	umbilicus	ribcage	nipple	shoulder	neck		nose	ear	top
Length	0	152	210	400	522	576	0	106	164	267
Perimeter	914	787	799	988		391		498	576	
Width	321	298	272	334	334					
Depth					169					

Left Arm

Level	shoulder	midarm	elbow	forearm	wrist		thumb	knuckle	nails
Length	0		250	338	520	0	65	88	195
Perimeter	383	309	261	282	180		255	215	132
Width					63		101	85	48

Right Arm

Level	shoulder	midarm	elbow	forearm	wrist		thumb	knuckle	nails
Length	0		253	338	521	0	63	86	194
Perimeter	383	312	264	277	178		257	213	130
Width					63		106	86	51

Left Leg

Level	hip	crotch	midthigh	knee	calf	ankle		heel	arch	ball	nails
Length	0	101		400	573	805	0	19		139	198
Perimeter		499	469	341	335	204		303	225	217	140
Width										86	58
Depth								117			

Right Leg

Level	hip	crotch	midthigh	knee	calf	ankle		heel	arch	ball	nails
Length	0	109		408	567	807	0	19		147	202
Perimeter		508	478	334	330	205		295	230	218	140
Width										89	57
Depth								115			

Height 1732

Weight 69.9 kg